Wintertime Cloud Systems over the Colorado Rockies: Three Case Studies

by
Robert Ray Lee

Department of Atmospheric Science
Colorado State University
Fort Collins, Colorado

Colorado
State
University

Department of
Atmospheric Science

WINTERTIME CLOUD SYSTEMS OVER THE

COLORADO ROCKIES: THREE CASE STUDIES

By

Robert Ray Lee

Department of Atmospheric Science
Colorado State University
Fort Collins, Colorado

December 1980

Atmospheric Science Paper No. 331

ABSTRACT OF THESIS

WINTERTIME CLOUD SYSTEMS OVER THE COLORADO ROCKIES: THREE CASE STUDIES

This study focuses upon the mechanisms by which mountains and
synoptic weather systems interact to produce characteristic orographic
cloud systems. In each of the three case studies, a synoptic cloud
component, an orographic cloud component, and a convective cloud compo-
nent were identified through the analysis of rawinsonde data, vertically
pointing radar data, and visual observations.

The following are considered to be the major findings of this
study: i) wintertime cloud systems over the Colorado Rockies form by
vertical velocity components which act on different size and time scales
(synoptic, orographic, and convective); ii) at times, a fourth cloud
component, generated by the mesoscale structure of the synoptic distur-
bance (e.g., travelling gravity wave, moving convective bands, or organ-
ized convective lines, etc.) invigorates the entire cloud system,
iii) upwind blocking is very important to the orographic lift and the
lifted cloud system; iv) the deduced cloud is very sensitive to the
lifting model and the upwind profiles of temperature and moisture; and
v) synoptic storm tracks, travelling mesoscale phenomena, large scale
vorticity, moisture and temperature advection, synoptic and topographic
forcing of wind direction and speed, vertical structure of temperature
and moisture, cold air pooling, nocturnal valley inversions, blocking,
and stagnation all constitute controls on orographic cloud systems.

The timing and interaction of the above physical processes deter-
mine the formation and behavior of the complete cloud system and define

how the local mountain terrain and environment interact with synoptic
weather patterns to produce each characteristic orographic cloud system
and the accompanying precipitation.

Robert Ray Lee
Atmospheric Science Department
Colorado State University
Fort Collins, Colorado 80523
Fall, 1980

ACKNOWLEDGEMENTS

HIGH FLIGHT

Oh, I have slipped the surly bonds of earth,

And danced the skies on laughter-silvered wings;

Sunward I've climbed and joined the tumbling mirth

Of sun-split clouds -- and done a hundred things

You have not dreamed of -- wheeled and soared and swung

High in the sunlit silence. Hov'ring there,

I've chased the shouting wind along and flung

My eager craft through footless halls of air.

Up, up the long delirious, burning blue

I've topped the wind-swept heights with easy grace,

Where never lark, or even eagle, flew;

And, while with silent, lifting mind I've trod

The high untrespassed sanctity of space,

Put out my hand, and touched the face of God.

By John Gillespie Magee, Jr.

TABLE OF CONTENTS

LIST OF TABLES

LIST OF FIGURES

xi

CHAPTER I INTRODUCTION

The formation of many orographic cloud systems can be attributed to the passage of synoptic scale migratory waves. These atmospheric disturbances provide the moisture and circulation, when sufficiently forced by the mountains, to form this type of cloud system. This is especially true of continental orographic cloud systems which play a significant role in establishing the winter snowpack in the Colorado Rocky Mountain region.

Precipitation in mountainous terrain can be thought of as being made up of three components: (a) the synoptic precipitation component, (b) the orographic precipitation component, and (c) the convective precipitation component. These three precipitation components are directly related to the vertical motion fields associated, respectively, with migratory waves, terrain lifting, and the local release of convective instability (Elliott, 1966; Rhea, 1972; Rhea, 1978). Visual observations by Marwitz (1974), radar observations by Furman (1967), satellite observations by Reynolds and Morris (1978) and Morris (1979), and precipitation network analysis by Elliott and Hovind (1964) and Elliott and Schaffer (1962), point to the existence of precipitation components associated with each of these mechanisms.

The economical importance of the winter snowpack to the Colorado Rocky Mountain region (e.g., ski industry, avalanche prediction, snow removal) calls for an understanding of how synoptic, migratory waves form different types of precipitating orographic cloud systems. This can be achieved by recognizing the fact that the characteristics of each cloud system are determined by a combination of the components as the synoptic scale disturbance passes.

1

1.1 Objectives

This study presents an analysis of three different orographic cloud systems which occurred during the winter months over the Park Range of northwest Colorado and attempts to understand the differences and similarities in light of the structure and motion of each accompanying synoptic scale disturbance.

PRIMARY OBJECTIVES

Determine the principal mechanisms by which mountains and synoptic weather systems interact to produce characteristic orographic cloud systems.

Analyze the synoptic, orographic, and convective components that comprise an orographic cloud system and identify the important physical processes which determine each.

SECONDARY OBJECTIVES

Develop analysis methods utilizing rawinsonde data taken in the vicinity of the target barrier which can be used to describe the synoptic, orographic and convective components of continental, winter, orographic cloud systems.

Analyze the interrelationships between the various components of the orographic cloud system.

Determine the degree of instability present within winter storm systems as they impinge upon the northwestern Colorado Rockies.

1.2 Literature Review

Various vertical velocity components combine constructively and destructively to determine specific orographic cloud systems. Ultimately, the shape and track of the migratory wave has the major control over the cloud system that forms.

Synoptic scale vertical velocity components, $\sim$ 0.01 m/sec, are determined by differential vorticity advection and airmass lifting by frontal systems. An existing orographic cloud can be invigorated by the synoptic vertical velocity ahead of the upper atmospheric disturbance or suppressed by subsidence behind the disturbance (Chappell, 1970; Rhea, 1972; Grant, et al., 1974; Rhea, 1978).

Orographic vertical velocity components, $\sim$ 0.3 m/sec, (stable airflow forced vertically by the topography) are the dominant components in that they provide a more persistent vertical velocity motion field in time. They are dependent upon airflow direction and speed, moisture and mountain barrier shape and orientation (Schaffer, 1950; Scorer, 1954; Myers, 1962; Rhea, 1972; Reid, 1976; Walsh, 1977; Rhea, 1978). Synoptic scale disturbances provide the moisture and forced airflow that induces the pure orographic cloud (Myers, 1962; Rhea, 1967; Grant, et al., 1968; Rhea, et al., 1969; Chappell, 1970; Grant, et al., 1974; Cooper and Saunders, 1976; Plooster and Vardiman, 1976; Vardiman et al., 1976). The orographic cloud component of the cloud system may fluctuate slowly in time or may remain relatively constant over a long period of time as long as the airflow and thermodynamic parameters do not change significantly.

As a cloud system's stability decreases, the dynamics of the orographic airflow are changed. In the period before convection sets in,

it has been shown that the character of the orographic airflow depends upon the upwind airflow, topography, and stability (Corby, 1947; Queny, 1947; Scorer, 1949, 1951, 1953a,b, 1954; Schaffer, 1950; Queny, et al., 1960; Sawyer, 1960; Elliott and Schaffer, 1962; Myers, 1962; Berkofsky, 1964; Wallington, 1970; Willis, 1970; Orgill, 1971; Grant, et al., 1974; Mahrer and Pielke, 1975; Rhea, 1978). For broad mountains, half width >20 km, the height at which the orographic vertical velocity first becomes zero is proportional to one over the square root of the Scorer parameter (Willis, 1970).

$$\ell^2 = g/u^2 \ \frac{\partial Ln\theta e}{\partial Z} \ b \qquad \text{(Scorer parameter for saturated air)}$$

$$\ell^2 = g/u^2 \ \frac{\partial Ln\theta}{\partial Z} \qquad \text{(Scorer parameter for dry air)}$$

$$b = \frac{1 - \gamma_m/\gamma_d}{1 - c_p T/\varepsilon L} \qquad \text{(Fraser, 1970; Fraser, et al., 1973).}$$

γ_m = saturated adiabatic lapse rate

γ_d = dry adiabatic lapse rate

T = temperature

ε = .622

L = latent heat of vaporization

c_p = specific heat at constant pressure

By calculating Scorer parameters for typical winter airmasses which impinge upon the Colorado Rockies, Rhea (1978) showed that the height at which the orographic vertical velocity first becomes zero is between 2 to 3 1/2 times as far above the mountain ridge for cloudy air as for clear air over the Colorado Rockies. Therefore, even the presence of moisture within the stabily stratified air can change its flow characteristics. When the cloud system becomes unstable and convection sets

in, the above airflow models break down and the convective component
of the orographic cloud system establishes itself. The degree of in-
stability dictates whether the convective motions will remain embedded
within the cloud system or if they will dominate the vertical velocity
field.

A convective vertical velocity component, > 1 m/sec, can be in-
duced and modified by thermodynamic stratification of the atmosphere,
the orographic lift encountered, advective processes of thermodynamic
variables, daily cycles of solar insolation, radiative losses, surface
roughness, vegetation, snow cover, small to medium scale turbulent
motions, wind shear, and microphysical processes (Orgill, 1971; Orgill,
et al., 1971; Derrickson, et al., 1973; Nickerson, et al., 1976; Reid,
1976; Reid, et al., 1976; Walsh, 1977). Convection may be superimposed
upon the orographic cloud and this instability can be caused by a com-
bination of destabilization by synoptic scale advective processes and
airmass lifting by the topography (Scorer, 1953; Saucier, 1955; Hess,
1959; Elliott and Schaffer, 1962; Myers, 1962; Elliott and Hovind, 1964;
Furman, 1967; Rhea, et al., 1969; Wong and Kao, 1970; Rhea, 1972;
Fraser, et al., 1973; Grant, et al., 1974; Marwitz, 1975; Marwitz,
et al., 1976; Walsh, 1977; Reynolds and Morris, 1978). This component
of the total cloud system is highly variable in time and space as
temperature and moisture fields are advected into the cloud system and
the air is lifted over the barrier (Elliott and Schaffer, 1962; Dept.
of the Air Force, 1969; Fraser, et al., 1973; Vardiman, et al., 1976).
The variability may occur with a diurnal cycle, a synoptic storm pro-
gression, or from storm to storm as each storm track, moisture content,

temperature structure, and source region vary (Rhea, et al., 1969; Chappell, 1970; Orgill, 1971; Grant, et al., 1974; Marwitz, et al., 1976; Walsh, 1977).

The convective component of the orographic cloud system is important because it can physically alter the shape, size, depth, dynamics, water contents, and microphysics of an otherwise stable system (Furman, 1967; Smith, 1970; Walsh, 1977). The presence of convective motions can directly alter the cloud microphysical processes. Imbedded convective elements can generate secondary ice crystals by transporting crystals from higher levels, accumulating ice nuclei or crystals at a given cloud level, multiplying ice crystals, or by generating seed crystals which grow by aggregation as they fall through lower cloud layers (Chappell, 1970; Grant and Elliott, 1974; Hobbs, et al., 1976; Marwitz, et al., 1976, Walsh, 1977). Previous research suggests that accretional, as well as diffusional, crystal growth are important during unstable cloud conditions while only diffusional growth may be important in many absolutely stable orographic clouds (Marwitz, et al., 1976). Convective elements can penetrate to higher, colder levels where more ice nuclei can be activated and produce many more natural ice crystals (Grant, et al., 1968; Rhea, et al., 1969; Smith, 1970; Grant and Elliott, 1974; Grant, et al., 1974; Brown, et al., 1976). Ice crystal multiplication processes such as; 1) fragmentation of individual cloud droplets during freezing, 2) fragmentation of freezing droplets following their collision with ice particles, 3) mechanical breakup of delicate ice crystals due to thermal shock they receive when they collide with and nucleate supercooled droplets, 4) Hallett-Mossop multiplication mechanisms, 5) mechanical fracturing of fragile crystals due to random

collisions associated with turbulent air motions or ordered collisions caused by a difference in terminal fall velocities between particles, and 6) rimed ice evaporating in sub-saturated air, can occur when convective elements are present (Hobbs, 1969; Vardiman and Grant, 1972; Hallett and Mossop, 1974; Hess, 1974; Henmi and Grant, 1974; Aufender and Larson, 1976; Mossop, 1976; Mossop and Wishart, 1976; Vardiman, 1976). The updrafts of convective elements are a source of cloud water and condensate that a stable orographic cloud would lack (Grant, et al., 1968; Elliott, 1969; Grant, et al., 1974; Marwitz, 1975; Cooper and Saunders, 1976; Marwitz, et al., 1976). As the above microphysical mechanisms suggest, the presence of convective motions can significantly alter the precipitation processes from those found in stable orographic clouds (Elliott and Schaffer, 1962; Elliott and Hovind, 1964; Grant, et al., 1965; Furman, 1967; Rhea, et al., 1969; Orgill, 1971; Grant, et al., 1974; Marwitz, et al., 1976; Rhea, 1978; Reynolds and Morris, 1978).

In addition to altering the microphysical processes of the orographic cloud system, the convective component may also function as a transport mechanism for seeding material which is dispersed from ground-based generators. This transport mechanism may be a help or a hindrance to successful cloud modification (Rhea, et al., 1969; Elliott, et al., 1971; Marwitz, 1974, 1975; Cooper and Saunders, 1976). As is suggested above the presence or absence of the convective component strongly affects the potential for static and dynamic modification. A static modification potential may exist because of a difference between the condensate supply rate, and the ice growth rate within a cloud system. Evaporation also has an effect upon this modification potential. A

dynamic modification potential, on the other hand, may exist due to the fact that by treating a cloud system, an additional latent heat release may affect a change in the condensation rate by altering the vertical motion field (Elliott, 1966; Chappell, 1970; Elliott, et al., 1971; Vardiman and Grant, 1972; Grant, et al., 1974; Brown, et al., 1976; Cooper and Saunders, 1976; Marwitz, 1976; Nickerson, et al., 1976; Reid, 1976; Vardiman, et al., 1976; Rhea, 1978).

These three vertical velocity components are important to the entire cloud system in that they determine the physical processes which may or may not operate within the system. These three components are generated by the movement, forcing, strength, temperature and moisture structure of the synoptic-scale disturbance. A detailed analysis of these various elements may lead to an understanding of the workings and interactions of the cloud system components which in turn determine each characteristic cloud system.

1.3 Data Source

In order to investigate the interaction of the orographic cloud system components and the control that the synoptic-scale migratory wave has upon the cloud system, case studies were designed to describe three different cloud systems and their accompanying atmospheric disturbances. Data collected during the Colorado State University Orographic Seeding Experiments (COSE I- January, February, March, 1979 and COSE II - November, December, 1979) conducted over the Park Range of northwestern Colorado, shape the basis for these case studies (see Figures 1 and 2).

The specific objective of the CSU Orographic Seeding Experiments were: i) to quantitatively define the dispersion and transport of
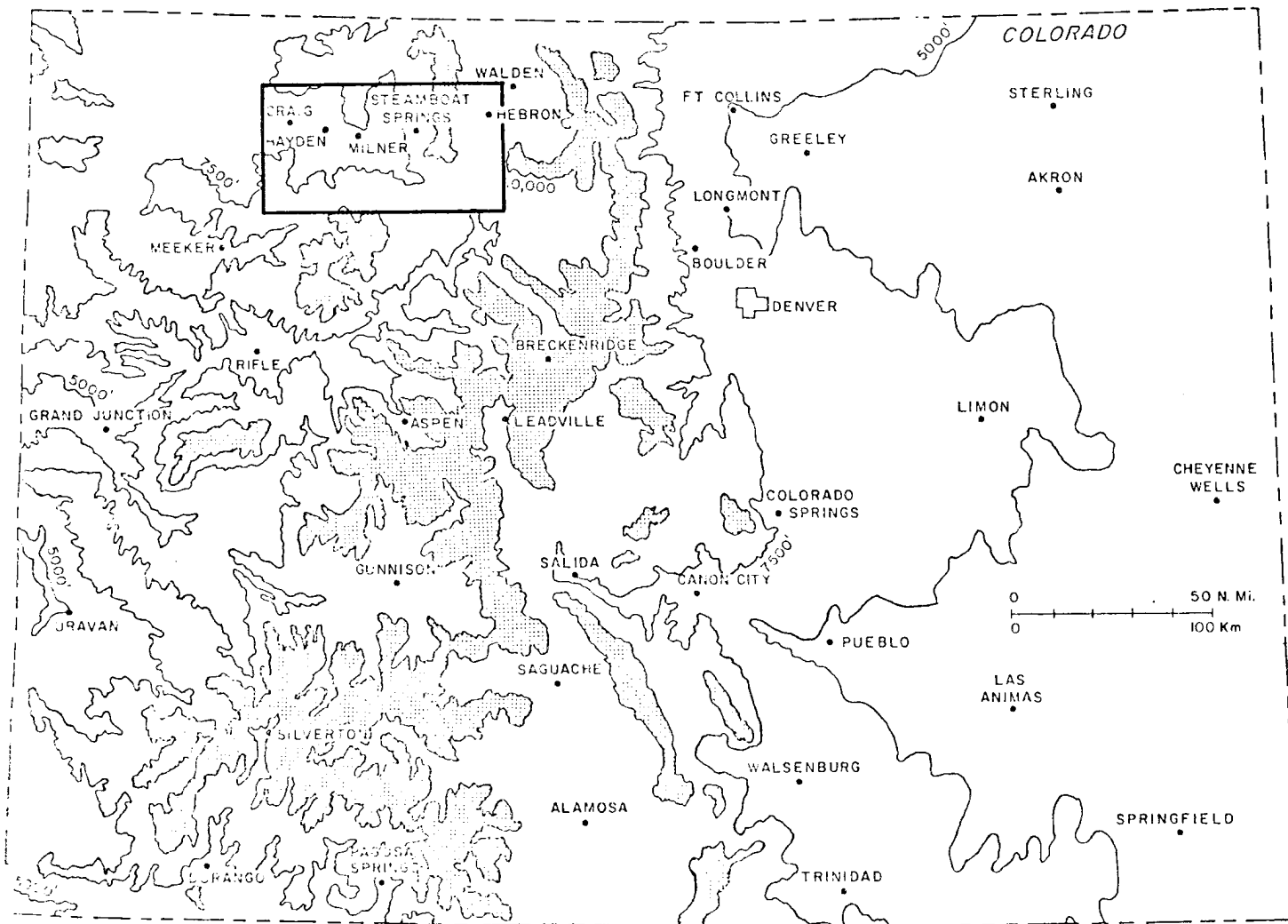
Figure 1. The state of Colorado and the COSE study area.
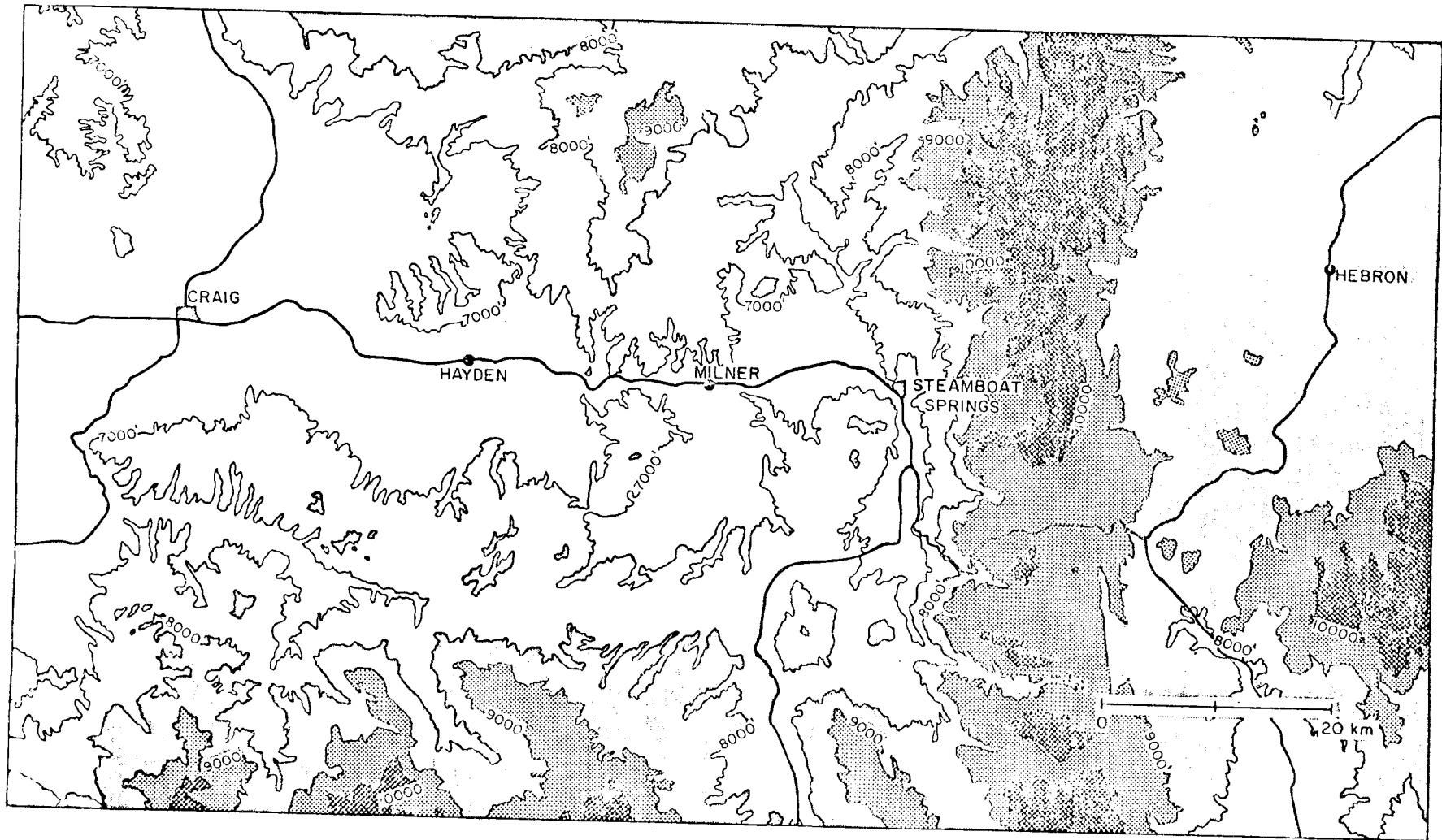
Figure 2. The COSE Study Area

seeding materials, ii) to describe the dominant microphysical processes, and iii) to seek the availability of atmospheric covariates (predictors) needed for analyses of research and applied weather modification programs. Basic data were obtained from (a) simultaneous rawinsonde observations upwind and downwind of the main barrier (the downwind rawinsonde was available during COSE II only), (b) observations with two aircraft equipped with cloud physics and state parameter packages (only one aircraft during COSE I), (c) vertically pointing Ku, K (COSE II only), and X (COSE II only) band radars, (d) ice crystal replicators at valley and mountain sites, (e) observations of atmospheric particulates and nuclei with Bigg-Warner and Mee ice nuclei counters, high volume and carbon cup (COSE I only) samplers, and snow samples to obtain snow for chemical analysis, (f) observations of boundary layer turbulent structure with an acoustical sounder, (g) surface meteorological observations of wind, temperature, humidity, and precipitation at a minimum of seven valley and mountain sites.

1.4 Data Used in Analysis

The necessary data for the analysis of the case studies included: rawinsonde measurements used to determine the upwind and lifted cloud components, radar observations taken vertically at the upwind base of the ridge, and visual observations, taken from the surface and aircraft, that described each overall cloud system. Rawinsonde data was gathered with an RD-65 rawinsonde unit upwind of the main barrier at Craig (see Figure 2). The sounding data set was comprised of 71 soundings taken during COSE I and 62 soundings taken during COSE II. In general, balloons were launched as often as every three hours during storm

periods and less often between storm events, depending upon the local weather conditions and the type of experimental day declared, i.e., transport and diffusion or microphysical studies. All raw rawinsonde data were carefully checked and double-checked for analysis errors and then reduced by the Environmental Data Network System operated by the Water and Power Resources Service, formerly known as the Bureau of Reclamation (Polete, et al., 1977). The EDNS provides for various formats of measured and derived meteorological parameters. For a general description of errors inherent in all rawinsonde data, see Air Weather Service (1955, 1974), Stringer (1972), and Wagner (1960a,b). The inherent errors within the rawinsonde raw data set are acceptable in light of the analysis to be performed.

The radar units consisted of a vertically pointing, .8 cm, K band radar provided to COSE II by the National Oceanice and Atmospheric Administration (NOAA) and a CSU vertically pointing Ku band, 1.8 cm, radar available during COSE I and COSE II. They were operated throughout storm periods and were located at the base of the upwind edge of the main barrier just southeast of Steamboat Springs. The criteria used to specify "cloud" for both radars was that the power returned must be three standard deviations above the receiver noise which was determined separately.

Cloud tops in the first and third case studies were determined from K band continuous fax strip chart data. Cloud top estimations from the fax data format were subject to reduction errors so the cloud tops could only be determined to the nearest 150 meters. Cloud top determinations for the second case study were determined from Ku band radar digital data. The resolution of the Ku radar analysis is 100 meters in the

vertical. A comparison of the two radar sets revealed that, in general, the K band radar was more sensitive and could detect smaller and fewer ice crystals than the Ku band radar. Therefore, the K band radar observed cloud top approximately 200 meters higher than the Ku band radar. This is consistent with the wavelength differences between these two radars. The reflectivity data, used in the first two case studies, was taken from the Ku band digital data.

1.5 Climatological Study of Steamboat Springs Precipitation

In order to place the following case studies in perspective with respect to the precipitation that was produced by each different synoptic regime, a ten year climatological study was performed. Daily precipitation, accumulated from sunset to sunset during the winter months November to April from 1970 to 1980 was recorded. Then a storm type was assigned to each disturbance which produced a measurable amount of precipitation, .01 inches at the precipitation gage located in Steamboat Springs, Colorado.

The ten year study revealed that less than .1 inches of precipitation fell on 37% of the days, on 64% of the days less than .2 inches fell, on 80% of the days less than .3 inches fell, and on 97% of the days .6 inches or less fell at Steamboat Springs. Storm types were classified according to the movement of the vorticity maximums within the 50 kPa (kilopascals) synoptic waves. Table 1 illustrates various characteristics of historical storms that were similar to those of each case study.

Notice that none of these storm types were very frequent or produced the greatest percentage of the total precipitation with respect

to the historical record. Storms similar to case study #1, however, did produce, on the average, the greatest amount of precipitation per storm event.

TABLE I

Climatology of Storm Type and Precipitation for Steamboat Springs

	Historical Weather Systems Similar to Those Analyzed in		
	Case Study #1	Case Study #2	Case Study #3
Frequency of storm type that produced measurable precipitation in 24 hours at Steamboat Springs	14%	13%	22%
Percentage of total precipitation produced by each storm type in the ten year period at Steamboat Springs	18%	13%	23%
Average amount of precipitation produced by each storm type in the ten year average at Steamboat Springs (inches)	.27	.21	.21

CHAPTER II ANALYSIS METHODS

2.1 Stability Analysis

The convective component of the orographic cloud system takes several different forms as the degree of instability increases; an embedded Bernard Cell type of convection, stationary convective lines, and vigorous, moving convective bands (Marwitz, 1976). Many different stability analyses and indices have been used by various investigators (Saucier, 1955; Schuetz, 1957; Hess, 1959; Gates, 1960; Elliott and Schaffer, 1962; Elliott and Hovind, 1964; Rhea, 1967; Dept. of the Air Force, 1969; Chappell, 1970; Fraser, 1970; Orgill, 1971; Grant, et al., 1974; Plooster and Fukuta, 1974; Seinfield, 1975; Marwitz, et al., 1976; Vardiman, et al., 1976).

Parcel methods for analyzing stability can be used to detect large scale instability (Elliott, 1969). If a parcel of air is lifted to its LCL (Lifted Condensation Level), by an orographic lift for example, and the environmental lapse rate in the vicinity of the LCL is such that $\Gamma_{saturated} < \Gamma_{environment} < \Gamma_{dry\ adiabatic}$ (conditional instability), the parcel will continue to rise due to buoyancy ($\Gamma = -dT/dZ =$ lapse rate). As the parcel rises, the temperature difference between the parcel and the environment will accelerate the parcel upwards while entrainment of environmental air will tend to decelerate it. When the temperature of the parcel again equals the temperature of the environment, the parcel will no longer be accelerated by buoyancy.

There are two types of layer methods which can be used to detect smaller scales of instability: layer conditional instability and potential, convective instability. The first method applies the concepts of conditional instability to an atmospheric layer. The layer is

classified according to (a) absolutely stable: $\Gamma_{environment} < \Gamma_{saturated}$, (b) conditionally unstable: $\Gamma_{saturated} < \Gamma_{environment} < \Gamma_{dry\ adiabatic}$, or (c) absolutely unstable: $\Gamma_{dry\ adiabatic} < \Gamma_{environment}$. The classification (b) is conditional upon moisture, if the layer is saturated, then the layer is stable. Processes which bring a conditionally unstable layer to saturation or drive a saturated absolutely stable layer to conditional instability will bring about convective motions through the release of latent heat as water vapor condenses to liquid water and liquid droplets freeze. Both of these processes may operature during an orographic lift. Layers are lifted and cooled, so that condensation takes place. On the other hand, vertical airmass stretching upon lifting can drive the lapse rate of a saturated layer past the saturated adiabatic so that conditional instability may be realized (Saucier, 1955; Hess, 1959; Elliott and Hovind, 1964).

The second method, potential convective instability, can also be applied to an atmospheric layer. A layer is potentially unstable when $\partial\theta_e/\partial Z < 0$ and non-saturated. If the layer is stable, lifted, and cooled to saturation, it will become convectively unstable. When $\partial\theta_e/\partial Z > 0$, non-saturated and stable, the layer is potentially stable. After lifting to saturation, it will remain stable (Saucier, 1955; Hess, 1959). Because layer conditional instability is unable to account for the vertical gradient of latent heat which may be present within the layer, convective potential instability is a preferred analysis technique (see Appendix A).

Table II displays a summary of parcel and layer stability analysis performed upon the COSE I and COSE II sounding data sets.

TABLE II

Parcel Stability vs Layer Stability for COSE I and COSE II

Time Period	Total Number Of Soundings In Data Set	Number of Soundings With Some Amount of Positive Area Generated (Parcel Method, Not Necessarily Realized)				Total Number Of Positive Area Soundings	% of Total
		Vertical Extent of Positive Area					
		0-2.5 kPa	2.5-5.0 kPa	5.0-10.0 kPa	>10.0 kPa		
COSE I	73	3	2	6	6	17	23.3
COSE II	62	1	0	0	0	1	1.6

Time Period	Total Number Of Soundings In Data Set	Number of Soundings With Some Potential Layer Instability Present (Layer Method, Not Necessarily Realized)	% of Total
COSE I	73	67	91.7
COSE II	62	41	66.1

(The COSE II experimental period happened to be exceptionally dry for the Park Range area.) It becomes obvious that the degree and frequency of instability experienced over the Park Range of Colorado is not exceptionally large and since the layer analysis method is more sensitive to this degree of instability, the layer potential instability analysis, rather than the parcel method, is best suited for this area.[1]

In order to analyze for the convective cloud components present within each sounding of the case studies, equivalent potential temperature (θ_e) was plotted as a function of height and the convective potential instability was defined in the following way:

A. Potential instability base equals the point at which the θ_e profile begins to decrease with height. (PIB)

B. Potential instability top equals the point at which the θ_e profile again equals the θ_e value at the layer base. (PIT)

The layer is lifted according to the simple model used to define the composite cloud (see Cloud Analysis section 2.3). The convective cloud component generated by the instability is determined from the following:

C. Convective instability base was taken as the LCL of the potential instability base. (CIB)

D. Convective instability top was taken as the potential instability top if the top of the layer became saturated with respect to water or it was equal to the cloud top if the water saturated top was below the potential instability top. (CIT)

---

[1] This general lack of extensive instability has been expected because winter storms which favor precipitation over the Park Range are generated by modified maritime polar airmasses (Rhea, et al., 1969, pp. 108-109).

The analysis procedure outlined above is the same method used by Marwitz, et al., (1976) to describe the convective cloud component present in San Juan storms (see also Marwitz, 1980). Therefore, the convective cloud component will be defined as the layer that lies between the convective instability base and convective instability top (see Figure 3 below).
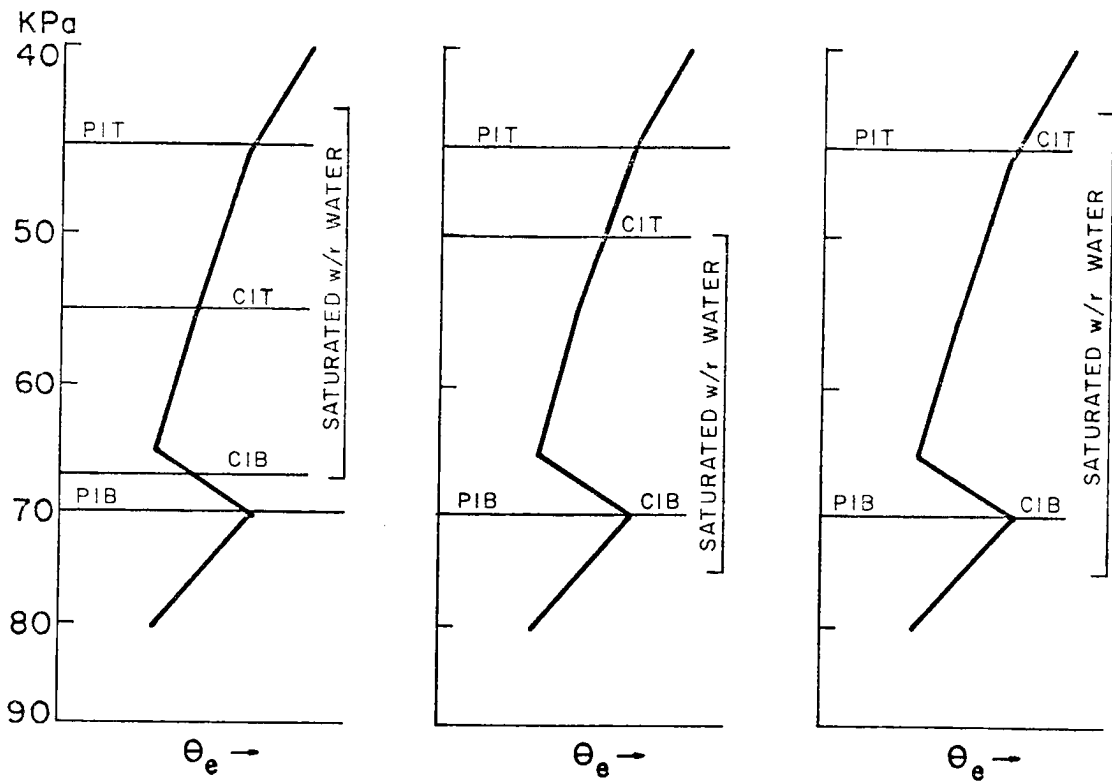
Figure 3. Examples of convective cloud components.

At some point, θ_e must begin to increase with height in order to determine the top of the layer as defined by B. This seems to imply some degree of potential stability within the layer of potential instability. As long as the base of the layer is determined as defined by A, θ_e will decrease with height from layer base to layer top and an average conditional instability will exist throughout the layer.

2.2 Blocking Analysis

A serious difficulty encountered in a two-dimensional analysis of airflow past a ridge is the inability to describe the motion of air which fails to pass over the barrier. This may be caused by any of the following: downslope valley winds in lower layers, thermodynamic stagnation, cold air pooling, light winds which pile air up against the ridge, or winds which encounter the barrier and turn to parallel it without ascension. These conditions are termed blocking flows (Kao, 1965; Wong and Kao, 1970; Orgill, 1971; Fraser, et al., 1973; Marwitz, et al., 1976; Reid, 1976; Rhea, 1978).

Blocking conditions may vary in time and have a large effect upon the orographic lift which, in turn, determines the orographic as well as the convective cloud components which form over the ridge. The blocking flow has been defined with respect to wind direction, a transbarrier wind component, and even a combination of transbarrier wind component and temperature profile (Myers, 1962; Elliott, 1969; Fraser, et al., 1973; Marwitz, et al., 1976; Rhea, 1978; Marwitz, 1980).

The criteria for blocking chosen for this study is similar to that of Rhea (1978). A layer will be termed blocked if the transbarrier wind component is less than 2 m/sec or if $dT/dP < 0.4°K/5$ k Pa. This

criteria will insure that blocking will be accounted for and that the orographic lift will be reduced by an appropriate amount. (If the lowest atmospheric layers are blocked from ascending the barrier, the upwind airflow will be exposed to a lift that will be less than the topographical height of the barrier. See also Marwitz, 1980.)

2.3 Cloud Analysis

In order to accurately reconstruct each storm event, it becomes necessary to define the three proposed components of the cloud system. This includes the upwind portion of the system which is not orographically lifted (the synoptic component), the topographically forced portion of the cloud system (the orographic component), and the portion of the cloud system in which convective motions are expected to occur by the release of potential convective instability (the convective component). The first two components must be defined from rawinsonde cloud base and cloud top criteria, while the convective component is defined from a stability analysis performed upon the rawinsonde data and the lifting of the sounding (see Stability Analysis section 2.1).

There are many ways to define a cloud from rawinsonde data. Water saturation, ice saturation, an arbitrarily defined dew point depression, or an arbitrarily defined relative humidity, are a few of the criteria used (Dept. of the Air Force, 1969; Elliott, 1969; Rhea, 1972; Dumont, et al., 1974; Dumont, 1975; Marwitz, et al., 1976; Vardiman, et al., 1976; Rhea, 1978). Depending on which criteria is used, a cloud top may vary by as much as 20 kPa! The upwind synoptic component of the cloud system will be defined as that portion of the sounding which is saturated with respect to ice. This criteria will be used with the

understanding that the cloud extent may be over estimated simply
because there may be no cloud present and the air is saturated with
respect to ice. Practically, the synoptic cloud component was
determined from each sounding by comparing the observed dewpoint
depression with the dewpoint depression necessary for ice saturation.
The ice saturation dewpoint depression is approximately equal to one-
tenth of the absolute magnitude of the temperature in degrees Celsius,
e.g., a parcel of air which has a temperature of -25°C is said to be
saturated with respect to ice if its dewpoint depression is 2.5°C or
less. This relationship was developed by Hill (1977), see also Hill
(1974), Dumont, et al., (1974) and Dumont (1975).

The lifted orographic cloud was defined by lifting the sounding
and then classifying a "cloud" by both water and ice saturation. These
criteria should give lower and upper estimates of cloud dimensions.
Note that the determined orographic cloud is not a purely "orographic
cloud". The figures which include the orographic component, may also
contain elements of the synoptic component above 40 kPa. Above this
level, the synoptic cloud component was simply "advected" toward the
barrier.

In addition to this "advection" effect, moisture present due to
the synoptic component alone may also be involved with moisture which
was condensed during the orographic lift. Nothing can be done to sub-
tract this synoptic component out of the soundings before they are
lifted by the topography. Therefore, the composite clouds which are
analyzed as existing over the ridge may contain elements of each of the
three components; synoptic, orographic, and convective.

The orographic lift is contingent upon the transbarrier wind component, the temperature structure of the lower layers, the airmass stability upwind of the barrier, blocking flow, and any convective motions which are present. The lifted orographic cloud was determined by employing a simple model which approximates the orographic forcing and yet attempts to account for blocking. The primary lift was defined as the ascent that air near the surface undergoes in order to be raised over the barrier, i.e., 10 kPa if no blocking is present. If blocking is present, the primary lift is reduced by the thickness of the blocked layer. The lift experienced at upper levels is decreased as higher altitudes are reached and becomes zero above 40 kPa. This is reasonable in light of airflow model results (Myers, 1962). It was shown that for uniform slight stability in the troposphere, the first streamline which was not displaced by the orographic influence, as defined from a minimum kinetic energy outflow criteria, lies close to but below the tropopause. For airflow which possess greater stability, by virtue of less moisture or stable lapse rates, the critical level, as defined above, will be found at a lower elevation. The greater stability of continentally modified maritime polar airmasses suggests a critical level around 40 kPa. The criteria used to lift the soundings and determine the orographic cloud, is shown in Table III. This lifting model has the following features: (1) blocking can be accounted for, (2) streamline displacement decreases with height up to 40 kPa, (3) airflow characteristics control the lift, (4) soundings are not lifted en masse, i.e., a decrease of lift with height is accounted for, and (5) lift is scaled towards stable airmass conditions. However,

this model is incapable of describing lift contributions from stability

changes, convective motions, or synoptic scale vertical velocities.

TABLE III

Orographic Lifting Model

Layer	Lift
From the top of the blocked layer or from the surface (80 kPa) to ridge top (70 kPa)	Primary Lift
70.0 kPa to 60.0 kPa	1/2 · Primary Lift
60.0 kPa to 52.5 kPa	1/4 · Primary Lift
52.5 kPa to 45.0 kPa	1/8 · Primary Lift
45.0 kPa to 40.0 kPa	1/16 · Primary Lift

Note: 1000 mb = 100 kPa

CHAPTER III CASE STUDIES

3.1 Case Study #1

December 10 19Z → December 12 00Z 1979

The first case study analysis was performed on a well-organized short wave system which passed over the study area on the 10th and 11th of December 1979. The surface low pressure center formed along the U.S.-Canadian border and moved to the east-southeast passing well to the north of Colorado. However, the trailing surface cold front extended from the low to the southwest down over California and moved quickly to the southeast, passing through the study area around 03Z on the 11th.

The upper air disturbance, most evident at 70 kPa consisted of a strong short wave which also moved through the study area around 03Z on the 11th. Considerable cold air advection and a substantial amount of moisture accompanied the wave. Since this disturbance moved so quickly, it produced heavy precipitation for a relatively short period of time (see Figures 4a-c).

Figures 5a-c illustrate the 1103Z, 1106Z and 1109Z soundings taken from Craig. An analysis of the serial soundings reveals the detailed temperature and moisture structure of the storm. Note the strong cooling in the lowest 20 kPa as the disturbance passed.

Figures 6-7 show the time sections of temperature (T), potential temperature (θ), and equivalent potential temperature (θ_e), respectively, as derived from the upwind Craig rawinsonde. Note the sharp cooling, especially in the lower layers, beginning around 04Z on the 11th.

Figure 8 shows a time section of the winds, again as derived from the Craig rawinsonde data. The winds in the lower layers at Craig,
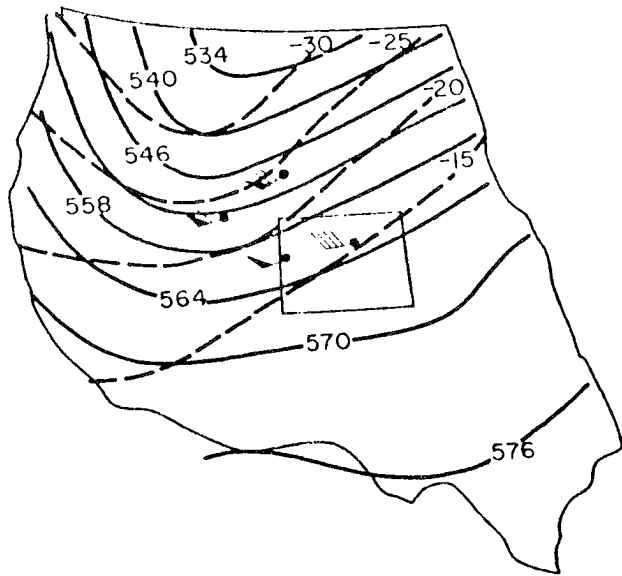
a. 50 kPa Height and Temperature
   Fields for 1100Z.
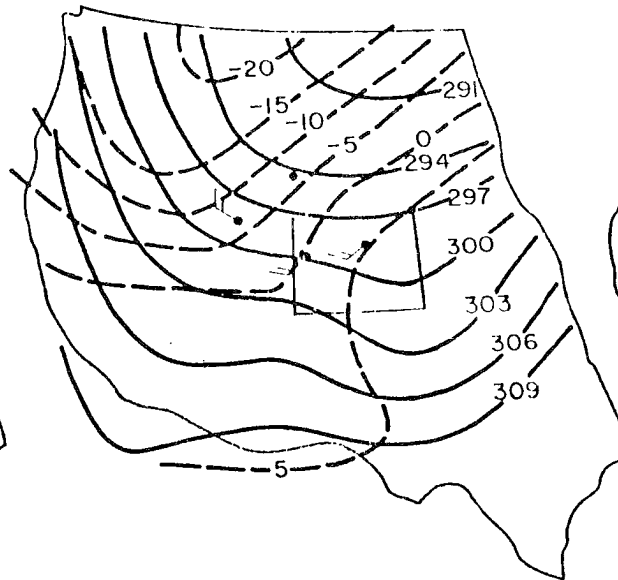
b. 70 kPa Height and Temperature
   Fields for 1100Z.
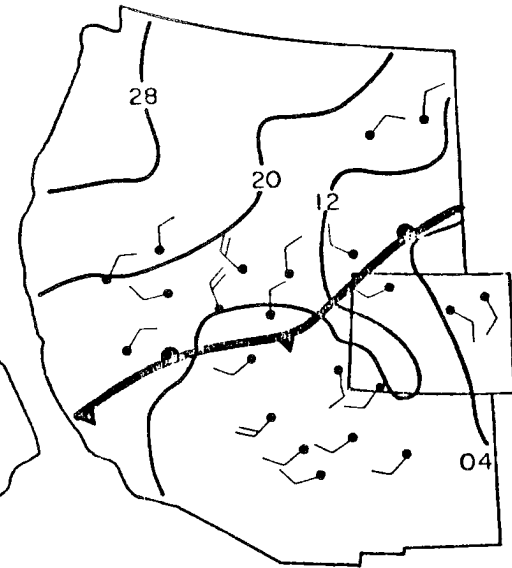
c. Surface Synoptic Chart
   for 1100Z.

Figure 4.   Synoptic Charts for Case Study #1.
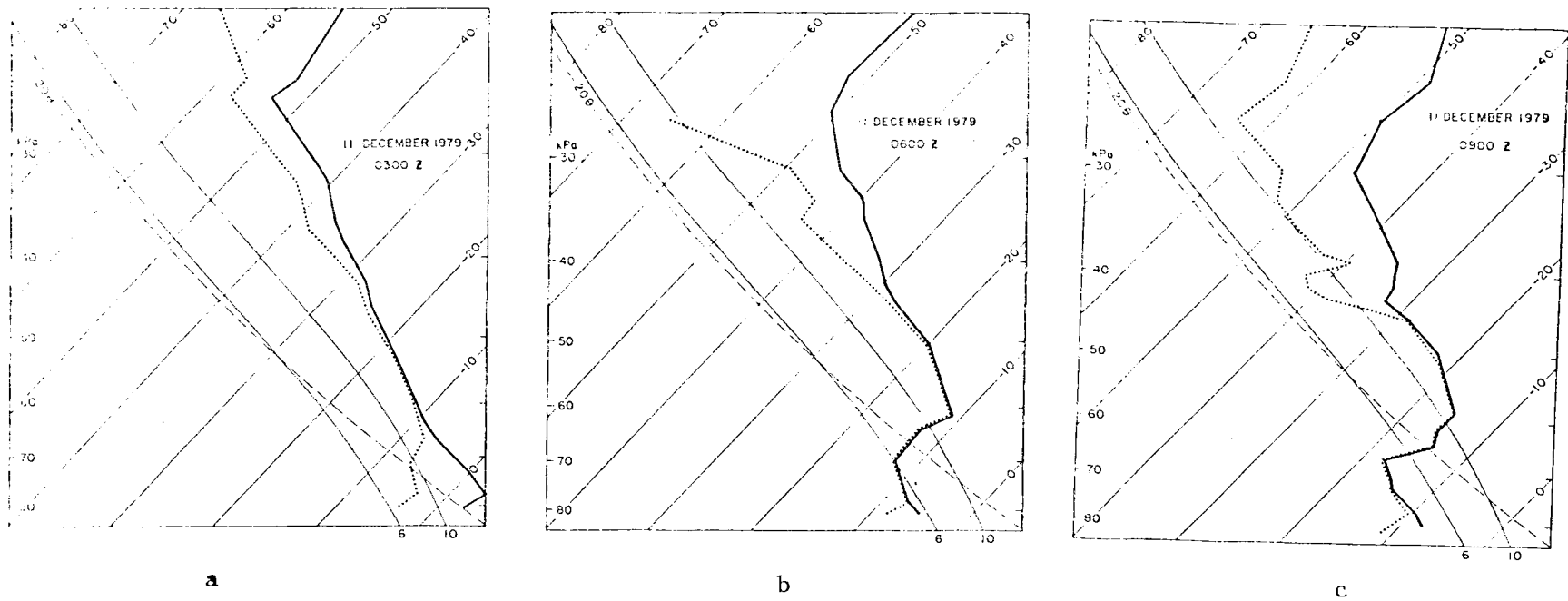
Figure 5. Soundings for Case Study #1.
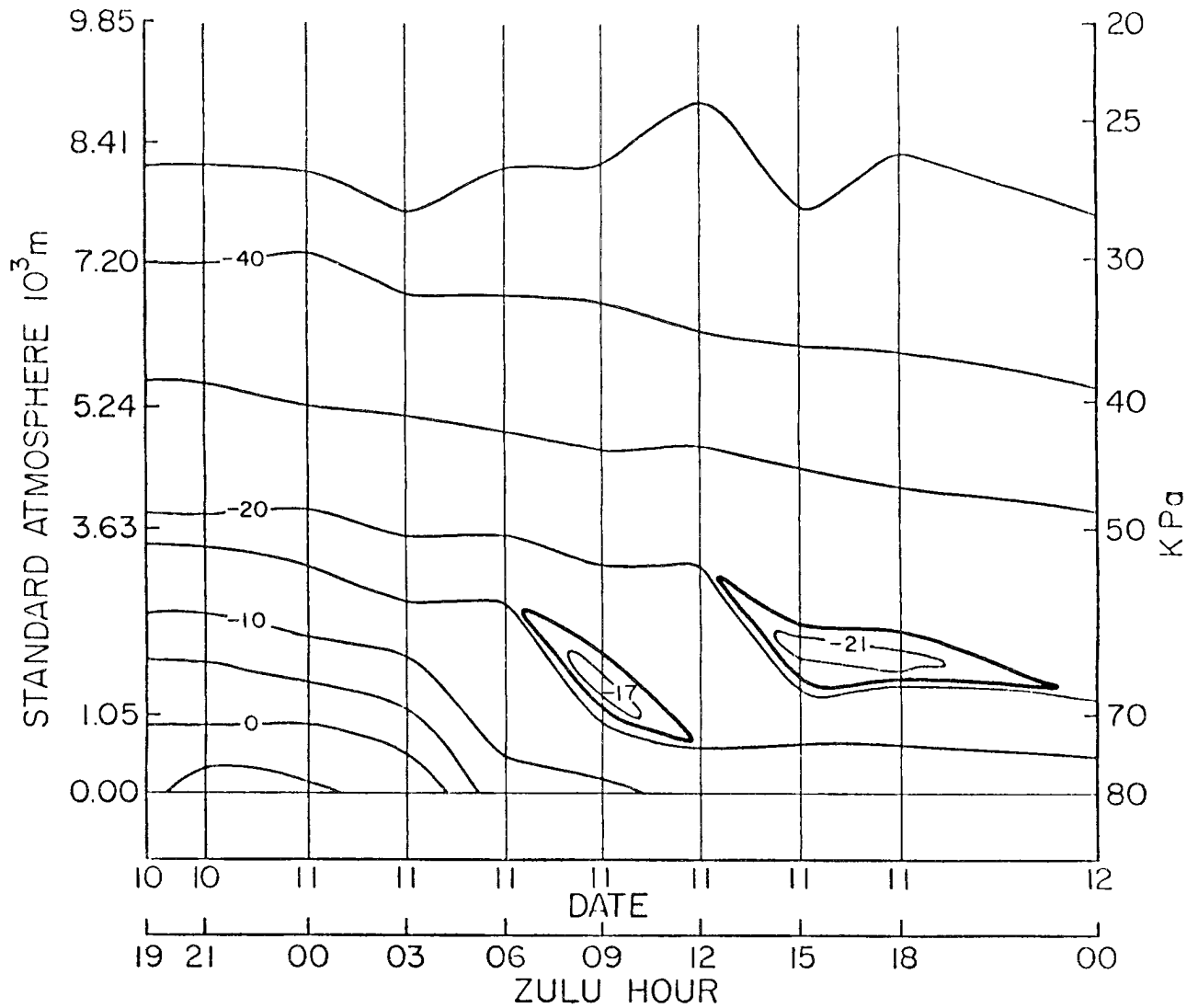
Figure 6. Time Cross-Section Analysis of Temperature of Case Study #1. At temperatures warmer than -20C, temperatures are analyzed every 5°, and at temperatures colder than -20C, temperatures are analyzed every 10°.
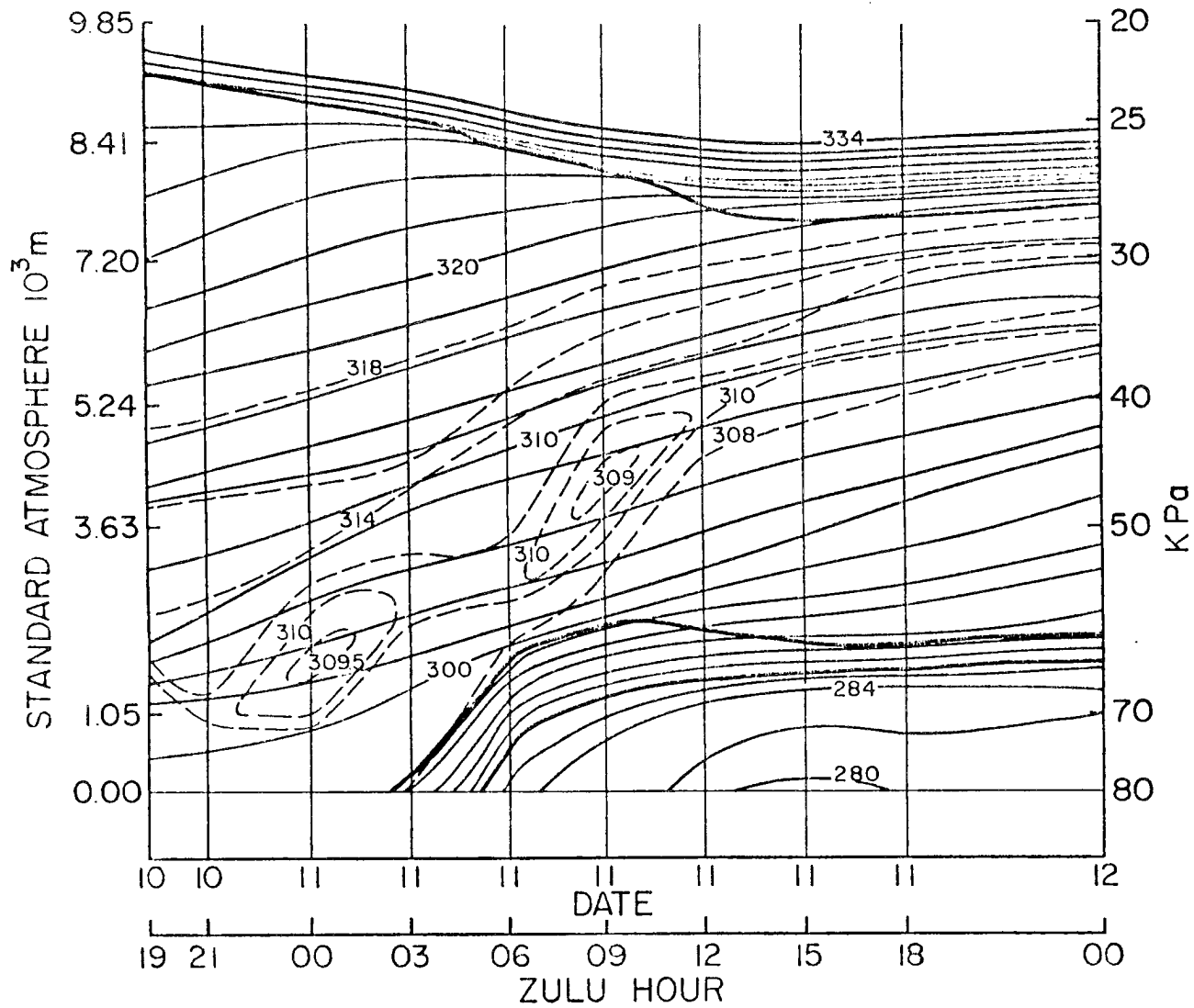
Figure 7. Potential and Equivalent Potential Temperature Time Cross-Section Analyses of Case Study #1. θ (solid lines) and θ_e (dashed lines) have been analyzed every 2°C. Heavy solid lines depict boundaries of stable layers.
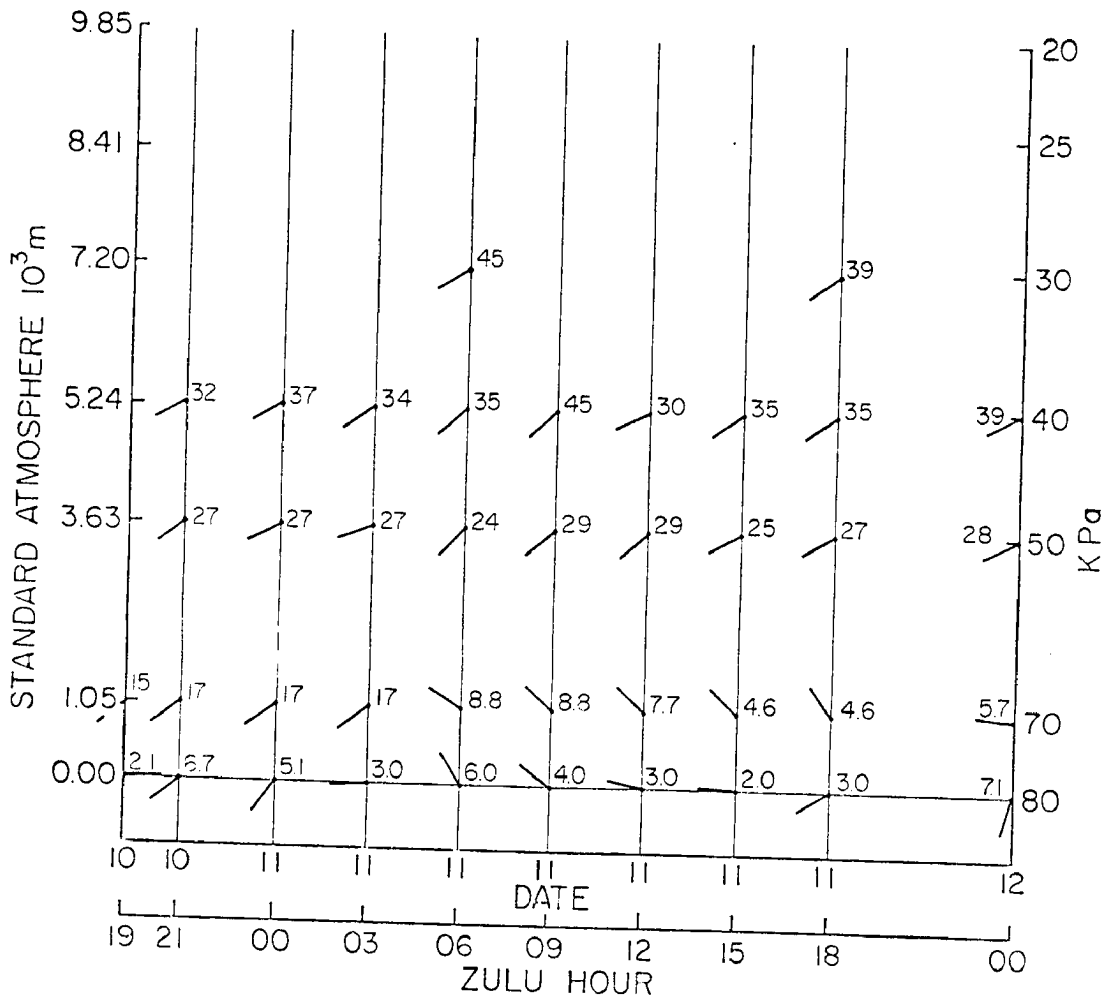
Figure 8. Time cross-section analysis of the wind direction and wind speed of Case Study #1. Wind speeds are in m/sec.

for the most part, maintained strong westerly components so that block-
ing was not important. Prior to 1106Z, however, a mesonet wind station
at Milner measured a weak easterly wind component (Note that 1106Z and
all other such designations within the text indicate a day and hour,
e.g., 06Z on the 11th. This is due to the fact that all rawinsonde ob-
servations were taken on the hour. Such a time designation provides
for a short hand notation in referring to events within the case
studies). After this time, the rawinsonde analysis revealed a veering
of wind direction to the northwest in time and an increase in wind
speed as the strong surface disturbance approached. This implies that
some nighttime cold air pooling acted in response to a diurnal pattern
of valley airflow. Since only one mesonet wind station measured this
downvalley flow, the cold air pooling was not strong or widespread
within the valley. Even though the flow was not blocked at Craig, the
air closer to the barrier may indeed have been blocked or stagnated.
The 70 kPa winds at Craig and all surface winds at the observation sites
throughout the valley veered towards the northwest in time as well as
increased in speed as a response to the short wave passage, while the
upper level winds remained strong out of the southwest.

Figure 9 shows the time-variation of the analyzed ice-saturated
cloud which formed over Craig in time.[2] This portion of the cloud
system has been defined as the synoptic component since the soundings
have not been lifted by the topography. Note the trough passage times
and the general lack of blocking at Craig. (The Craig surface pressure
remains sufficiently close to 80 kPa to call this pressure the surface
in the pressure coordinate system.)

---

[2] See the definition of ice saturated cloud in section 2.3.
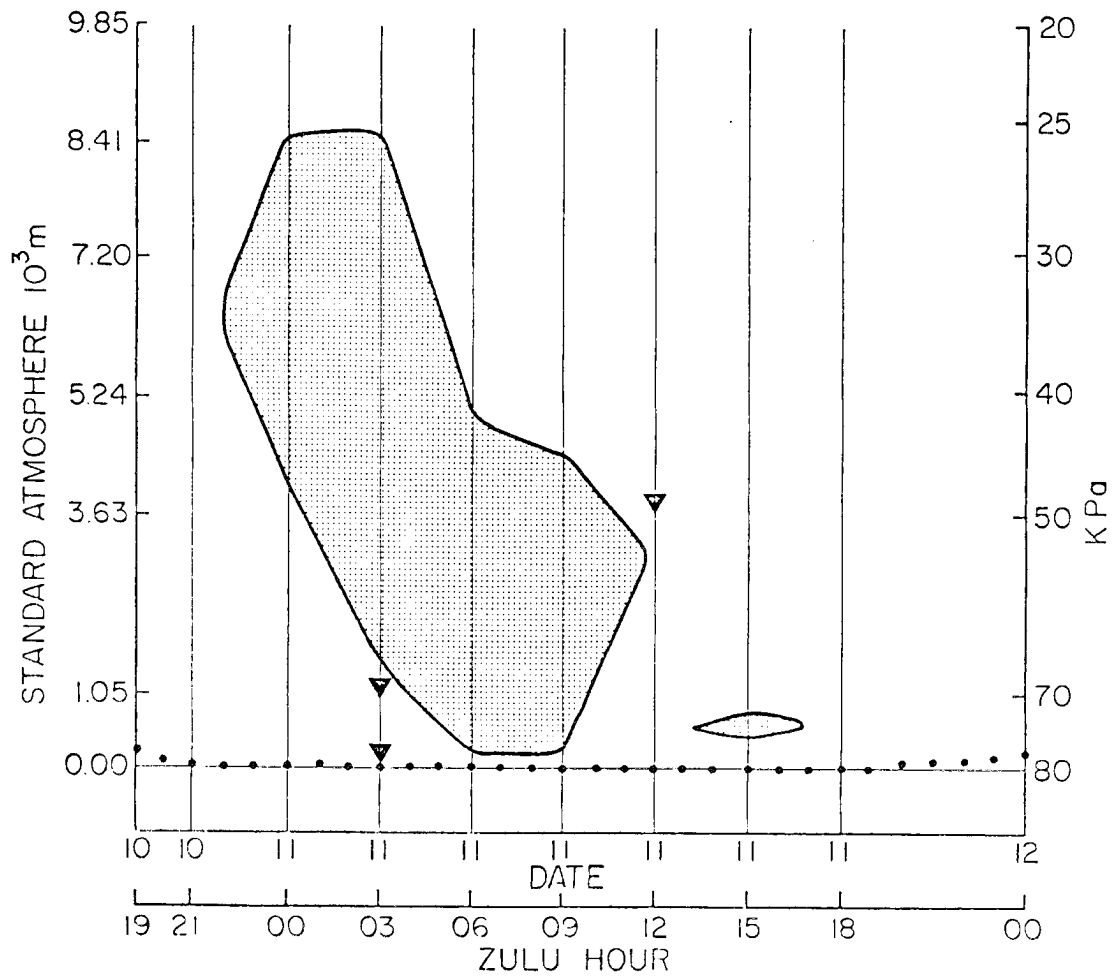
Figure 9. Time cross-section analysis of the synoptic cloud component of Case Study #1. The stippled area depicts the upwind, non-lifted synoptic cloud component. The area between the surface, 80 kPa, and the solid dots depicts the blocked layer. Triangles indicate trough passage at the surface, 70 kPa, and 50 kPa.

Figure 10a illustrates the derived cloud which formed over the
ridge. This composite cloud contains elements from each component.
The soundings were lifted according to the previously defined model.
Ice and water saturated clouds were determined.[3] Note that an
orographic cloud did form during the later stages of the storm when no
upwind cloud existed. The stippled area represents the convective
component of the cloud system and was defined as the zone where the
potential convective instability was released. Figure 11 illustrates
why the convective component was shallower than the derived orographic
ice and water clouds. The air was stable up to the point that θ_e
decreased with height near 50 kPa. Above 50 kPa, the air was
potentially unstable. Since the layer between 50 kPa and 42 kPa became
saturated with respect to water upon lifting, it also became convec-
tively unstable as outlined in section 2.1. The depth of the derived
convective component extended only to the CIT (convective instability
top). Also note that at 1112Z the analysis delineated the existence
of two cloud decks while the radar apparently did not observe two
separate decks. (Several distinct cloud decks have been frequently
observed by the radar during both COSE I and COSE II field experiments.)

As indicated in section 2.3, Cloud Analysis, the lifting model
could describe the first order effects of the orographic forcing, but
it is a crude model at best. In order to test the sensitivity of the
cloud component that formed as a consequence of the topographical
lifting as a function of the lifting model and various temperature and

---

[3]See the definition of orographically forced ice and water saturated
clouds in section 2.3.

34
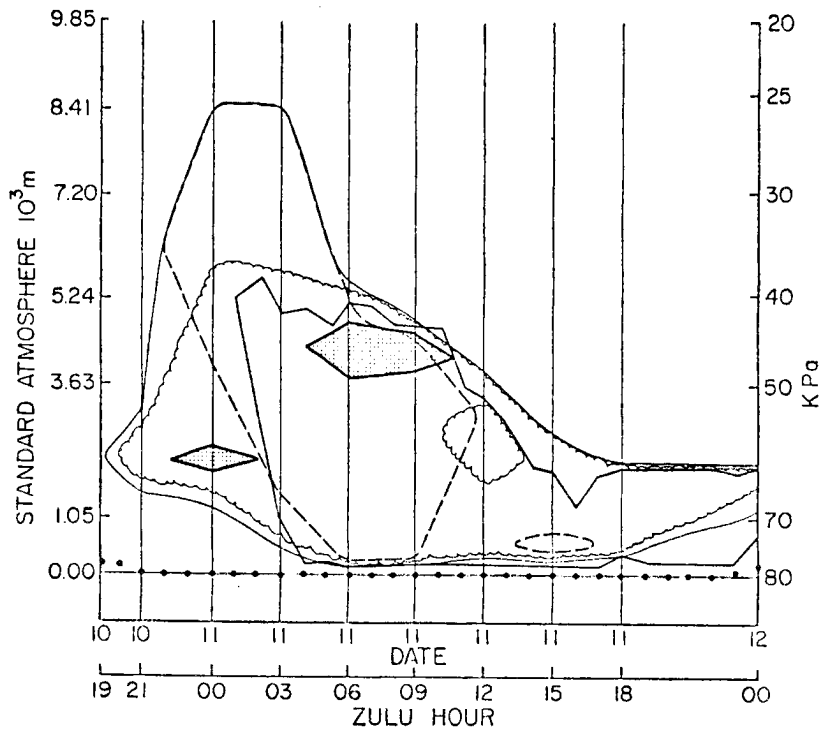
Figure 10a. Time cross-section analyses of the composite cloud system of case study #1. The area within the dashed line depicts the upwind, non-lifted cloud. The area within the thin solid line depicts the lifted, ice-saturated cloud. The area within the convoluted line depicts the lifted, water-saturated cloud. The area within the heavy solid line depicts the radar observed cloud. The stippled area depicts the convective cloud component, θ_e, decreasing with height in a water-saturated layer. The area between the surface, 80 kPa, and the solid dots depicts the blocked layer.
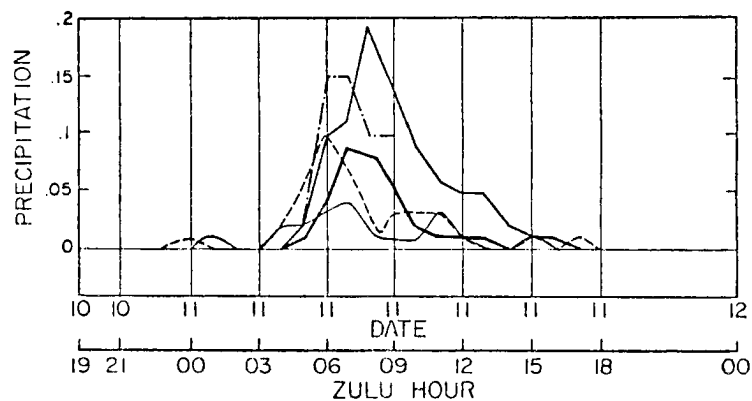
Figure 10b. Time plot of hourly precipitation at various points across the Park Range barrier for case study #1. The heavy solid line (———) corresponds to Radar Base. The dotted-dashed line (—·—) corresponds to False Top. The medium solid line (———) corresponds to Picnic Area. The dashed line (— — —) corresponds to Highway Camp. The thin solid line (———) corresponds to Colubmine Lodge.

PIB = POTENTIAL INSTABILITY BASE
PIT = POTENTIAL INSTABILITY TOP
CIB = CONVECTIVE INSTABILITY BASE
CIT = CONVECTIVE INSTABILITY TOP
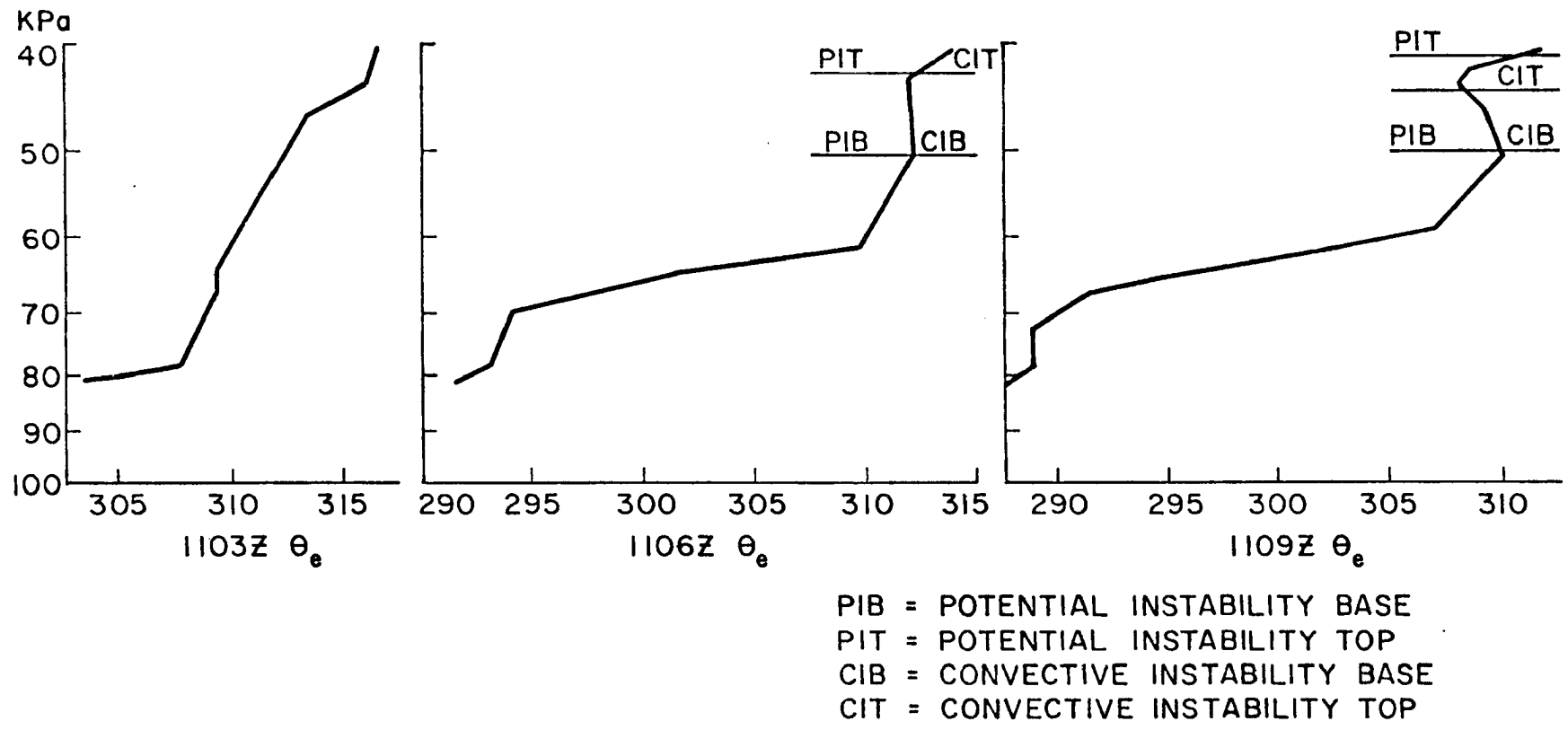
Figure 11. Convective cloud components of Case Study #1.

moisture profiles, an analysis using a slightly different lifting model was attempted. This time the primary lift was apportioned linearly between the surface and 30 kPa. Prior to 1109Z, the new analysis indicated that cloud tops were generally higher than the first analysis, at most 7.5 kPa higher (e.g., at 45 kPa, the first lifting model indicated a lift of 1/16 x primary lift while the alternate lifting model indicated a lift of 6/16 x primary lift). After 1109Z, however, a strong subsidence inversion was established and there was no appreciable difference in the two analyses. This shows that with certain temperature and moisture profiles, the lifting model is critical in determining the lifted cloud top, while different profiles of temperature and moisture clearly indicate the position of cloud top no matter what kind of model is used.

The analyzed water-saturated cloud tops were only slightly higher than those observed by the K band radar. On the other hand, the radar did not detect the early stages of the storm progression as delineated by the analysis in Fig. 10a. This latter discrepancy is reconciled in light of the fact that the air continued to rise over the ridge after it passed the point at which the vertical pointing radar observations were made. It is possible that the cloud formed over the top of the ridge and did not extend upwind far enough for the radar to "see" it. In general, discrepancies between the radar observed and derived cloud top may be attributed to the fact that the moisture, temperature, and windfields observed at Craig, nearly 60 km upwind of the radar site, may not be representative of atmospheric conditions in the immediate vicinity of the ridge.

Early in the storm period, 1100Z and 1103Z, the extreme depth of

the ice-saturated cloud is questioned. The air was likely to be

saturated with respect to ice, but the question remains, Was there ac-

tually a cloud present at this extreme altitude? This question is

difficult to answer, however, since the radar did not observe a "cloud"

anywhere near the indicated tops. The answer is probably that the air

was saturated with respect to ice, but no cloud or else an extremely

thin cloud (below radar detection) was present. Therefore, at these

two times, more emphasis should be placed on the water saturated

analysis.

The problem of delineating a cloud from rawinsonde data can be

illustrated in the following example. Different cloud tops were deter-

mined from the 1100Z and 1103Z soundings using different definitions

of "cloud" (see Table IV). Which criteria correctly identifies "cloud"

from "non-cloud"? Note that the dewpoint depressions used are much

smaller than the $6^{o}C$ dewpoint depression recommended by the Department

of the Air Force (1969) for this type of analysis.

TABLE IV

Various Cloud Top Pressures (kPa) as Determined from Different Cloud
Top Criteria

	Relative Humidity		Dewpoint Depression			Ice Saturation
	80%	85%	$2^{o}C$	$3^{o}C$	$4^{o}C$	
1100Z	35.0	36.3	35.5	32.0	24.0	25.0
1103Z	38.0	40.0	40.0	35.0	25.0	25.0

High radar reflectivities, as documented by Ku band radar data,

corresponded well in time with the analyzed release of convective in-

stability. This fact was true especially between 1106Z and 1109Z (see

Figure 12). The level of maximum reflectivity tended to lie between
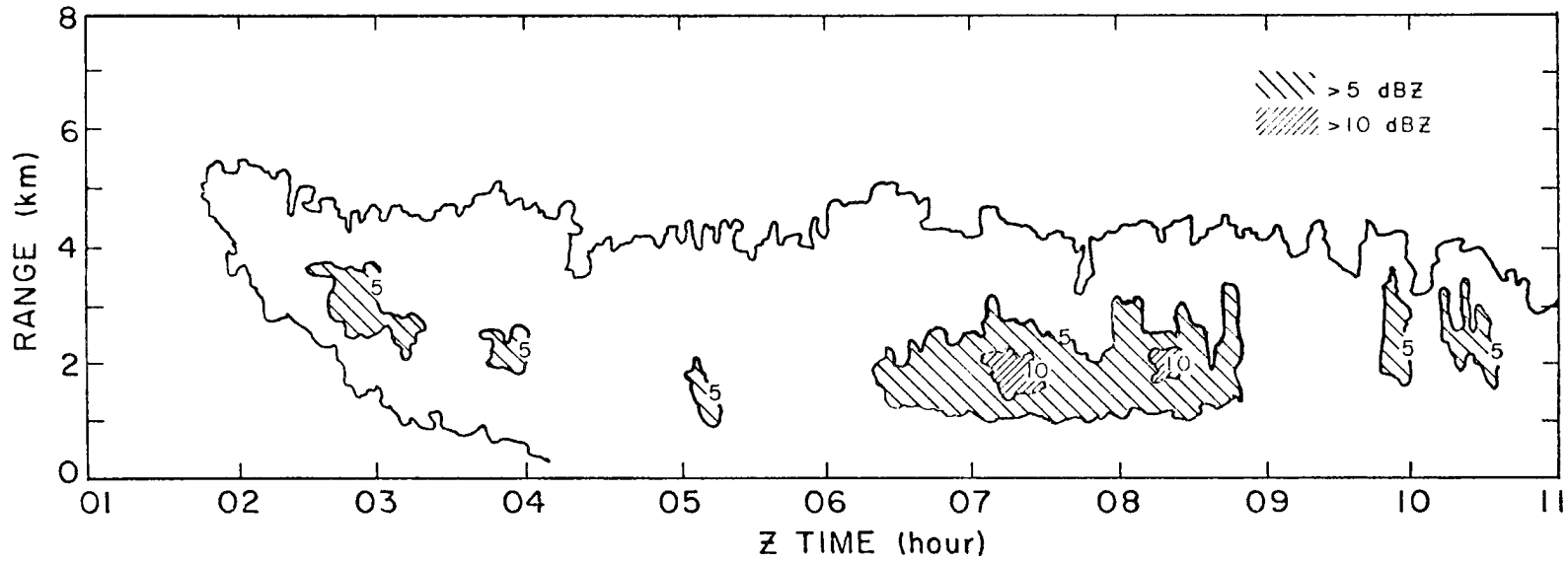
Figure 12. Ku band radar reflectivities of Case Study #1 beginning at 01Z on the 11th.

66 kPa and 56 kPa, well below the analyzed zone of convective insta-
bility. Note that in this layer, the non-lifted temperatures from the
Craig rawinsonde analysis were roughly between $-14^{\circ}C$ and $-17^{\circ}C$. This
temperature range approximately defines the dendritic ice crystal
growth zone. It is hypothesized here that ice crystals fell into the
dendritic growth zone from the zone of convective instability release
and produced the higher radar reflectivities. The maximum reflectivity
values tended to be 10 dBz greater than the rest of the storm reflec-
tivities.

The analysis did quite well in portraying the radar observed com-
posite cloud system. This case study illustrates the importance of
using the analysis together with the radar observations to describe the
complete cloud system.

Figure 10b shows water equivalent precipitation, accumulated during
the indicated hour, as a function of time. The stations, in order of
elevation and distance away from the radar site at the western base of
the ridge, are as follows: Radar, Picnic Area, False Top, Highway Camp,
Columbine. The ridge is relatively broad and flat at its top and
Columbine is at the far eastern edge before the terrain falls off into
the North Park area. Note that all of the precipitation was post-
frontal. It peaked quickly at the beginning of the storm period and
then fell off slowly in time as the post-frontal orographic cloud
established itself. The precipitation started sooner and lasted longer
at the higher elevation sites than at the base of the ridge. The fact
that the snow started sooner at the highest elevation, easternmost
sites, before the trough passed, indicates that this precipitation
was probably due to an orographic precipitation component. If a

synoptic precipitation component had been present, it seems likely that the other snow gages would have indicated snowfall at this time also.

Visual observations made within the Yampa Valley agree quite well with the rawinsonde analysis presented in Figure 10a. A thin layer of clouds formed over the ridge at 2130Z on the 10th. By 2300Z on the 10th, cirrus and stratus clouds were observed to be moving from west to east at Craig. One hour later, 000Z on the 11th, an altostratus layer invaded the valley. At this time, cloud bases over the Park Range were still well above ridge top. In the next four hours, cloud bases dropped below the ridge top, precipitation began at the radar, and moderate to heavy snow was falling halfway up the ridge. Snow continued throughout the night on the ridge and finally stopped at 1400Z on the 11th. Cloud bases remained below the Park Range ridge top throughout the rest of the day up to 0000Z on the 12th, even though upwind from Steamboat Springs, the cloud in the Yampa Valley had dissipated. Soon after 0000Z on the 12th, the orographic cloud itself dissipated. Further detailed visual observations are presented in Appendix B.

3.1.1 The Main Findings of the First Case Study

A closer look at the preceding analyses reveals important relationships between the migratory wave and the components of the orographic cloud system.

1) Rapid cooling occurred in the T, θ, and the θ_e fields following the short wave passage, especially at lower levels.

2) The synoptic cloud component became apparent as the short wave passed.

3) The synoptic cloud component moved into the area at mid-levels, deepened, and then dropped to lower levels. This is presumably due to variable moisture advection, strong vorticity advection, which occurred during the earlier portions of the storm period, or the transient mesoscale structure of the disturbance. (The absolute cloud tops of the synoptic component were difficult to determine.)

4) The migratory wave track was slightly north of the study area so that the low level winds were strong enough to provide for a constant, low level lift.

5) The cloud system which formed over the ridge was governed by moisture advection and lifting. This cloud formed slightly before and lasted many hours after the synoptic upwind cloud component dissipated.

6) The composite cloud system quickly thickened prior to the short wave passage as did the synoptic component. This may be due to the strong vorticity and moisture advection which was present in the earlier part of the storm.

7) A pure orographic cloud did form when an upwind synoptic cloud was not detected late in the storm period.

8) The convective cloud component developed relatively early within the cloud system that formed over the Park Range.

9) Strong cooling in the lower layers, in response to the frontal passage, established an inversion which stabilized the lower portions of the cloud system. Convective instability was not associated with the cooling in these lower layers as the front moved through.

10) Slight convective instability formed at 1106Z due to a moisture decrease with height and differential cooling of a 4 kPa layer centered around 60 kPa. Stabilization occurred as a consequence of a

relative moisture increase with height. The potential instability

present in the 1106Z and 1109Z soundings developed in association with

differential cooling in the 45 kPa and 50 kPa layer. This cooling

caused the lapse rate to be slightly greater than moist adiabatic and,

therefore, forced $\partial\theta_e/\partial Z < 0$. Lifting and condensation released the

potential instability (see Figures 5a-c and 11).

11) The convective instability was associated with the wave

passage. It was not, however, generated on a large scale by the dis-

turbance itself, i.e., neither strong cold air advection aloft nor

strong warm air advection in the lower layers caused the lapse rates to

become unstable. The instability was associated with fine scale tem-

perature and moisture advective processes which operated within a

4-5 kPa layer. The differential cooling tipped an already near moist

adiabatic lapse rate past this value so that $\partial\theta_e/\partial Z$ was negative. The

layer became convectively unstable when the air was able to reach

saturation after lifting.

12) It is hypothesized that ice crystals, falling from a zone of

convective instability release, fell into the dendritic crystal growth

zone, $-14^\circ C$ to $-17^\circ C$, and were responsible for the higher radar reflec-

tivities at this time.

3.1.2 Important Conclusions from Case Study #1

A very important fact illustrated in this first case study is that

the derivation from the rawinsonde data of the cloud system which formed

over the ridge was, at times, very sensitive to the lifting model.

Temperature and moisture profiles determined to a large extent this

"sensitivity". When the moisture slowly decreased with height, the

lifting model became important in that the streamline displacement

determined how the air was lifted and cooled to saturation. If the

streamline displacement is not accurately determined, a "lifted" cloud

can not be analyzed with confidence at all times (i.e., if the moisture

slowly decreases with height, the lifting model is critical).

3.2 Case Study #2

February 22 12Z → February 24 18Z 1979

The second case study analysis was performed on a complex long

wave system. Aloft, a small wave passed over the study area at a time

prior to 2212Z (Note that 2212Z and all other such designations within

the text indicate a day and hour, e.g., 12Z on the 22nd. This is due

to the fact that all rawinsonde observations were taken on the hour.

Such a time designation provides for a short hand notation in referring

to events within the case studies). Slight ridging occurred over

Colorado as the long wave developed over the western U.S. As the long

wave passed over the study area about 2400Z, the storm track generally

moved from the west-southwest. Strong cold air advection and ridging

followed behind the upper air trough.

At the surface, at 2212Z, a low pressure area was centered in

northeastern Colorado while the accompanying cold front trailed off to

the southwest through New Mexico. A secondary cold front was positioned

off the Oregon coast and another weak stationary front extended through

Montana to the southeast, generally northeast of Colorado. In time,

the front off the Oregon coast propagated quickly to the east while the

stationary front to the northeast slowly retrograded to the southwest.

During this time, cold arctic air moved into the Great Plains from the

north. As it did so, it pushed westward toward the Continental Divide and deepened. The two fronts merged very close to the study area about 2400Z and then proceeded to the east together. By 2500Z, a high pressure system had strengthened into the Great Basin area (see Figs. 13a-f).

Figures 14a-g show selected soundings from Craig throughout this storm period. A comparison between Figure 20 and Figure 14a-g illustrates the relationship between θ_e and the soundings. Note that θ_e decreases with height when the lapse rate becomes less than moist adiabatic or the dewpoint depressions increase quickly with height.

Figures 15-16 show the upwind time sections of T, θ, and θ_e, respectively. The field gradients were much weaker than in the first short wave case study. This disturbance seemed to be more spread out in time as the long wave moved slower than the previous short wave of the first case study. Both time sections indicate cooling in the lower levels between 2306Z and 2312Z. This can be attributed to nocturnal cooling and valley cold air pooling. During the nighttime hours, after 2306Z and before 2312Z, the soundings indicated that a valley inversion had been established. This formation of a very stable layer undoubtedly contributed to the blocking and accounted for the cold air pooling at this time. During the nighttime periods, however, between 2400Z and 2412Z, no valley inversion formed. At this time, the blocking was attributable to southwesterly winds at 70 kPa which produced a cross-valley flow at upper levels and was not funneled toward the barrier. All three temperature fields, however, also indicated some cooling in response to the trough and surface passage after 2400Z. As shown in Figure 16, the θ_e field differed from the θ field implying the presence of moisture throughout the entire storm period. Note that at times
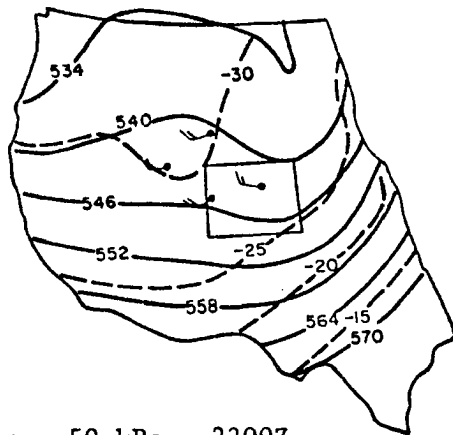
a. 50 kPa - 2300Z
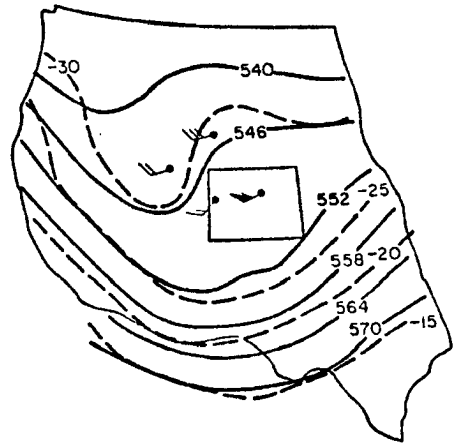
b. 50 kPa - 2400Z
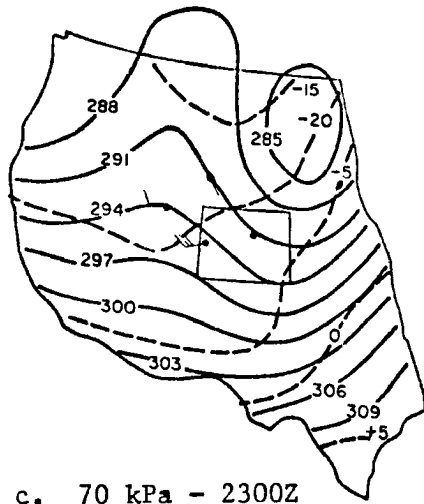
c. 70 kPa - 2300Z
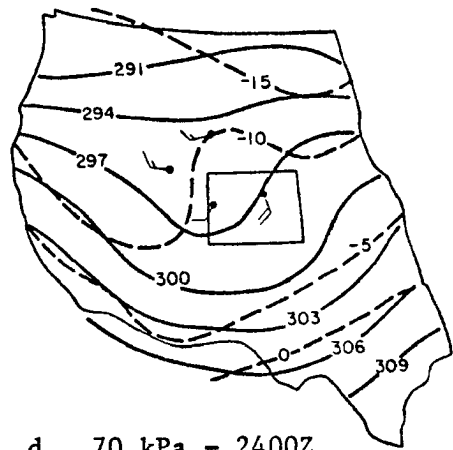
d. 70 kPa - 2400Z
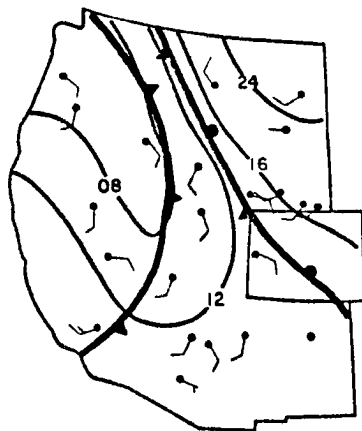
e. Surface - 2312Z
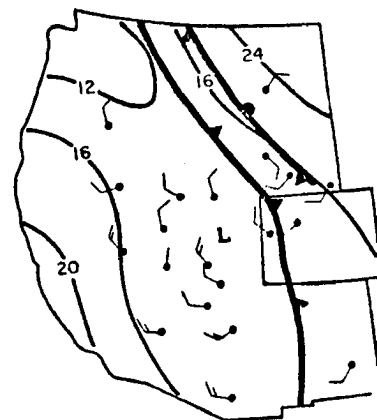
f. Surface - 2400Z

Figure 13. Synoptic Charts for Case Study #2.
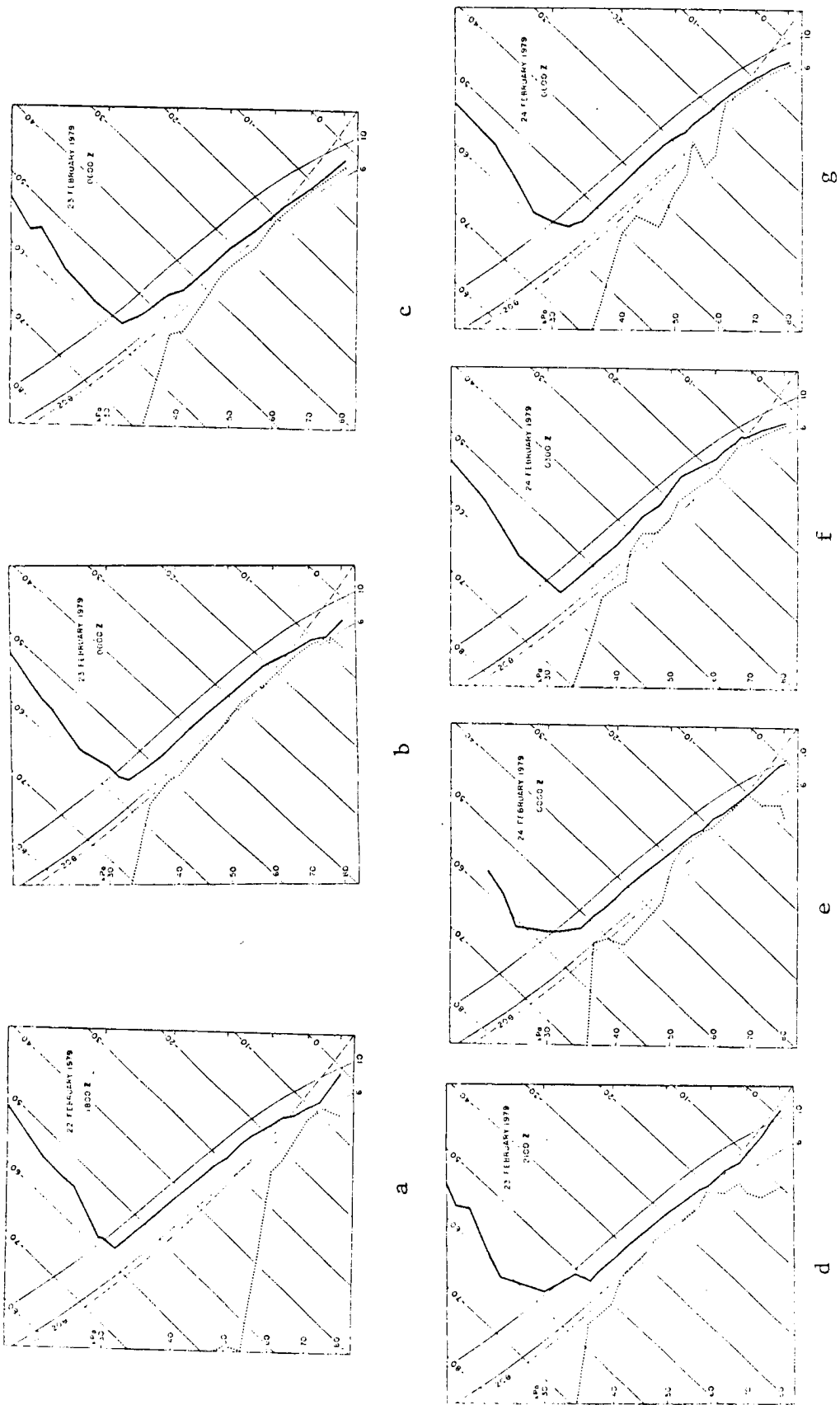
Figure 14. Soundings for Case Study #2.
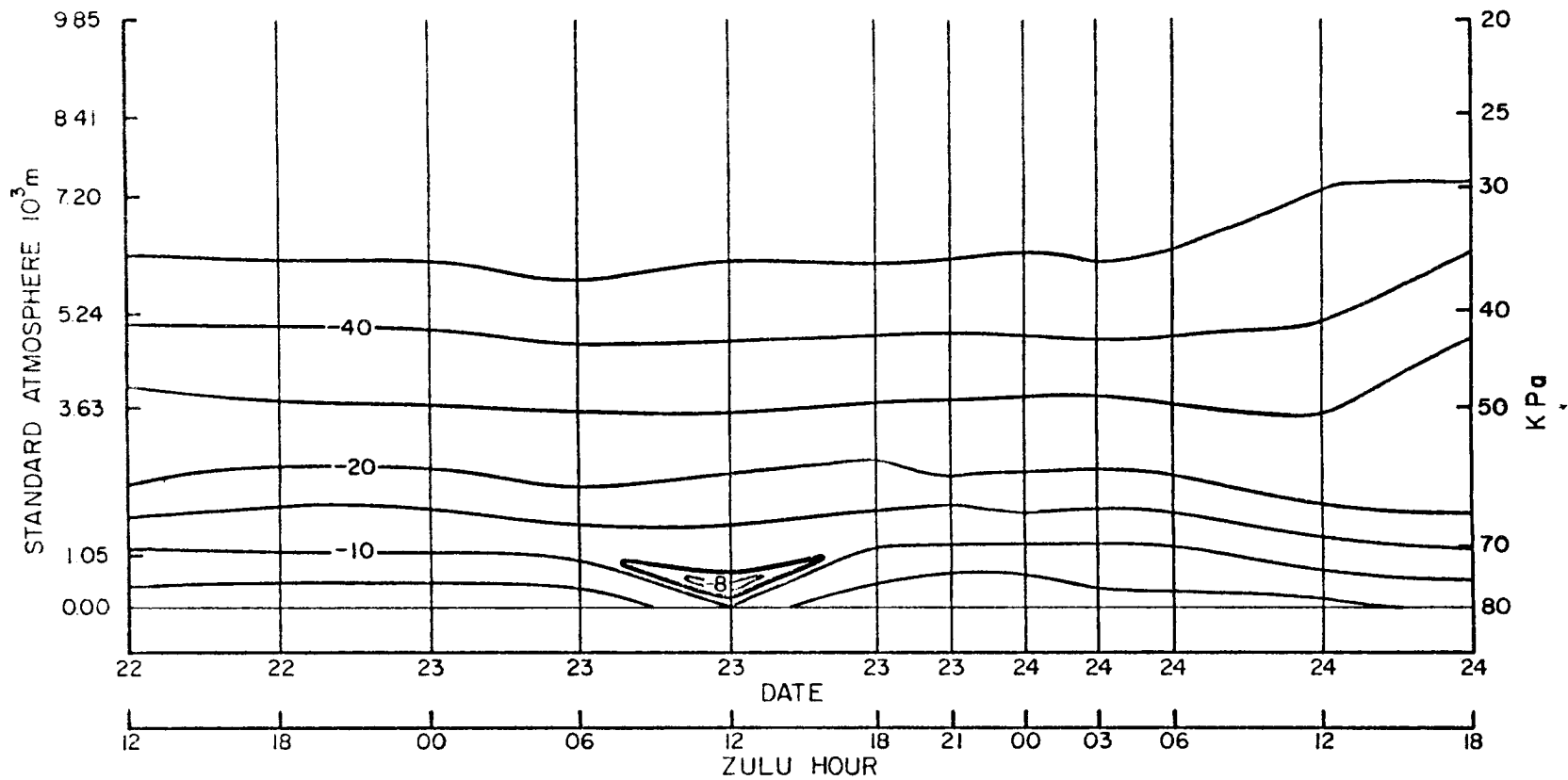
Figure 15. Time Cross-Section Analysis of Temperature for Case Study #2. For temperatures warmer than -20C, temperatures are analyzed every 5°, and for temperatures colder than -20C, temperatures are analyzed every 10°.

47
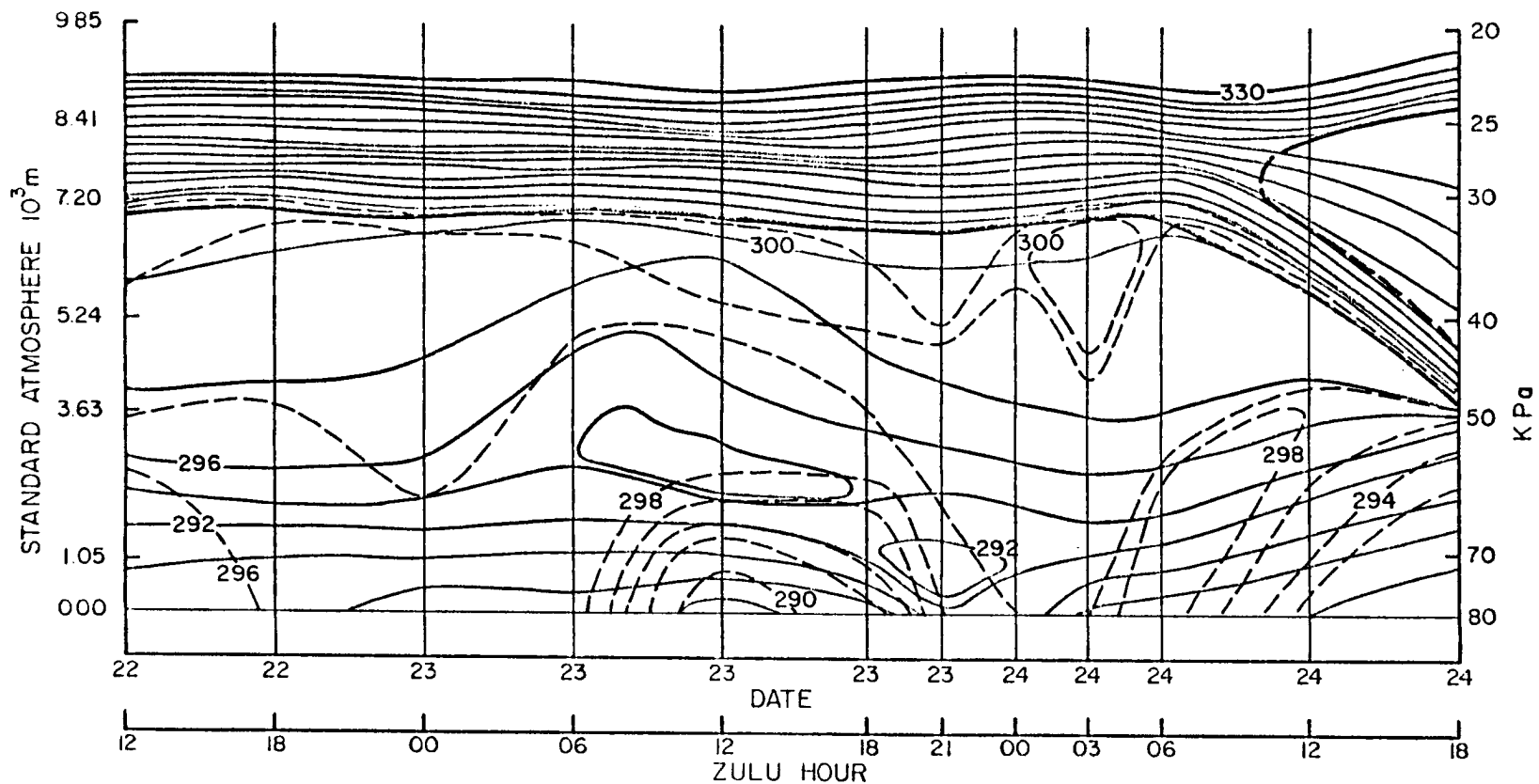
Figure 16. Potential and Equivalent Potential Temperature Time Cross-Section Analyses of Case Study #2. θ (solid lines) and θ$_e$ (dashed lines) have been analyzed every 2°C. Heavy solid lines depict boundaries of stable layers.

the θ_e analysis indicates pronounced weak vertical gradients. The important implications of this observation will be discussed with respect to the convective cloud component that was present within this storm.

Figure 17 illustrates a time section of winds as derived from the Craig rawinsonde data. The 50 kPa and 70 kPa winds reflected the long wave passage. They backed in time as the trough approached and then veered sharply soon after the passage. The lower level winds, however, were light and variable and produced a blocking condition as the disturbance passed. At approximately 2400Z, the storm track gave rise to winds that had strong southwesterly components and were unable to funnel efficiently into the west end of the Yampa valley. This contributed to the stagnation. The blocking between 2300Z and 2318Z, however, was produced by a local down valley drainage flow which gave rise to surface winds with easterly or northeasterly components. This fact was substantiated by rawinsonde data in that a valley inversion formed in conjunction with cooling of the temperature fields in time. Down valley drainage also explains the extreme depth of the blocked layer at 2312Z. In fact, several mesonet wind stations in the valley near Milner substantiated down valley flow between 2300Z and 2406Z. These observations strengthen the arguments for this diurnal valley airflow and cold air pooling which contributed to the extensive blocking prior to this storm passage.

Figure 18 shows the analyzed, upwind ice-saturated cloud. The moisture was advected into the area at relatively low levels. Note that the cloud deck thinned as slight synoptic scale ridging occurred between the pre-2212Z short wave and the primary 2400Z long wave trough
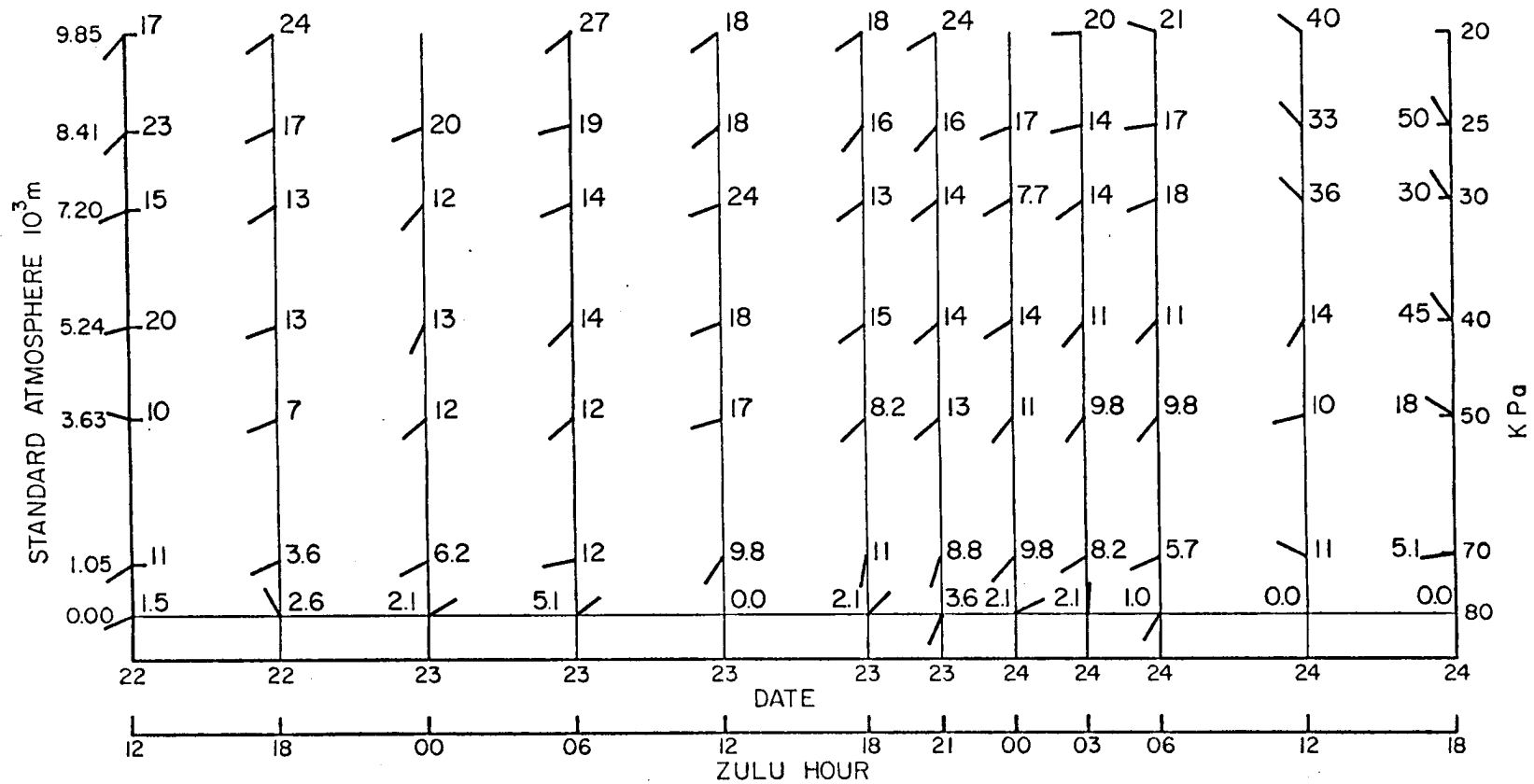
Figure 17. Time cross-section analysis of wind direction and wind speed of Cast Study #2. Wind speeds are in m/sec.
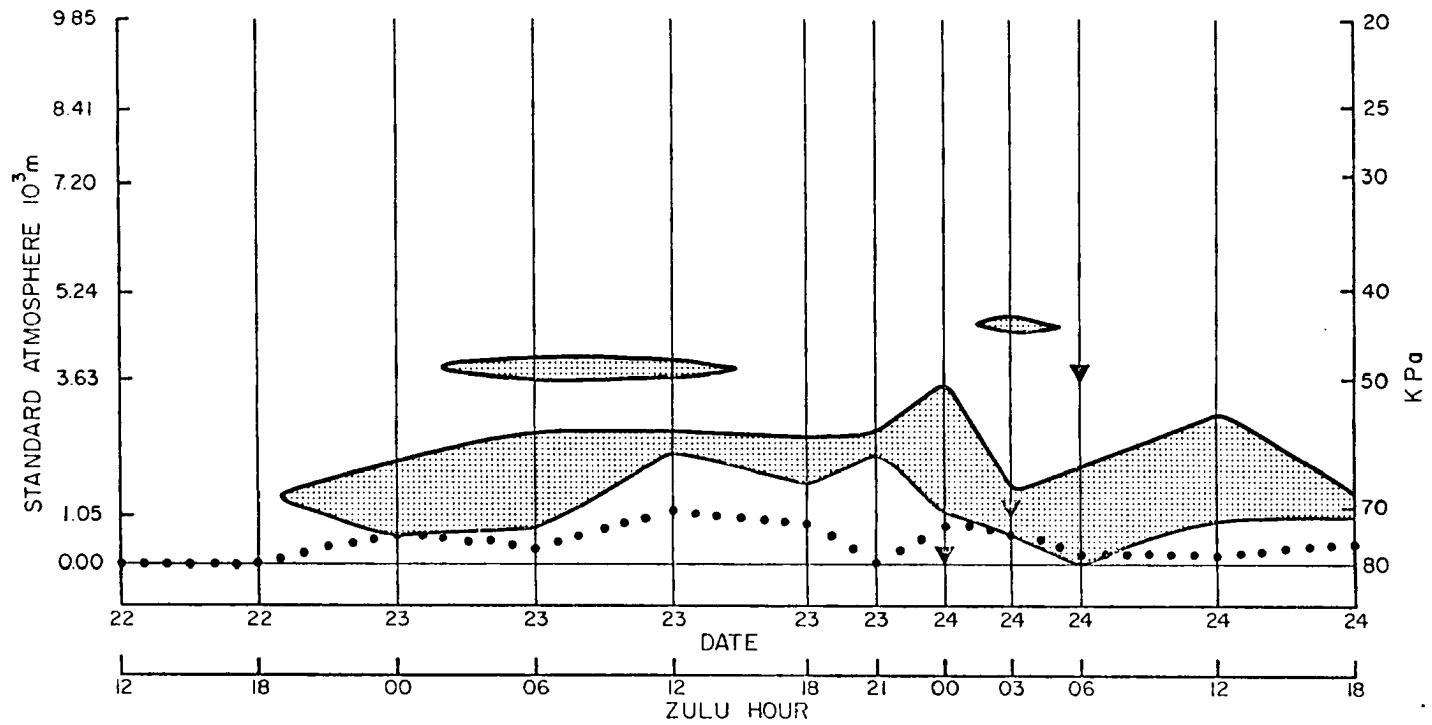
Figure 18. Time cross-section analysis of the synoptic cloud component of Case Study #2. The stippled area depicts the upwind, non-lifted synoptic cloud component. The area between the surface, 80 kPa, and the solid dots depicts the blocked layer. Triangles indicate trough passage at the surface, 70 kPa, and 80 kPa.

passage. This low level moisture preceded the primary 2400Z trough to such an extent that it was almost advected into the first, pre-2212Z short wave. Consequently, the synoptic and lifted cloud components persisted many hours. As the primary trough passed, the synoptic cloud thickened and dropped. The post-frontal synoptic cloud remained for many hours before it began to dissipate.

The analysis in Figure 18 also suggests the presence of cirrus above the primary synoptic cloud mass. If cirrus crystals were falling from the upper layer, they may have supplied secondary ice crystals to the lower cloud layer. There is however, no guarantee that cirrus ice crystals existed, only that the air was saturated with respect to ice. Assuming a crystal fall speed of 0.5 m/sec and mean wind speeds of 12 and 14 m/sec, from Figure 17, the crystals would have travelled to the lower cloud mass 23 and 34 km downwind from Craig, respectively. This means that the crystals could have entered the lower cloud mass over Milner, well ahead of the main barrier. From this point, they could have easily been injected into the orographic cloud system. This secondary source of ice crystals has important ramifications upon the seedability of this storm event.

Figure 19a shows a synthesization of the cloud system which formed over the Park Range barrier. A pure orographic component formed as a result of sub-ice saturated air being lifted to water saturation before the upwind cloud formed because of the moisture and lifting that was present.[4] Around 2312Z, the cloud system thinned to mid levels as a

---

[4]See the definition of orographically forced ice and water saturated clouds in section 2.3.
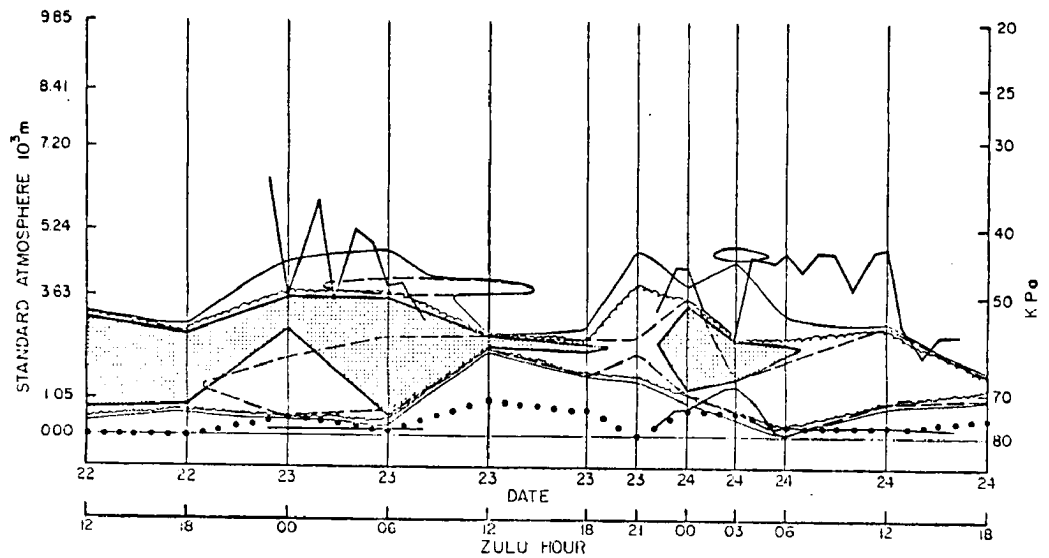
Figure 19a. Time Cross-Section Analysis of the Composite Cloud System of Case Study #2. The area within the dashed line depicts the upwind, non-lifted cloud. The area within the thin solid line depicts the lifted, ice-saturated cloud. The area within the convoluted line depicts the lifted, water-saturated cloud. The area within the heavy solid line depicts the radar observed cloud. The stippled area depicts the convective cloud component, θ_e, decreasing with height in a water-saturated layer. The area between the surface, 80 kPa, and the solid dots depicts the blocked layer.
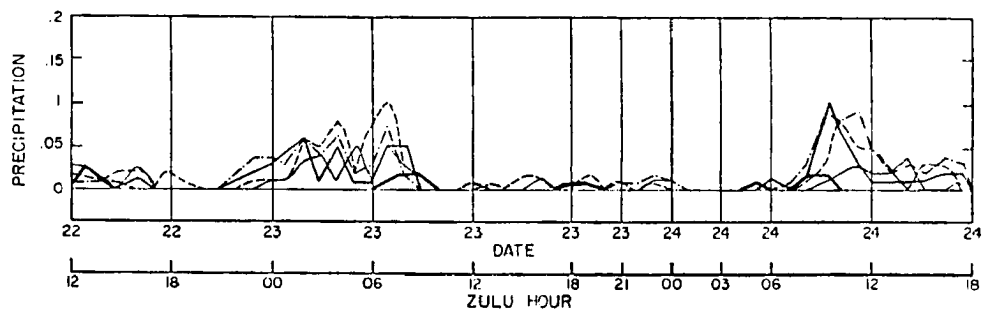
Figure 19b. Time Plot of the Hourly Precipitation at Various Points Across the Park Range Barrier for Case Study #2. The heavy solid line (———) corresponds to Priest Creek. The dotted-dashed line (—.—) corresponds to False Top. The medium solid line (———) corresponds to the Picnic Area. The dashed line (— — —) corresponds to Highway Camp. The thin solid line (———) corresponds to Columbine Lodge.

result of synoptic ridging which evaporated moisture by subsiding air and increased the blocking, which reduced the lift. In general, there was adequate moisture present throughout this storm to produce a substantial cloud but the amount of blocking severely decreased the amount of lift and, consequently, decreased the extent of the cloud system. As the primary long wave approached, the cloud thickened and the cloud base dropped below ridge top. After the disturbance passed, the postfrontal moisture was topographically lifted to water saturation for many hours until the moisture supply was cut off.

The convective component was very prominent in the early portions of the storm system from 2212Z to 2312Z, as was previously suggested in the time cross-section analysis of θ_e in Figure 16 and is shown in Figure 20. The major contributor to this instability consisted of a lapse rate which was nearly or slightly more than the moist adiabatic value in the lower levels. At higher levels, however, the moisture gradient effect increased the extent of the potential convective instability, making it deeper than it would otherwise have been if the lapse rate effect alone had been considered. As a consequence of lifting and saturation, the potential instability was realized as the convective component. This instability, in general, was either caused by cold air advection associated with the short wave which passed prior to 2212Z, or vorticity advection associated with the development of the primary wave before it passed at 2400Z. Without a detailed analysis of the pre-2212Z wave passage, it is difficult to determine exactly how the potential instability formed at this time (this trough passage was not analyzed due to the fact that rawinsonde data was not gathered with sufficient time resolution for it to be included in this case study).

An analysis of the thermodynamic diagrams revealed very little, if any, positive energy area which could support convection. The 2306Z sounding was the most unstable sounding at this time. Yet, the temperature difference between a moist adiabatically ascending parcel and the environmental temperature remained within one half of one degree Celsius. With the effects of entrainment, the sounding dries slightly above 60 kPa, strong convective motions as a result of instability and orographic lifting alone could not have been supported in this environment (see Figure 14b).

Between 2218Z and 2306Z, the depth of the convective component was reduced. Figure 20 illustrates the θ_e profiles from 2212Z, 2300Z, and 2306Z. The θ_e profiles indicate a fluctuation of θ_e with height, in time, which caused the potential instability first to disappear and then to reappear. The 2218Z sounding shows a conditionally unstable lapse rate below 73.3 kPa and a nearly moist adiabatic lapse rate from 73.3 to 66.5 kPa. The relative moisture gradient in the upper layer was such that it forced the θ_e profile to decrease with height. Hence, a large degree of potential instability was present throughout the lower levels of the 2218Z sounding. The 2300Z sounding shows a similar stability in the lowest layers as the 2218Z sounding did. Now, however, the relative moisture increased with height just above the surface. This cancelled the potential instability created by the lapse rate so that the net θ_e gradient with height was positive to neutral. Above this point, 74.8 kPa, moisture advection and a slight lapse rate decrease occurred in time. This reduced the effects of the moisture gradient which destabilized this layer before. By 2306Z, the moisture was still present, but the lapse rate had once again increased such
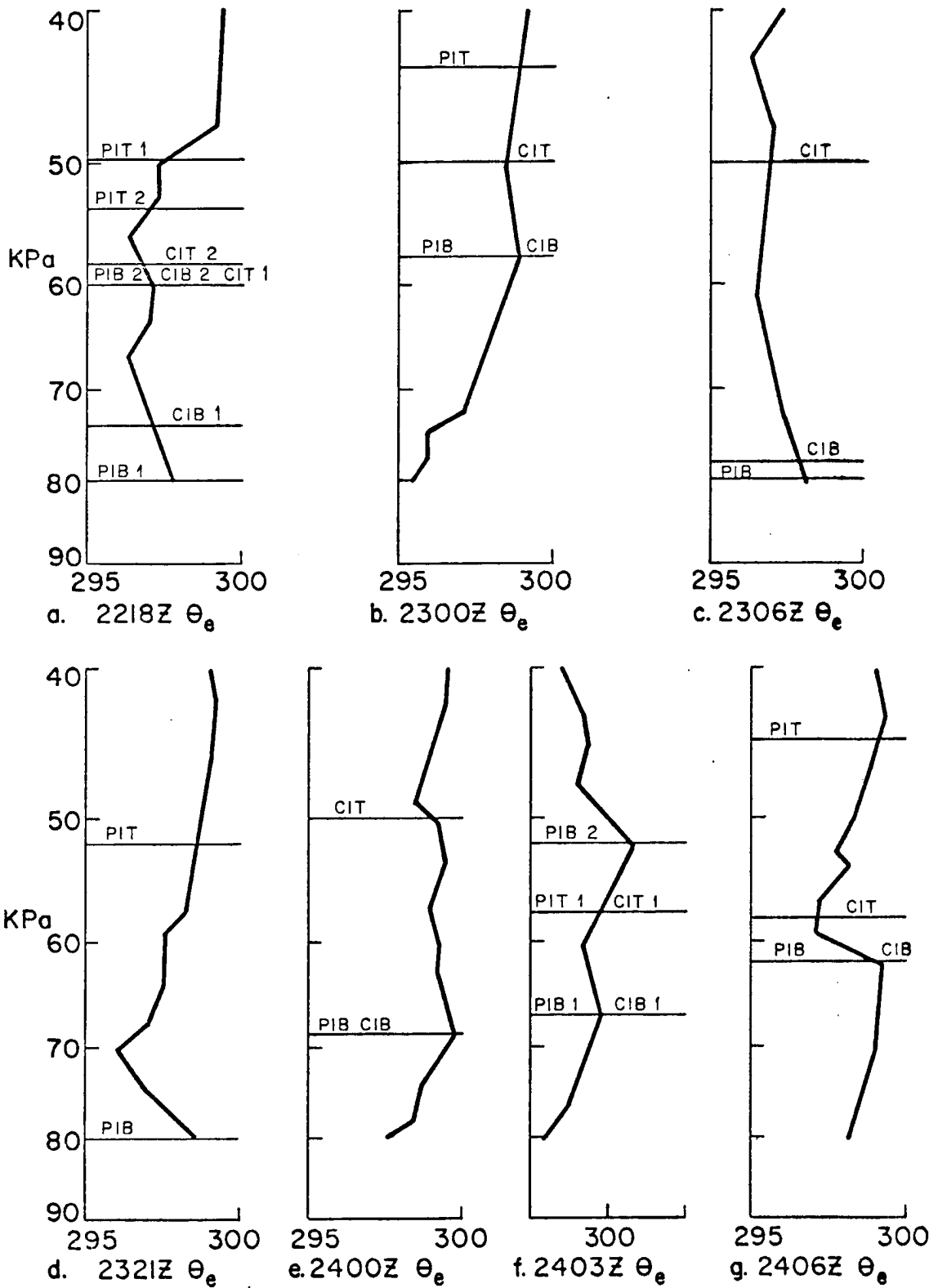
Figure 20. Convective cloud components of Case Study #2.

that it was slightly unstable with respect to the moist adiabatic value. The change of the θ_e vertical profiles in time explains how the potential convective instability varied in time. The instability could be realized only if the air was lifted to saturation, as is analyzed in the time section of Figure 19a. An examination of the vorticity fields associated with this portion of the storm reveals that two vorticity maxima were advected over the study area around 2218Z and 2306Z, respectively, while negative vorticity advection occurred between these two times. The vorticity advection may have affected the moisture and temperature profiles which, in turn, changed the potential instability. These vorticity fields must, however, have been associated with the first, unanalyzed, pre-2212Z short wave.

At the time of frontal passage, around 2400Z, the vertical velocity component that contributed to the complete cloud system through a release of convective, potential instability was generated by a lapse rate which was slightly unstable with respect to the moist adiabatic value. In fact, the unstable lapse rate was present 12 hours before 2400Z, but a relative moisture increase with height prohibited $\partial \theta_e / \partial Z$ from being less than 0. Consequently, the potential instability did not form. By 2400Z, moisture advection had taken place and the potential instability formed. Orographic lifting then provided the saturation necessary for the instability to be realized. In the 2400Z and 2406Z soundings, a sharp relative moisture decrease with height contributed to the instability (see Figure 20). The form that the instability took in time was very similar to the previous short wave case study and was not directly associated with the large scale post-frontal cold air advection at upper levels. As the disturbance passed, the soundings cooled uniformly

throughout the post-trough period. Destabilization corresponded to the disturbance passage, but in this case, a warming at or just above 70 kPa seemed to create the instability. After the wave had passed, the convective component disappeared and a stable cloud system was indicated by the analysis. Radar observations, however, do not verify this conclusion drawn from the analysis as will be shown.

At first glance, the analysis in Figure 19a appears not to agree very well with the Ku determined cloud tops. Since none of the analyzed cloud tops were appreciably above 40 kPa, an erroneously determined cloud top advected from an upwind synoptic analysis could not have contributed to cloud top discrepancies during this storm. Still, ice-saturated air may not represent a cloud, but more confidence can be placed in the analysis in that a cloud is present when the ice-saturated cloud top is near to the water-saturated cloud top. The analysis shows, however, that a large degree of convective potential instability was present and released between 2212Z and 2306Z. As mentioned before, however, parcel instability analysis indicated that the environment could not have supported strong vigorous convective motions at this time.

Figure 21 illustrates the Ku radar profile for this storm. As can be seen, the radar observed cloud was cellular with zones of higher reflectivity embedded in the cloud mass which seemed to pass over the radar in time. It is tempting to attribute these zones of higher reflectivity to a phenomena similar to the convective bands observed in California (Elliott and Hovind, 1964). Determinations of "zone" width and the distance between the "zones", using the mean wind speed in the layer, revealed dimensions similar to those observed in California (band width = 72 km, distance between bands = 99 km). A satellite
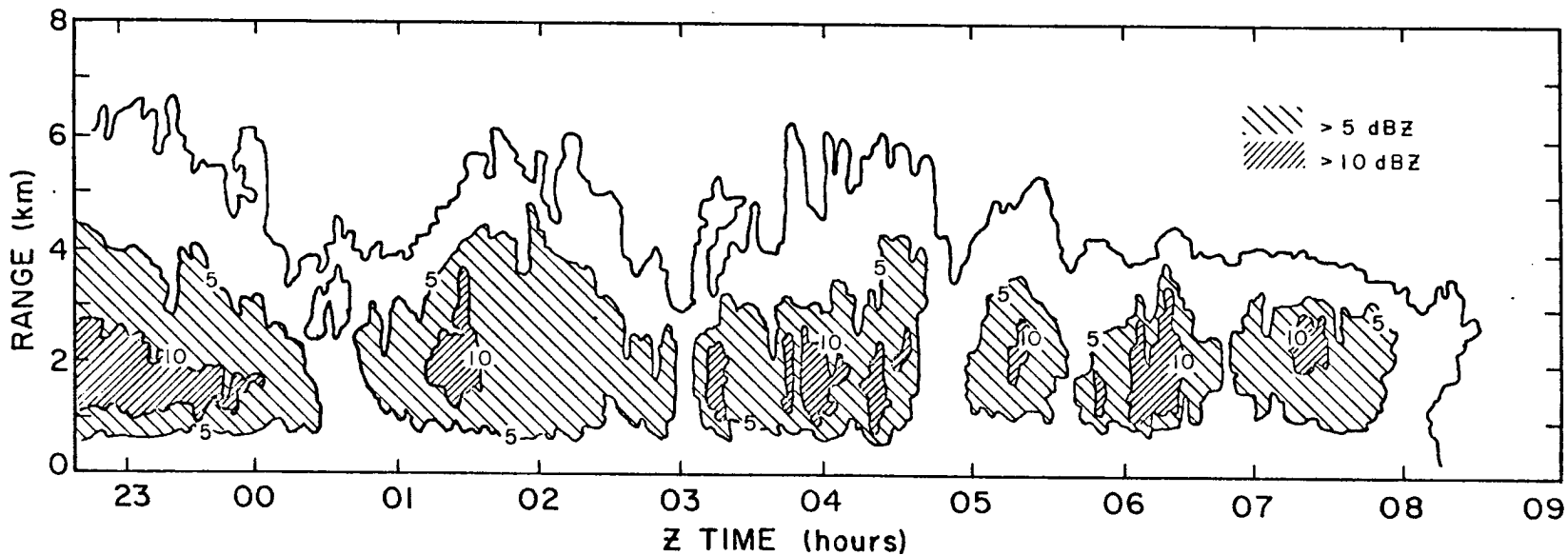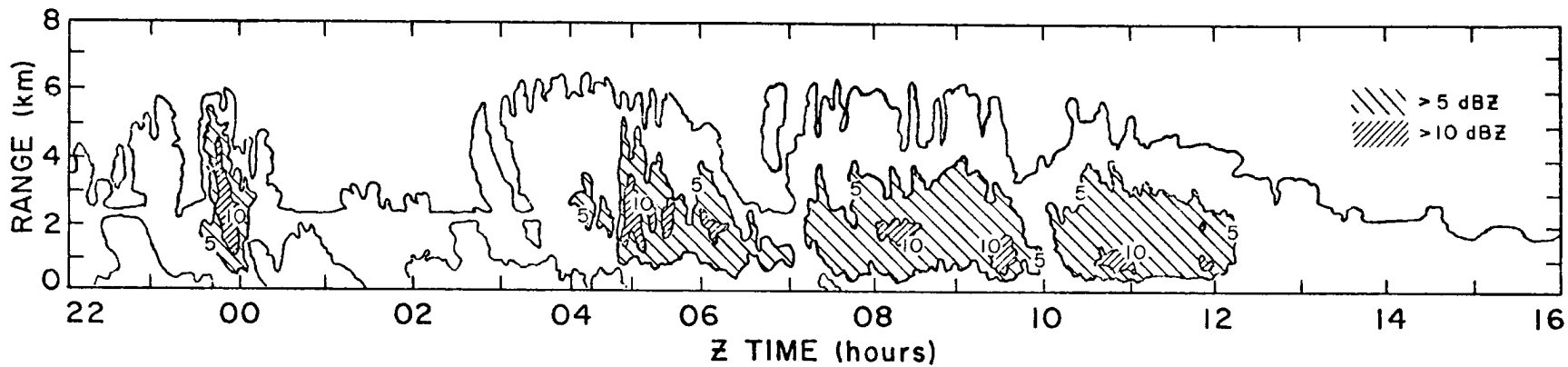
Figure 21. Ku band radar reflectivities of Case Study #2. The top figure begins at 22Z on the 23rd while the bottom figure begins near 23Z on the 23rd.

photograph, however, taken around 00Z on the 23rd did not reveal vigorous "convective bands". There did seem to be a smaller scale organization of several cloud lines, however, oriented from the northwest to southeast over northwestern Colorado (these could not have been orographic clouds oriented along the mountains because the mountains lie mostly north-south in this area of the state). It is hypothesized here that the zones of higher radar reflectivities could have been caused by a propagating mesoscale gravity wave (Lindzen and Tung, 1976; Houze, et al., 1976). This hypothesis explains the "banded structure" suggested by the zones of high reflectivity as well as the cellular nature of the radar observations. This same type of "banded structure" was observed in the Park Range area by Rhea, et al., (1969) and in the central Rockies by Furman (1967). The continuous precipitation record during this early storm period indicates several "pulses" of precipitation which may have corresponded to the high reflectivity zones observed by the radar (see also Marwitz, 1980; Cooper and Saunders, 1980).

The high radar reflectivities and convective instability release during this storm were not as easily linked to the crystals growing in the dendritic growth region. The -15°C isotherm averaged near 62 kPa but the instability was so deep in this area, that it was difficult to conclude that the crystals were falling from an area of convective instability release into the dendritic growth region, -14°C to -17°C.

Cloud top determinations from the rawinsonde analysis and the radar observations during the first unstable period between 2212Z and 2304Z were in good agreement at sounding times. Between the rawinsonde launch times, where the analysis was linearly interpolated in time, the radar observed cloud tops were highly variable and cellular in nature and did

not agree well with the rawinsonde analysis (see Figure 19a). This illustrates the importance of serial rawinsonde launches. One launch every three hours is reasonable in light of field operations and analysis requirements. In the sense of detecting cloud tops and convective instability at sounding times, the analysis, during this period, was successful.

In general, the radar cloud top determinations at 2400Z and 2403Z tended to agree with the analysis; while at 2406Z and 2412Z, there was disagreement. Beyond 2403Z, the radar indicated much higher tops than the analysis. Part of this discrepancy may be due to the interpolation problem and part may be due to the inability of the analysis to illustrate convective cloud tops. If higher cloud tops and a greater area of convective instability had been analyzed at 2406Z, along with a positive energy area which could support convective motions, the disagreement would have been less. In fact, Figure 20 shows a large degree of potential instability above 62 kPa, but Figure 14g indicates that with lifting only a very little amount of positive energy area could have been generated (this is an extremely borderline situation). Three possible explanations for the disagreement between the two cloud top evaluations beyond 2403Z can be advanced. First, the lifting model may be unable to simulate the orographic lift which actually saturated the air from 62 kPa to 54 kPa. In this case, cloud tops would have been raised and potential instability which existed between 62 kPa and 45 kPa would have been realized and the slightly positive area between 60 and 55 kPa could have contributed some convective motions to the cloud system. Second, the large degree of instability, a decrease with θ_e of nearly two degrees, was released as analyzed between 62 and 58 kPa.

Given the support of an existing positive energy area or the generation of such an area through lifting, the instability realization may have set off strong convective activity which would have then penetrated to higher and higher levels. A positive energy area could have been generated as the 68 to 52 kPa layer was lifted to saturation and the lapse rate forced past the saturated adiabatic value. As this occurred, air above 58 kPa would have become saturated and more convective instability would have been released. This process would have continued until the rising elements could have no longer saturated the air or the potential instability was no longer realized. (Note that the potential instability tops were near 45 kPa as was the observed radar tops.) No significant positive energy area was present, but the lifting and saturation of the 62 kPa to 58 kPa layer may, indeed, have tipped the lapse rate past the moist adiabatic value and generated a small area of positive energy.

A third explanation may also be advanced to explain the discrepancy between the analysis and radar observations since zones of higher reflectivity were present within the Ku band radar data (see Figure 21). As before, the cloud system may have been invigorated by a moving mesoscale gravity wave. These gravity waves may have been associated with the synoptic scale weather system or they may have been generated by mountains upwind of the Park Range. Unfortunately, no useable satellite data were available at this time.

Once again, an alternate lifting model was tested for this unstable storm event. The primary lift was apportioned linearly between the surface and 30 kPa, as before, in order to relax the condition that streamline displacement should decrease with height. This was done primarily

to test if higher levels of the soundings would become saturated by an
orographic lift that was not so severely restricted by stability. The
newly derived orographic and convective cloud components at times over-
estimated the cloud tops of the first analysis by no more than 5 kPa.
This indicates that stability plays an important role in controlling
the orographic airflow. Also, the temperature and moisture profiles
determine, to a large degree, how the derived cloud depth behaves under
different lifting models. For example, a strong subsidence inversion
at mid-levels will generate similar cloud top altitudes regardless of
the lifting model. On the other hand, a cloud top determination from a
sounding characterized by a slow increase of dewpoint depression with
height will be very sensitive to the lifting model employed.

Figure 19b shows the precipitation associated with this storm
event. Substantial precipitation fell at the higher elevations during
two separate periods, 2300Z to 2309Z and 2406Z to 2418Z, while precipi-
tation at Priest Creek, which is the most westerly station at the top of
the ridge, remained light and variable throughout the entire case study
period. Clearly, the period from 2406Z to 2418Z was associated with
the frontal passage. The highest precipitation amounts occurred early
in the storm period and then tapered off in time.

During the period 2300Z to 2309Z, however, a frontal passage did
not take place. A deep orographic cloud was established and a consider-
able amount of potential convective instability was realized. The three
cloud components combined to initiate significant precipitation at this
time. The continuous precipitation records indicated several "pulses"
of precipitation during this first period. The post-frontal continuous
precipitation records, however, did not reveal a similar observation.

When ridging occurred between the two wave passages, the precipitation and the cloud system decreased significantly.

Once again visual observations contributed to the interpretation of the rawinsonde analysis presented in Figure 19a. At 1600Z on the 22nd, skies were broken to clear in the Yampa Valley to the west and clouds were covering half the ridge that lies to the east of Steamboat Springs. Snow began falling at 2255Z on the 22nd at Steamboat Springs. At 1841Z on the 23rd, a few puffy cells of scattered cumulus were forming over the mountains as observed from the aircraft. The ceiling lowered over the ski area at 2250Z on the 23rd. Ten minutes later, a brief snow shower was reported at Steamboat Springs. At 2333Z on the 23rd, the top of the clouds in the Steamboat Springs vicinity were reported as being cumuliform while to the west in the valley, several stratiform decks appeared higher than the cumulus deck at Steamboat Springs. Twenty minutes later, the ceiling over thePark Range was noticeably lower and fairly thick while the cloud deck to the west was broken. Light intermittent snow continued to fall through 18Z on the 24th. After this time, these clouds dissipated. Further detailed visual observations can be found for this case study in Appendix B.

3.2.1 The Main Findings of the Second Case Study

This second case study reveals important similarities as well as differences between the first two cloud system case studies.

1) The T, θ, and θ_e fields indicated cooling after the frontal passage.

2) These thermodynamic gradients were not nearly as strong as in the previous short wave case study.

3) The synoptic cloud component formed and fluctuated in time as the moisture and vorticity advection varied.

4) The synoptic cloud component thickened and cloud bases dropped in response to the trough passage.

5) The synoptic storm track forced upper airflow from the southwest.

6) The moisture tended to move in at lower levels rather than at higher levels.

7) Upper portions of the general synoptic cloud mass may have been "seeded" by ice crystals falling from a high cirrus layer. If ice crystals were indeed falling from this upper cirrus layer, the crystal trajectories may have been such that they fell into the cloud mass well ahead of the main barrier and were introduced into the existing orographic cloud system.

8) The 50 kPa and 70 kPa winds were out of the southwest around 2400Z which tended to cause a stagnation in the valley upwind of the main barrier. Stagnation reduced the amount of lift and, as a result, the extent of the orographic cloud.

9) According to T, θ, and θ_e analyses, rawinsonde data, and surface micromet station data, blocking was caused by cold air pooling, down valley airflow and the formation of a valley inversion during the nighttime hours around 2312Z.

10) The ridge top cloud system quickly thickened and cloud base dropped prior to the trough passage. Therefore, the composite cloud may have been invigorated by the synoptic disturbance as it brought more moisture into the system.

11) A pure orographic cloud did form when no upwind synoptic cloud was analyzed early in the storm period.

12) The convective component, prior to the 2400Z trough passage, formed in response to slight instability with respect to the moist adiabatic lapse rate and moisture gradients.

13) The realization of the potential instability prior to 2400Z may have been caused by voriticity advection and the lifting of moist air to saturation. Radar data indicated the passage of zones of high radar reflectivity during this period and was supported by continuous precipitation records. This invigoration of the cloud system may have been due to the passage of a mesoscale gravity wave.

14) A convective component formed in conjunction with the 2400Z frontal passage. As in the first short wave case, the instability was not a direct consequence of the frontal passage and large scale post-frontal advection.

15) Potential instability was created by small scale temperature and moisture perturbations which forced lapse rates that were nearly moist adiabatic to become greater than this value. The potential instability was then released by orographic lifting and saturation.

16) In the period after 2400Z, the composite cloud may have been invigorated by a) saturation of potentially unstable layers by an orographic lift which was not as severely restricted by airmass stability, b) the release of convective activity which saturated higher layers which in turn released more convective instability, and c) a travelling mesoscale gravity wave.

17) There was some suggestion in the precipitation record that at times, a variable convective precipitation component existed.

3.2.2 Important Conclusions from Case Study #2

Again, in this second case study, the lifting model was very important in determining the lifted cloud under certain conditions of moisture and temperature. At this time, the sensitivity of the lifting model not only affected the depth of the "orographic component", but it also had important ramifications upon the convective component.

Physical processes, however, which complicated the details of the lift are seen to be of even greater importance because of their impact upon the streamline displacement. The physical mechanism which has the strongest impact upon the orographic lift is blocking. The stagnation of air upwind of the mountain barrier helps to determine the primary lift, that streamline displacement which determines the lift at upper levels. As was shown, blocking did occur in the Yampa Valley upwind of the Park Range and, therefore, strongly affected the analysis. To ignore this physical process may bring about serious errors in the resulting analysis and interpretation. This blocking phenomena, to some degree, depends on the local topography immediately upwind of the main ridge. The Yampa Valley seems conducive to blocking. This is reflected in the surface wind observations and the rawinsonde data. Strong temperature stratification in the lower layers also contributed to blocking and stagnation.

A second important finding of the second case study was that even after all the proposed cloud components were taken into account, there were still discrepancies between the analysis and the observations. Some evidence pointed to the fact that the cloud system could have been invigorated by a moving mesoscale gravity wave. Whether the discrepancy was due to a gravity wave or some other type of moving mesoscale

phenomena imbedded within the synoptic wave, the proposed explanation

indicates that the analysis was correct to the first order of magnitude.

If this is indeed the case, a fourth cloud component may be present

within this storm, i.e., a cloud component associated with the detailed

mesoscale structure of the synoptic wave.

3.3 Case Study #3

December 21 14Z → December 23 14Z 1979

The third case study analysis was performed on a cutoff low which

strongly affected the area of study. Aloft, the winds became easterly

which greatly complicated the analysis. There are several reasons,

however, to attempt an analysis of this complicated system: i) the

final results can be compared to the other two case studies to provide

insight into the analysis techniques employed, ii) important facts may

be revealed about these cutoff synoptic circulations, and iii) these

storms do occur and are as important as one of the weather patterns

that affects snowfall in the area.

At 2212Z, two cold fronts were positioned to the west of the study

area (Note that 2212Z and all other such designations within the text

indicate a day and hour, e.g., 12Z on the 22nd. This is due to the fact

that all rawinsonde observations were taken on the hour. Such a time

designation provides for a short hand notation in referring to events

within the case studies). The primary front was located in central

Nevada and extended back to central California while a secondary front

lie along the Washington-Oregon coast. In time, the primary front

formed a strong surface low pressure center in central Utah by 2200Z.

By 2212Z, the low had drifted, almost over the study area to the

east-southeast and deepened in southeast Colorado. As the primary sur-
face disturbance moved eastward, the secondary cold front shifted to
the east. By 2212Z, it was located in Utah oriented north to south.
By 2300Z, the secondary front had drifted towards western Colorado,
weakened, and was not analyzed on this 00Z surface map (see Figures
22a-h).

At 70 kPa, the synoptic analysis revealed that at 2212Z, a long
wave trough had dug down to south central Nevada, oriented north-south,
while its upper portions lagged along the Washington-Oregon coast.
By 2212Z, a deep long wave trough with its southern portions over
Arizona and New Mexico, had formed. The center of the trough exhibited
weak height gradients while the wind fields over the northern Colorado
area suggested cyclonic circulation. By 00Z on the 23rd, a closed low
had formed at 70 kPa over western Kansas. At 50 kPa, the synoptic
analysis showed that at 2212Z a cutoff low had formed over the Texas
panhandle. This circulation was evident even in northwestern Colorado.
From this time on, the cutoff low at 50 kPa moved first to the north
and then to the northeast. This general motion at 50 kPa was coinci-
dent with the formation of a long wave at 70 kPa and a breakdown of the
cutoff low. This wave at 70 kPa extended from northern New Mexico to
Michigan. As this wave was established by 2312Z, a ridge built to the
west of the 70 kPa trough from southern California to Montana. The
important features of this atmospheric disturbance are: 1) the time
and position of the surface low pressure center as it moved past the
study area, and 2) the formation and movement of the upper level cutoff
low (see Figures 22a-h).
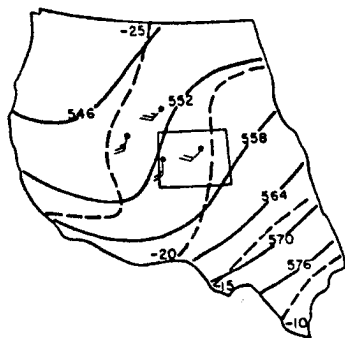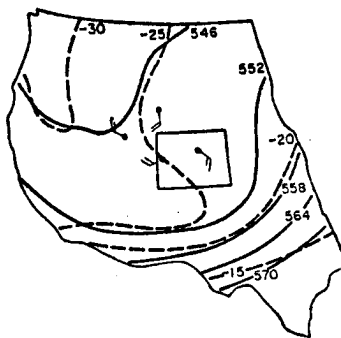
a. 50 kPa – 2200Z b. 50 kPa – 2212Z c. 50 kPa – 2300Z
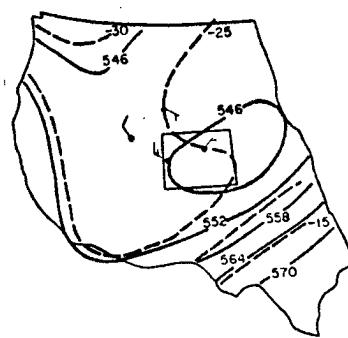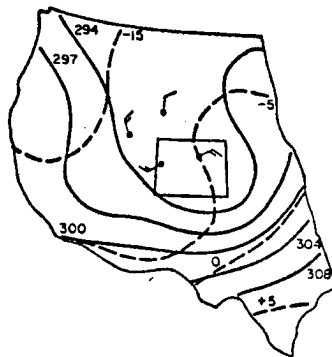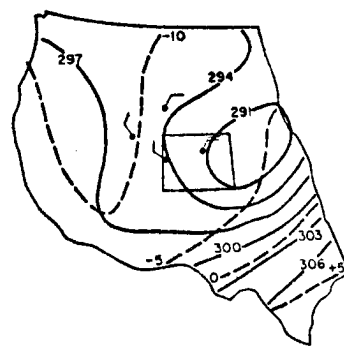
d. 70 kPa – 2212Z e. 70 kPa – 2300Z
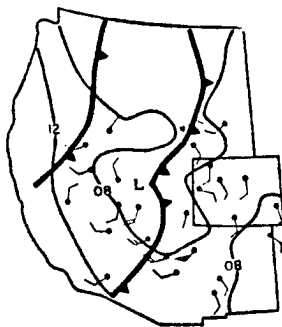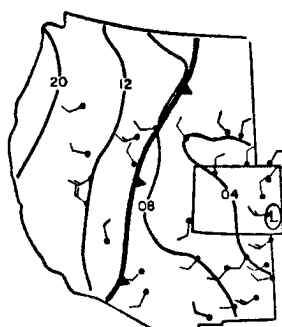
f. Surface – 2200Z g. Surface – 2212Z h. Surface – 2300Z
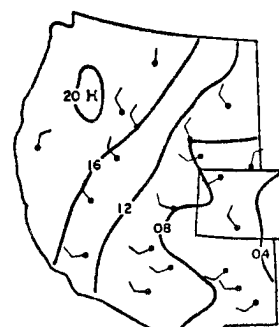
Figure 22. Synoptic Charts for Case Study #3.

Figures 23-24 show the T, θ, and θ$_e$ fields, respectively. They all

indicate that cold air pooling occurred between 2300Z to 2212Z. The

soundings also illustrated the formation of a strong deep valley inver-

sion which points to the cold air pooling at this time. The pooling may

have been associated with the blocking or stagnation flow as in the

previous long wave case study. The surface wind network data did not,

however, clearly substantiate the down valley drainage as before. The

Mount Harris mesonet wind station elevated above the valley floor,

measured an easterly component between 2214Z and 2220Z, but the Milner

site experienced westerly winds. There seems to be no simple connection

between down valley flow and cold air pooling at this time. Cold air

pooling and a valley inversion was suggested by the rawinsonde data;

but these may not have been associated with any valley scale drainage.

The temperature analyses reveals a slow uniform cooling after the

surface and upper level disturbances passed. The θ$_e$ field differs from

the θ field and contains weak gradients at certain times. This implies

the presence of moisture and potential instability as in the second case

study.

Figure 25 illustrates a time section of the winds as observed by

the Craig rawinsonde. Due to the fact that this case study dealt with

a cutoff low aloft, the wind analysis was vital in determining the form

of the cloud system. This storm system can easily be broken into two

wind regimes in the vertical, a lower level westerly flow and an upper

level easterly flow.

Prior to 2215Z, a low level blocking flow was observed. This was

probably controlled by: 1) nighttime cold air pooling as indicated by

the T, θ, and θ$_e$ fields, and 2) a small to zero westerly transbarrier
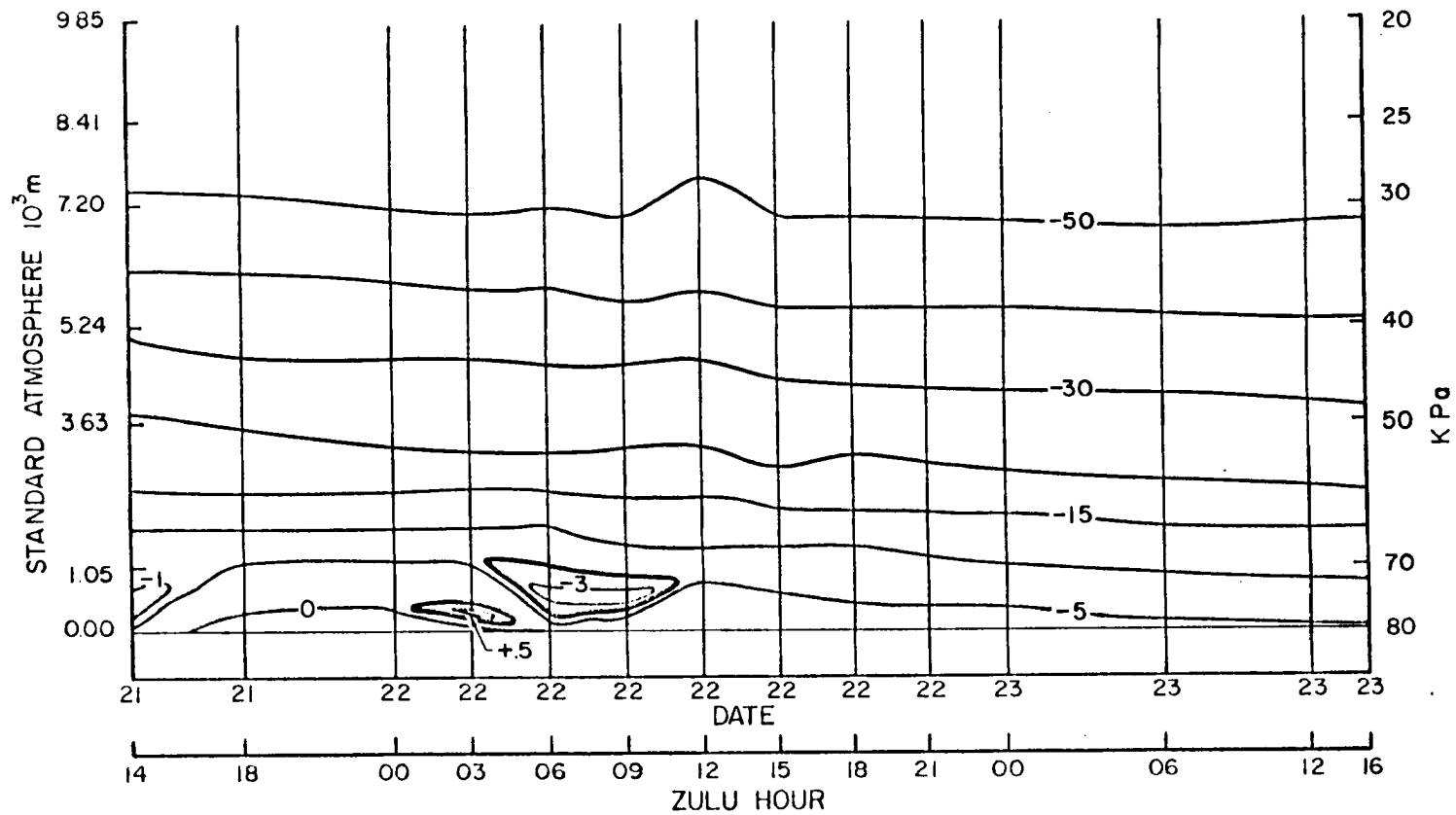
Figure 23. Time Cross-Section Analysis of Temperature for Case Study #3. For temperatures warmer than -20C, temperatures are analyzed every 5°; and, for temperatures colder than -20C, temperatures are analyzed every 10°.

72
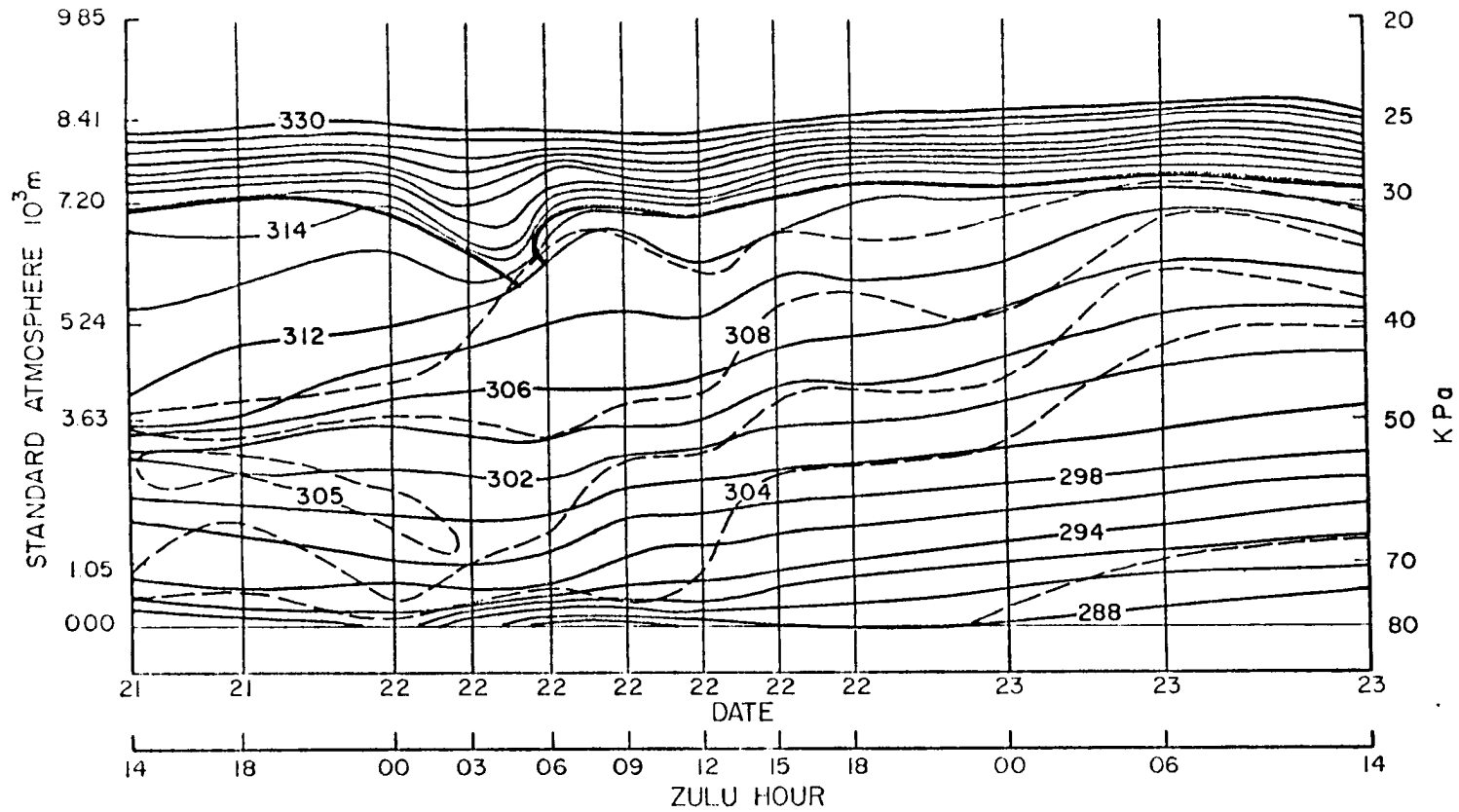
Figure 24. Potential and Equivalent Potential Temperature Time Cross-Section Analysis of Case Study #3. θ (solid lines) and θe (dashed lines) have been analyzed every 2°C. Heavy solid lines depict boundaries of stable layers.

73
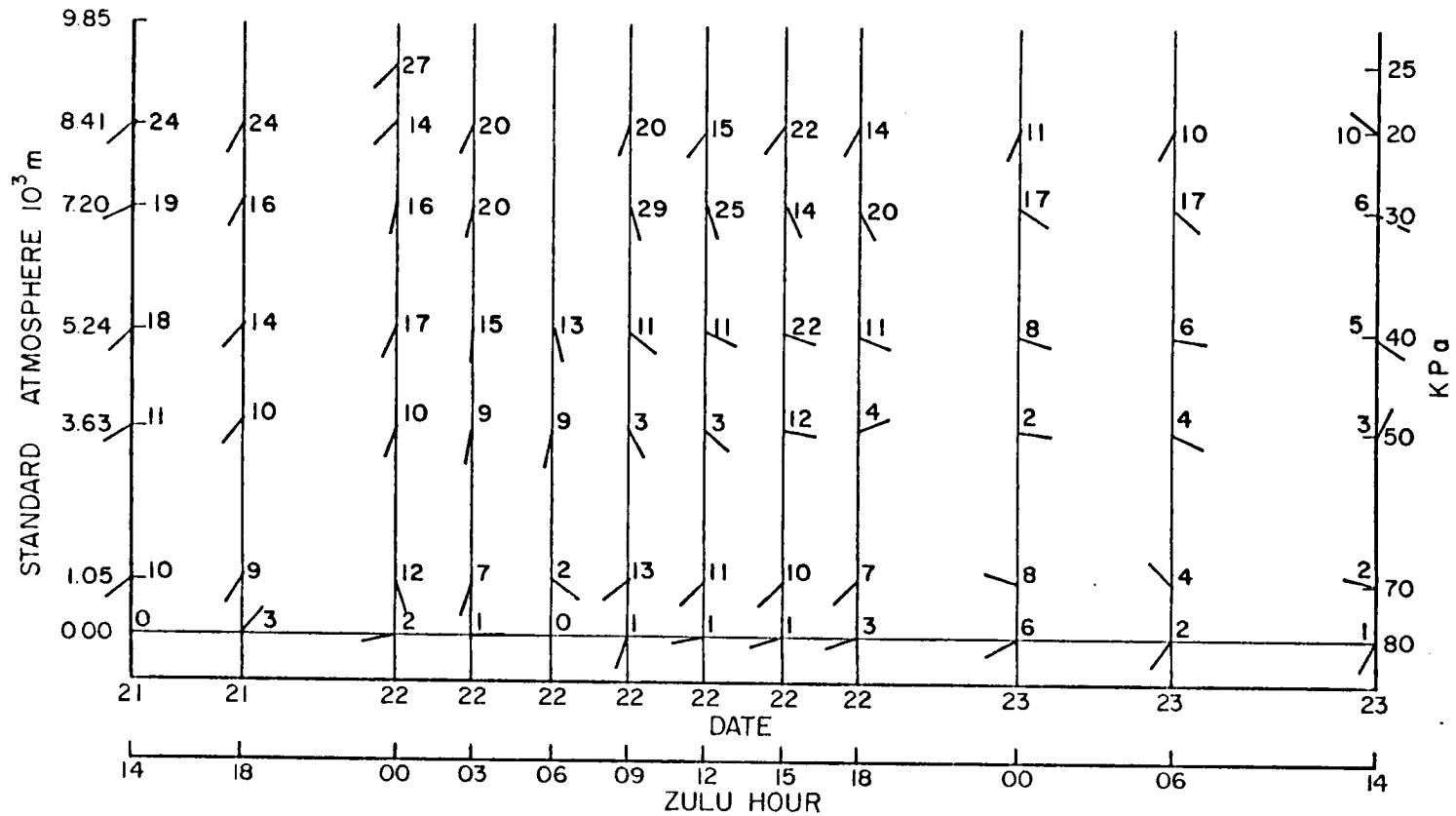
Figure 25. Time Cross-Section Analysis of Wind Direction and Wind Speed of Case Study #3. Wind Speeds are in m/sec.

wind component at 70 kPa. The 70 kPa wind apparently contributed to the stagnation within the valley. When the 70 kPa wind was out of the southwest or south, blocking occurred. When the wind shifted to the west and northwest, the blocking was eliminated. This seems reasonable when the topography of the region is taken into account (see Figure 2). By the veering of the 70 kPa winds in time, a frontal passage was indicated at 2209Z, and the deep blocking reduced and disappeared as the wind shifted to the southwest.

As the blocking or stagnation zone decreased, a low level flow was lifted over the barrier. Also during this time, the synoptic cutoff low formed to the east-southeast of the study area and established an easterly flow regime at upper levels. The upper level winds of the time section clearly illustrate this development. Consequently, after 2209Z, two airflow regimes existed; a low level flow which lifted air from the west to saturation and an upper level flow which could have lifted air from the east to saturation. A thorough understanding of the basic air flow in the vicinity of the main barrier is needed in order to understand the formation of the orographic component.

Figure 26 shows the synoptic cloud component as derived from Craig rawinsonde data.[5] A main body of moisture moved in at high levels beginning at 2200Z. At the time of frontal passage, 2203Z, the moisture remained at upper levels. By the next morning, the post-frontal moisture became evident in the lower levels as the blocking decreased and cloud bases dropped. Moisture, which was indicated between 50 kPa and

---

[5]See the definition of the synoptic cloud component in section 2.3.
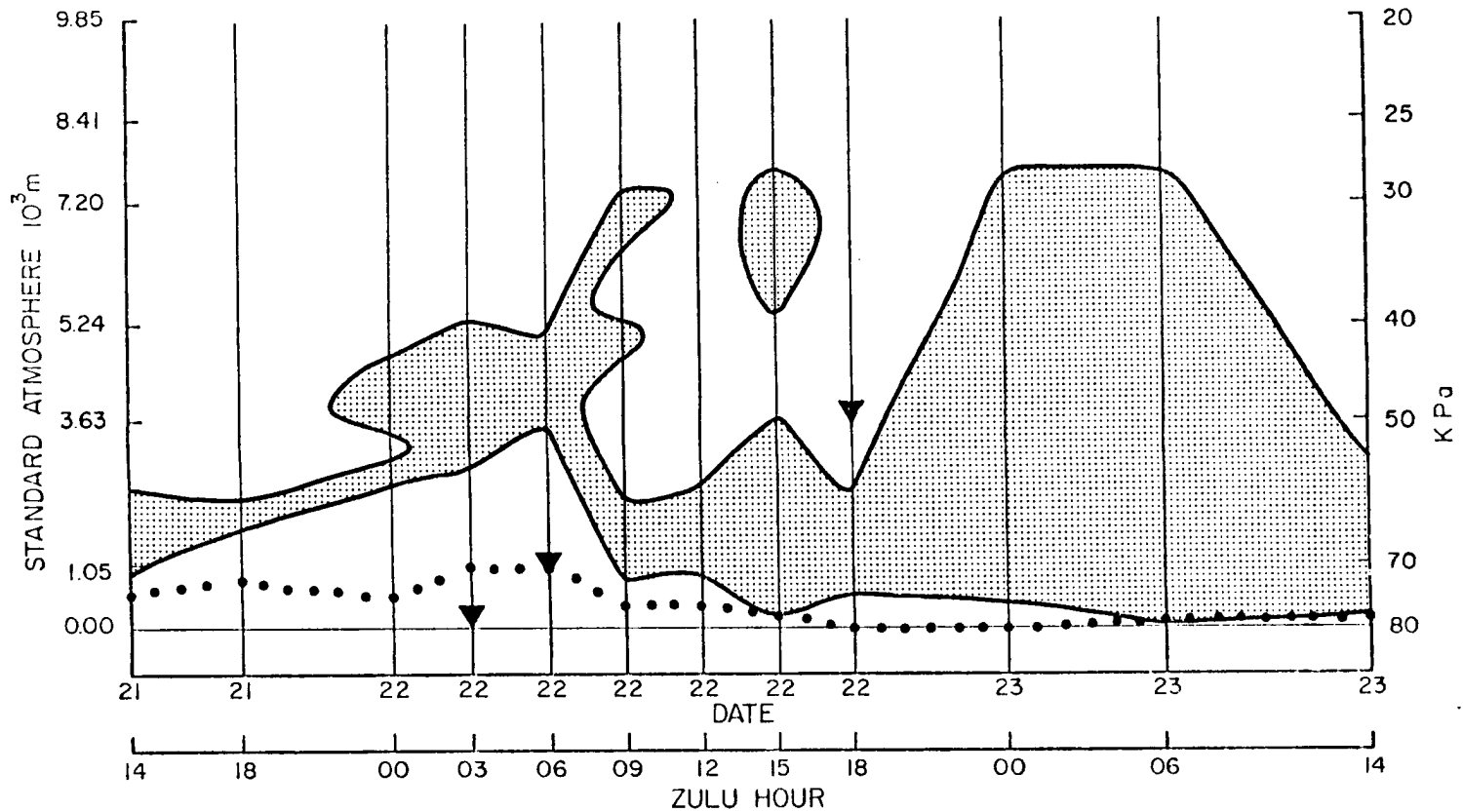
Figure 26. Time Cross-Section Analysis of the Synoptic Cloud Component over Craig of Case Study #3. Stippled area depicts the upwind, non-lifted synoptic cloud component. The area between the surface, 80 kPa, and the solid dots depicts the blocked layer. Triangles indicate trough passage at the surface, 70 kPa, and 80 kPa.

27 kPa after 2209Z, was advected from the east while above and below this layer, it was still being forced from the west.

In order to understand how much moisture was being advected toward the study area at upper levels, the rawinsonde data taken over Hebron, which lies to the east, was analyzed (see Figure 2). Figure 27 shows a time section of the synoptic cloud component which formed over Hebron. Some of this moisture was advected over the main barrier toward the Craig rawinsonde (The Hebron surface pressure level is near 75 kPa).

Figure 28 illustrates a time section of the cloud that formed over the Park Range with the assumption that winds at all levels had westerly, transbarrier components.[6] This assumption could produce errors which would invalidate the analysis. First, air from lower layers was lifted into a wind regime which was flowing away from the barrier, i.e., easterly. Second, air which originated within the regime of easterly flow was also advected towards the barrier and lifted according to the lifting model. Third, air which was advected from the east may, in fact, have been lifted and saturated. These three conditions have not been accounted for in Figure 28.

In order to correct for the above inaccuracies, an analysis of the airflow field between Craig and Hebron was performed. Figure 29 illustrates cross-sections in time of the wind field at Craig, to the left, and Hebron, to the right. This analysis shows that at the lower interface of easterly and westerly flow, the Craig winds back with height through 180° while the Hebron winds veer with height through 00°. At

---

[6]See the definition of the orographic and convective cloud components in section 2.3 and 2.1, respectively.
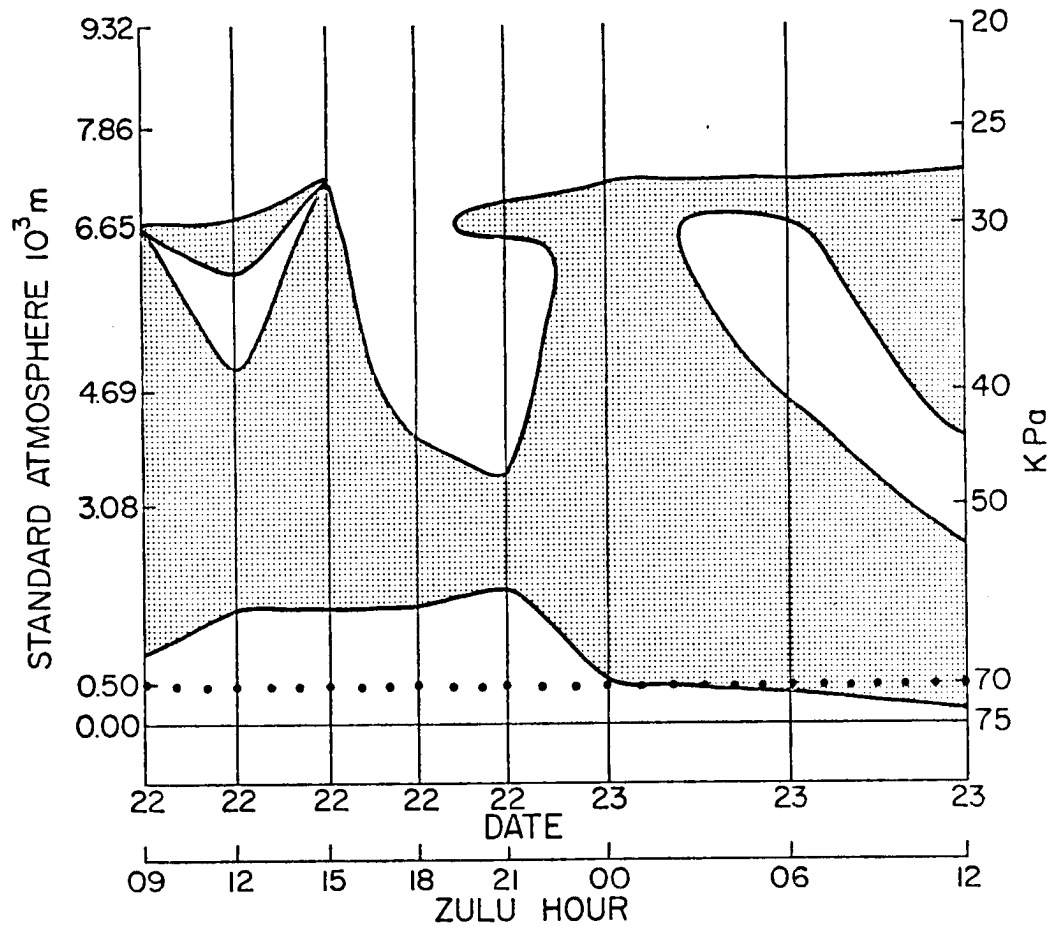
Figure 27. Time cross-section analysis of the synoptic cloud component over Hebron in case study #3. The stippled area depicts the non-lifted synoptic component. The area between the surface, 75 kPa, and the solid dots depicts the blocked layer.
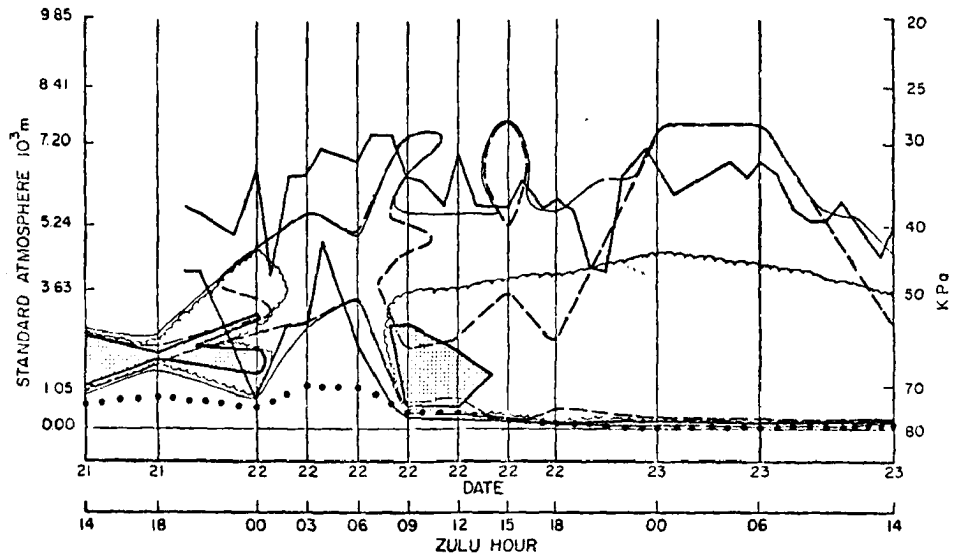
Figure 28a. Time cross-section analysis of the unadjusted composite
cloud system of case study #3. The area within the dashed
line depicts the upwind, non-lifted cloud. The area within
the thin solid line depicts the lifted, ice-saturated cloud.
The area within the convoluted line depicts the lifted,
water-saturated cloud. The area within the heavy solid
line depicts the radar observed cloud. The stippled area
depicts the convective cloud component, θ_e, decreasing
with height in a water-saturated layer. The area between
the surface, 80 kPa, and the solid dots depicts the blocked
layer.
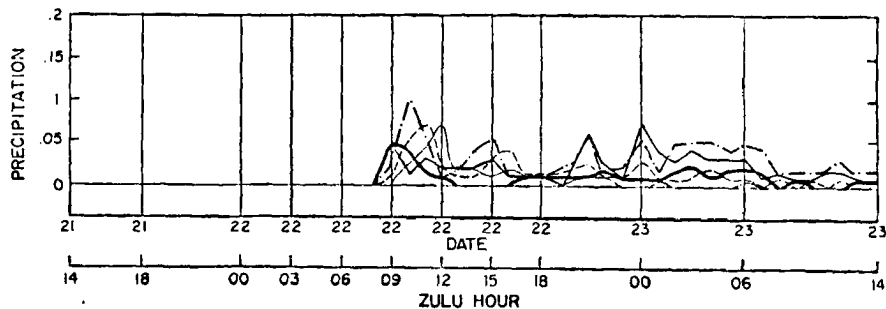
Figure 28b. Time plot of the hourly precipitation of various points
across the barrier for case study #3. The heavy solid
line (———) corresponds to Radar Base. The dotted-dashed
line (—·—) corresponds to False Top. The medium solid
line (———) corresponds to Picnic Area. The dashed line
(— — —) corresponds to Highway Camp. The thin solid line
(———) corresponds to Columbine Lodge.
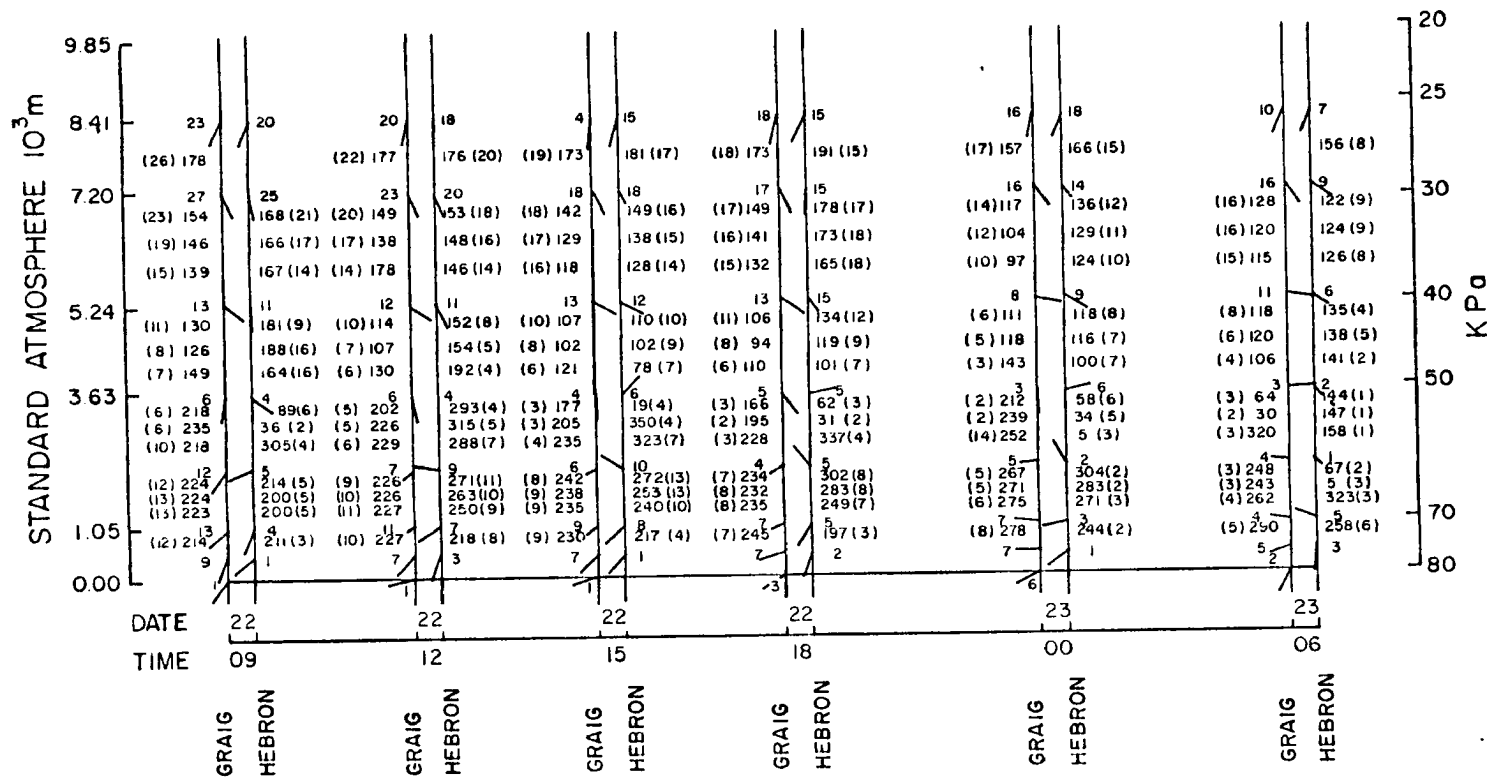
Figure 29. A detailed cross-section analysis of wind directions and wind speeds as observed by Craig and Hebron rawinsondes during case study #3. Wind directions (degrees - not within parentheses) and wind speeds (m/sec - within parentheses) are analyzed in 2.5 kPa intervals.

this interface either a mesoscale mountain wave effect in the horizontal caused the winds to flow out of the south at Craig and out of the north at Hebron, or mesoscale low pressure areas lie to the west of Craig and to the east of Hebron. The synoptic analysis gives no indication as to which of these possible explanations occurred. Above this point, the winds at the rawinsonde sites are in fair agreement.

Figure 30 shows an isentropic cross-section analysis in time between Craig and Hebron while Figure 29 shows a detailed analysis of wind directions and speeds over Craig and Hebron in time. Note that within the easterly component at upper levels, air that flows along the isentropes sometimes rises and sometimes sinks as it flows from Hebron to Craig.[7] From this fact is seems likely that, at times, portions of the cloud system could have been formed by air which travelled westerly from Hebron at upper levels and was lifted to saturation.

Figure 31a illustrates the adjusted orographic and convective cloud components of the third case study with the upper level easterly flow accounted for.[8] This composite cloud system was synthesized by lifting the Hebron soundings in the upper layers according to the airflow and isentropic analyses. This treatment of Craig to Hebron airflow in order to reconstruct the cloud system implies that the θ surfaces are flat across the mountain barrier. This may be a poor assumption and could introduce errors in the upper levels of the synthesized composite cloud system.

---

[7]This airflow lifting and sinking between Hebron and Craig my be attributed to a synoptic scale effect similar to over running air associated with a warm front or an upper air mesoscale effect due to the peculiarity of the synoptic circulation on a smaller scale.
[8]See the definitions of orographic and convective cloud components in sections 2.3 and 2.1, respectively.
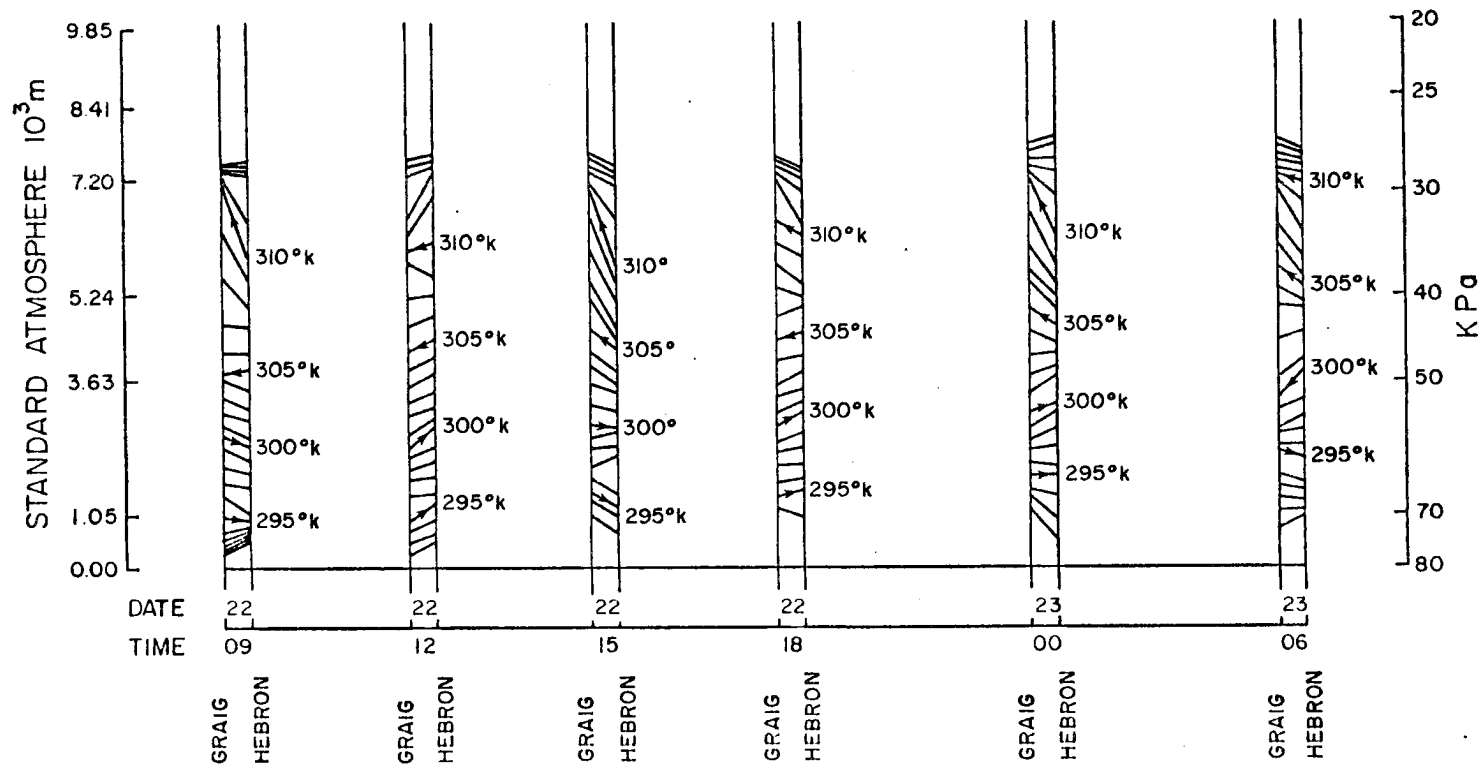
Figure 30. Isentropic Analyses for Craig-Hebron Cross-Sections in Time of Case Study #3. Isentropes are analyzed in one degree intervals and airflow directions are indicated on isentropes every 5°C.
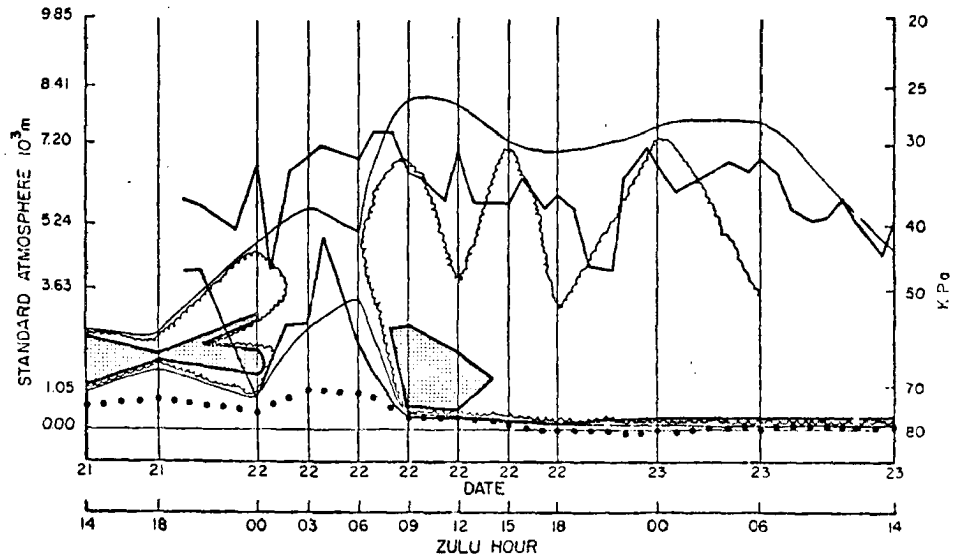
Figure 31a. Time Cross-Section Analysis of the Adjusted Composite Cloud System of Case Study #3. The area within the thin solid line depicts the lifted, ice-saturated cloud. The area within the convoluted line depicts the lifted, water-saturated cloud. The area within the heavy solid line depicts the radar observed cloud. The stippled area depicts the convective cloud component, θ_e, decreasing with height in a water-saturated layer. The area between the surface, 80 kPa, and the solid dots depicts the blocked layer.
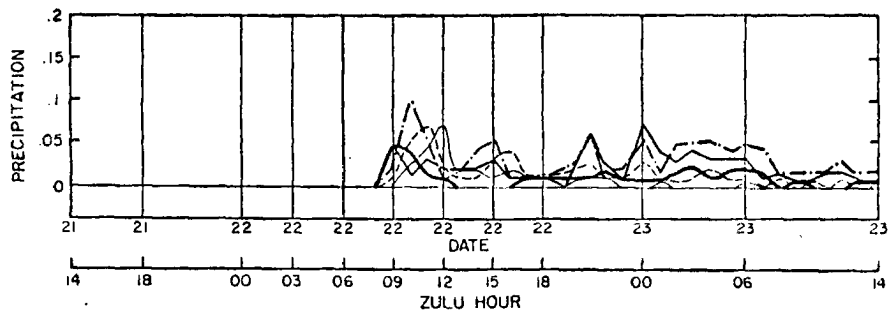

Figure 31b. Time Plot of the Hourly Precipitation of Various Points Across the Park Range Barrier for Case Study #3. The heavy solid line (────) corresponds to the Radar Base. The dotted-dashed line (─·─) corresponds to False Top. The medium solid line (────) corresponds to Picnic Area. The dashed line (───) corresponds to Highway Camp. The thin solid line (────) corresponds to Columbine Lodge.

The agreement between the K band radar observations and the analyzed orographic component was acceptable in the lower layers where the cloud base dropped below ridge top, 70 kPa. The disagreement at all high levels, however, even after an attempt was made to account for the complications of deep easterly flow, can be attributed to several factors. First, this cutoff synoptic system was accompanied by a complicated airflow system. Second, the soundings were generally characterized by temperature and dewpoint traces that were either parallel or slowly separating with height. This makes any lifting model critical in analyzing for saturation. Clearly the orographic lifting model used as well as the simple attempts to lift the upper levels of the Hebron soundings did not properly treat the actual airflow conditions. Third, the vertically pointing radar observed the cloud at the westerly edge of the barrier. Fourth, the analyzed cloud system only accounted for an orographic and an implied mesoscale lift which operated at upper levels. Synoptic vertical velocities which accompanied this complicated system could have easily added to the orographic cloud component since the moisture within the soundings was critical and only slowly decreased with height. Synoptic analysis of vorticity advection hinted that this may be the case, but no positive identification could be made. Last, but not least, the air that is indicated as being saturated with respect to ice may, in fact, not contain a "cloud".

A comparison between the Craig and Hebron soundings for coinciding launches of the third case revealed that in most, but not all, cases the "downwind" soundings were noticeably drier than the "upwind" soundings. This was true for Hebron in the lower layers, when the flow was from the west, and for Craig in the upper layers, when the flow was from

the east. This dryness within the "downwind" sounding may indicate that moisture was extracted as precipitation from the air as it flowed over the Park Range.

Figures 28b and 31b illustrate the observed precipitation which fell during this storm event. Once again, there is a sharp peak early in the period, then amounts fell off. The figure implies that convective showers occurred around 2220Z. No soundings were taken at this time and Ku radar reflectivity data could not be used to verify the analysis (The Ku radar had been moved to Milner for this storm. Its reflectivity data showed no hint of convective activity at this site). At 1227Z, in the visual observations section in Appendix B, there is a significant increase of snow accumulations as elevation increases. This points to the presence of a true orographic precipitation component.

Since two wind regimes were operating, one forcing air from the west and another forcing air at higher levels from the east, it is possible that ice crystals blowing from the east could have fallen into the lower cloud layers which were being formed from the low level flow. A simple calculation using the mean wind speeds in the easterly flowing air from Hebron and an assumed crystal fall valocity of 0.5 m/sec, revealed that crystals falling from these upper layers could have entered the lower cloud layers and westerly wind regime near Milner. Here the ice crystals could have been caught up into the cloud system and provided for a self-seeding mechanism. As mentioned above, this type of cloud system which seeds itself is sometimes referred to as a "seeder-feeder" system.

Visual observations of this third cloud system did help in reconstructing the storm progression but they did not greatly explain the complexities of this system. At 1400Z on the 21st, skies were broken at Craig as the storm began to move in. By 1630Z, a few hours later, a widespread orographic cloud deck was reported over the Park Range with no convection observed. At 0013Z on the 22nd, aircraft observations documented some patchy scud clouds over the area with a higher cloud layer all the way up to 25,000 feet or so. Snow began to fall at Steamboat Springs at 0850Z on the 22nd. By 1227Z on the 22nd, one-half inch of snow had accumulated at Milner, one inch at Steamboat Springs, and one and one-half inches halfway up the ridge. Snow continued to fall in the area through 1400Z on the 23rd. Further detailed visual observations can be found in Appendix B.

3.3.1 The Main Findings of the Third Case Study

This closed low case study supported findings from other cases that revealed important relationships between the migratory wave and the components of the total cloud system:

1) The moisture moved in at high levels and then deepened after the low pressure center, at the surface and aloft, had passed.

2) Some of the moisture at the highest levels, later in the storm period, had been advected from the east due to the easterly wind regime established by the upper air disturbance.

3) The composite cloud formation was delayed until the 70 kPa winds, moisture, and cold air pooling provided for a circulation which eliminated blocking and provided for lifting and saturation. The cold

air pooling was weakly supported by surface airflow and to a greater
extent by the presence of a nocturnal valley inversion.

4) In this storm, the cloud over the ridge was formed by two
different wind regimes; a low level orographic lift, and an upper air
mesoscale lift.

5) Even after all orographic and mesoscale lifting had been con-
sidered, the analyzed orographic component could still not be matched
to radar observations. This may be due to inaccurate lifting models,
inability to include synoptic vertical velocities, errors in specifying
whether a cloud is present or not, or the difficulties associated with
analyzing a disorganized atmospheric system.

6) The complicated east-west wind regime associated with the syn-
optic storm circulation, which formed this cloud system, may have
created a "seeder-feeder" cloud system. The cloud blowing from the
east, aloft, may have fed the lower cloud layers, which were formed as

air was topographically lifted from the west, with ice crystals.

7) "Downwind" soundings tended to be drier than "upwind" sound-
ings. This indicates that precipitation and the removal of moisture
occurred between the two rawinsonde sites.

8) The convective component occurred in the lower levels which
was within the westerly wind regime and was orographically lifted.

9) The form of the convective component during the trough passage
was very similar to the other case studies.

10) The convective component occurred fairly early in the storm
period and the greatest amount of instability developed with respect to
the orographic cloud that formed after the disturbance passed.

11) All of the instability associated with the early portions of this storm existed potentially at 2100Z and after. It was released after an orographic component was formed by condensation of this potentially unstable air.

12) The instability was not caused on a large scale by the synoptic scale disturbance.

13) The precipitation record at times suggested the presence of a showery, convective precipitation component, while at other times, a steady, orographic precipitation component was suggested.

3.3.2 Important Conclusions from Case Study #3

Once again the upwind blocking significantly affected the cloud system. During the field experiments of COSE I and COSE II, the blocking phenomena was observed fairly regularly in the Yampa Valley. In this region at least, it is very important to attempt to measure the amount of blocking and account for its effects.

As illustrated in the third case study, the type of lifting model is not only critical when the moisture slowly decreased with height, but also when the general airflow in the vicinity of the ridge is not uniform. Strong wind direction changes with height complicated the lifting model and only very rough approximations of lifting could be made which yielded less than perfect agreement between the analysis and the observations.

CHAPTER IV SUMMARY AND CONCLUSIONS

This study has focused upon the mechanisms by which mountains and synoptic weather systems interact to produce characteristic orographic cloud systems. Case studies were constructed from rawinsonde data, radar data, visual observations, surface winds, temperature, and precipitation observations and synoptic analyses. These cloud systems were described with respect to three principle air motion components of which they were comprised: synoptic, orographic, and convective components.

The three storm systems studied were quite different in the sense that each represented a different type synoptic scale: short wave, long wave, cutoff low. This was fortunate in that the analysis methods could be applied to different types of storms so that their different structure could be envisaged. It was, however, unfortunate in that analyses of similar type storms could not be made to document the variability within storm types. All three storms studied possessed some degree of convective instability, and in all cases, the presence of upwind blocking was important to the topographic lift. Other similarities include storm tracks that provided wind flows which produced favorable orographic lift, and all three storms produced significant precipitation for the Park Range.

In terms of climatological distribution, the storms analyzed in this study did not represent the most frequent storm type that produces the highest percentage of precipitation which falls in the Steamboat Springs area. Storms similar to that of case study #1, however, do produce the greatest amount of precipitation per storm event.

Precipitation at Steamboat Springs is characterized as being fairly light and occurring at frequent intervals. This is illustrated by the fact that .3 inches of precipitation or less fell on 80% of the days which produced snowfall at Steamboat Springs during the past ten years. The storm systems which produce greater amounts than the .3 inches of precipitation per storm event are important in that even though they are fairly infrequent, a lack of such events may result in seasonal snowfall deficiencies. This is what happened during the drough years of 1976-1977 throughout the entire state of Colorado.

The climatology of mountain precipitation as given by Grant, et al, (1974) indicates a strong diurnal precipitation maximum between midnight and 7:00 a.m. local time. Four of the five largest precipitation periods during the three case studies also indicated this nighttime maxim. It appears that the synoptic disturbances passed through the study area during the early evening hours, but it is difficult to believe that even in the climatological averages, the synoptic storms completely control the early morning precipitation maxima. It can be hypothesized that as the air continues to cool in its diurnal cycle, it is unable to hold as much water vapor as it could at warmer daytime temperatures. Another explanation may be that as air is cooled in its diurnal cycle, downslope valley winds converge with inflow air from the west and an effective lift is realized due to convergence in the valley upwind of the main barrier.

4.1 Major Findings

The important findings in this study are:

1) Wintertime cloud systems over the Colorado Rockies are formed by vertical velocity components that, in turn, are generated by very

different physical processes. Synoptic scale velocity components are determined by differential vorticity advection and airmass lifting by frontal systems. Orographic vertical velocity components are determined by stable airflow that is forced vertically by the topography. Convective vertical velocity components are determined by the release of convective instability as layers of air are lifted to saturation. These vertical air motions combine constructively and destructively in time to produce the individual characteristics of each cloud system.

2) It is significant that the second case study cloud system may have been invigorated by a mesoscale disturbance associated with the synoptic storm structure. Rhea, et al., (1969) and Furman (1967) have made radar observations in the Colorado Rockies similar to those made in this study. They both concluded that the observed radar characteristics were due to convective activity organized into banded structures. The banded zones of higher radar reflectivity as observed in 1967, 1969, and 1979 may be attributed to a moving mesoscale phenomena. In addition to the radar studies, weak gravity waves have been observed within cloud systems over the San Juan Mountains of Colorado (Marwitz, 1980; Cooper and Saunders, 1980). All of these observations imply that, at times, a fourth cloud-forming component is also important.

3) Barrier blocking was very important in determining the orographic component of the lift and the depth of the "lifted" cloud. Blocking or stagnation occurred in conjunction with nighttime cold air pooling, nocturnal valley inversions, weak surface winds, and cross-valley airflow out of the southwest at 70 kilopascals (kPa) that prevented efficient channeling and forcing of the lower elevation winds into the Yampa Valley and over the Park Range barrier. Neglecting this

physical process can lead to serious analysis errors.

4) The lifted cloud analysis was sensitive to the type of lifting model employed. In a sense, the temperature and moisture profiles determine the potential for saturation. When the moisture slowly decreased with height, the physical synoptic cloud was difficult to identify and the model used to lift the sounding became critical in defining the depth of the "lifted" cloud. When the moisture sharply decreased with height, as at a subsidence inversion, these two problems were eliminated.

5) Synoptic storm track, large scale vorticity, moisture and temperature advection, travelling mesoscale phenomena associated with cyclonic waves, synoptic and topographic forcing of wind direction and speed, vertical structure of temperature and moisture, cold air pooling, nocturnal valley inversions, blocking, stagnation, and orographic lift all combine in time to define the actual orographic cloud. The timing and interaction of these physical processes determine the formation and behavior of the complete cloud system and define how the local mountain terrain and environment interacts with synoptic weather patterns to produce each characteristic orographic cloud system and the accompanying precipitation.

4.2 Additional Findings

1) Various cloud components occurring within these winter orographic storm systems were deduced from rawinsonde analysis, physical reasoning, and vertically pointing radar data. Case studies based on radar observations or thermodynamic analysis alone, however, leads to erroneous conclusions or incomplete descriptions with respect to

dynamical and microphysical processes which occur within the cloud systems.

2) Both spring and fall 1979 sounding data sets indicate that most cloud systems that formed over the Park Range of Colorado experienced only a small degree of instability that was responsible for convective vertical velocity motions. Therefore, microphysical processes associated with convective motions were not of primary importance within these cloud systems.

3) Because the lifted cloud analysis was so sensitive to the upwind profiles of wind, temperature, and moisture, rawinsonde operations and data reduction should be closely monitored to maintain the highest standards of quality.

4) The case study method serves as a valuable tool in describing the important physical properties of cloud systems and the mechanisms by which they are produced. This approach, however, requires detailed observations in time of thermodynamic and microphysical properties. Radar as well as visual observations are fairly continuous in time. Rawinsonde observations, on the other hand, are restricted in time by the preparation of the instrument package, the ascension time of the balloon, and the initial data reduction. Since the preceding operations can be performed in 2 to 2 1/2 hours, serial rawinsonde launches at intervals of no more than every 3 hours are recommended for a reasonably detailed characterization of cloud systems in a case study format.

5) The K band radar analysis of cloud top agreed well with the analysis methods used in the first case study except when the air, as depicted by the analysis, was saturated with respect to ice at extreme altitudes, but no "cloud" was "seen" by the radar. Most of the time,

the Ku radar was found to underestimate the cloud tops of both the K band radar and the analysis. The K band radar was more sensitive than the Ku band radar because it was capable of detecting a lower threshhold of "cloud". When the Ku radar indicated cloud tops substantially higher than the analysis indicated, however, as in the second case study, it was inferred that the discrepancy was due to the deficiencies of the analysis to indicate convective turret cloud tops or discriminate a meso-scale gravity wave disturbance which invigorated the composite cloud system.

6) In the first case study, it was hypothesized that ice crystals fell from a layer of conditional instability into the dendritic crystal growth region centered on the -15°C isotherm and that this accounted for a zone of higher radar reflectivities observed at this time. A detailed crystal trajectory analysis and a complete cross-sectional analysis would have to be performed in order to verify this hypothesis.

7) In the second and third case studies, it is also hypothesized that these storms could have had a "self-seeding" mechanism operating. Again, a detailed crystal trajectory analysis would have to be performed to substantiate the hypothesis.

8) Visual observations upwind of the main barrier tended, in all cases, to validate the use of the defined ice-saturated cloud for non-lifted soundings, although the extent of the analyzed cloud overestimated the visually observed cloud. This was expected, however.

9) Approximately 17 percent of the time, a purely "orographic" cloud did form when no upwind synoptic cloud was indicated by the rawin-sonde analysis or visual observations. This indicates that a synoptic cloud component produced by synoptic scale vertical velocities is not

necessary to the formation of these wintertime cloud systems.

10) The low level winds upwind of the main barrier were not always the only dominant controlling airflow in the formation of the composite cloud system. As was noted in the last case study, upper atmospheric synoptic or mesoscale circulations may have a strong influence in lifting air to saturation from any direction.

11) In all cases, the composite cloud thickened while the bases dropped below ridge top level in response to the synoptic disturbance passage.

12) The convective potential instability analysis ($\partial\theta_e/\partial Z < 0$ in a saturated layer) can be properly used to identify the instability responsible for the convective vertical velocity cloud component. This conclusion is supported by the fact that the strongest vertical velocity components, as deduced from the stability analysis, were accompanied by high radar reflectivities and radar "cloud tops" that were cellular in nature. In contrast, the radar data taken when the instability was not as deep or as strong was characterized by high reflectivities embedded within a cloud mass which was non-cellular. The maximum radar reflectivity observed in any of these storms was 25 dBz.

13) The cloud system of case study #2, at times, existed in an unstable airmass. This illustrates the fact that some cloud systems that formed over the northwestern Colorado Rockies can generate convective vertical velocity components. These orographic systems may support a completely different microphysical regime than most of the stable orographic types that are common to this continental mountainous area.

CHAPTER V RECOMMENDATIONS FOR FURTHER RESEARCH

The type of case studies performed here provides insight into the workings of orographic cloud systems. Advances need to be made in defining various physical processes that control orographic clouds: specifically, complexities that relate vertical displacement of an airflow as a function of topography and stability, lifted and non-lifted cloud formation, and blocking and stagnation as defined from rawinsonde data.

More detailed studies of the physical interactions between the various lifting processes which contributed to cloud formation over mountainous terrain are necessary for a proper understanding of orographic cloud systems. Future research should focus on the mechanisms, locations and times that the various vertical motion components interact to form cloud systems. Satellite data may be of some help in making some of these determinations. Care must be taken to choose the proper radar system, its location, and the mode of operation.

More work needs to be done in the area of detecting and analyzing mesoscale gravity wave formation and propagation. Radar observations, in both the PPI and vertically pointing modes, can be used to study how gravity waves propagate and how they physically influence pre-existing cloud systems.

The most important parameter to be understood is the precipitation that forms as a consequence of the interactions between the various orographic cloud components in time and space. Perhaps a combination of accurate, qualitative cloud descriptions, microphysical data which

can be used to infer precipitation formation, and crystal trajectory calculations may reveal an answer to this difficult question.

CHAPTER VI REFERENCES

Air Weather Service, 1955: Accuracies of radiosonde data. Technical
Report 105-33, H.Q., Air Weather Service, USAF, Washington, D.C.,
12 pp.

Air Weather Service, 1974: Analysis of weather data. Career Develop-
ment Course for Weather Technicians, USAF, Vol. 3, 204 pp.

Aufdernauer, A.N., and H.R. Larson, 1976: Ice multiplication through
grazing collisions. International Conference on Cloud Physics,
AMS, Boulder, Colorado, July 26-30, pp. 152-156.

Berkofsky, L., 1964: The fall-off with height of terrain-induced verti-
cal motions. J. Appl. Meteor., 3, 4, 410-414.

Brown, K.J., R.D. Elliott, and J.R. Thompson, 1976: Seeding convective
bands in winter storms and the observed large scale effects.
Second WMO Scientific Conference on Weather Modification, Boulder,
Colorado, August 2-6, pp. 465-472.

Chappell, C.F., 1970: Modification of cold orographic clouds. Ph.D.
Dissertation, Department of Atmospheric Science, Colorado State
University, Fort Collins, Colorado, 196 pp.

Cooper, W.A., and C.P.R. Saunders, 1976: Microphysical observations in
San Juan storms. Second WMO Scientific Conference on Weather Mod-
ification, Boulder, Colorado, August 2-6, pp. 93-98.

Cooper, W.A., and C.P.R. Saunders, 1980: Winter storms over the San
Juan mountains. Part II: Microphysical processes. J. Appl.
Meteor., 19, 927-941.

Corby, G.A., 1954: The airflow over mountains. Quart. J. Roy. Met.
Soc., 80, 491-521.

Department of the Air Force, 1969: Use of the skew T, log P diagram in
analysis and forecasting. Headquarters, Air Weather Service
(Mac) Scott Air Force Base, Illinois, AWS Manual 105-24, July,
142 pp.

Derrickson, R.G., E.C. Nickerson and J.A. Peterka, 1973: A numerical
simulation of a cold orographic cloud system. Fluid Mechanics
Program, College of Engineering, Paper No. CER72-73RGO-ECN-JAP19,
Colorado State University, Fort Collins, Colorado, February, 127 pp.

Dumont, R.J., 1975: Determining the seedability of the winter oro-
graphic clouds from satellite observations. Masters Thesis,
Department of Atmospheric Science, Colorado State University,
Fort Collins, Colorado, 48 pp.

Dumont, R.J., D.W. Reynolds, L.O. Grant, and T.H. Vonder Haar, 1974: Determining the seedability of winter orographic clouds from satellite observations. Preprints: Fourth Conference on Weather Modification, Ft. Lauderdale, Florida, AMS, pp. 454-461.

Elliott, R.D., 1966: Effects of seeding on the energy of systems. J. Appl. Meteor., 5, 5, 663-668.

Elliott, R.D., 1969: Cloud seeding area of effect numerical model. By Aerometric Research, Inc., California (CFSTI, Springfield, Virginia), January, 67 pp.

Elliott, R.D. and E.L. Hovind, 1964: On convection bands within Pacific coast storms and their relation to storm structure. J. Appl. Meteor., 3, 143-154.

Elliott, R.D., and R.W. Shaffer, 1962: The development of quantitative relationships between orographic precipitation and air-mass parameters for use in forecasting and cloud seeding evaluation. J. Appl. Meteor., 1, 218-228.

Elliott, R.D., P. St.Amand, and J.R. Thompson, 1971: Santa Barbara pyrotechnic cloud seeding test results, 1964-1970. J. Appl. Meteor., 10, 785-795.

Fraser, A.B., 1970: Airflow through a cap cloud. Second Weather Modification Conference of the AMS, Santa Barbara, California, April 6-9, pp. 14-17.

Fraser, A.B., R.C. Easter and P.V. Hobbs, 1973: A theoretical study of the flow of air and fallout of solid precipitation over mountainous terrain: Part I. Airflow model. J. Atmos. Sci., 50, 801-812.

Furman, R.W., 1967: Radar characteristics of wintertime storms in the Colorado Rockies. Atmospheric Science Paper #112, Department of Atmospheric Science, Colorado State University, Fort Collins, Colorado, 53 pp.

Gates, W.L., 1960: Static stability measures in the atmosphere. J. Meteor., 18, 526-533.

Grant, L.O., C.F. Chappell, and P.W. Mielke, Jr., 1968: The recognition of cloud seeding opportunity. Proc. First National Conference on Weather Modification, Albany, New York, April 28-May 1, pp. 372-385.

Grant, L.O., C.F. Chappell, L.W. Crow, J.M. Fritsch, P.W. Mielke, Jr., 1974: Weather modification - a pilot project. Final Report to the Bureau of Reclamation, Appendices A-I, pp. 1-98.

Grant, L.O., and R.D. Elliott, 1974: The cloud seeding temperature window. J. Appl. Meteor., 3, 355-363.

Grant, L.O., J.D. Marwitz, C.W. Thompson, 1965: Application of radar to snow surveying. Proc. 33rd Annual Meeting Western Snow Conference, Colorado Springs, Colorado, April 20-22, pp. 42-48.

Hallett, J. and S.C. Mossop, 1974: Secondary ice particle production during the riming process. International Conference on Cloud Physics, AMS, Tucson, Arizona, October 21-24, pp. 165-168.

Harris, F.I., 1976: Doppler radar observations of precipitation structure and convective motions in an evaporating ice cloud. 17th Weather Radar Conference, Seattle, Washington, October 26-29, pp. 220-225.

Henmi, T., and L.O. Grant, 1974: Secondary ice particle production from rimed ice. Conference on Cloud Physics, Tucson, Arizona, October 21-24, pp. 158-164.

Hess, S.L., 1959: Introduction to Theoretical Meteorology. Holt, Rhinehart, and Winston, New York, New York, 362 pp.

Hess, W.N., 1974: Weather and Climate Modification. John Wiley and Sons, Inc., New York, New York, 842 pp.

Hill, G.E., 1974: Results of a cold orographic cloud seeding experiment in the northern Washatch Mountains. Fourth AMS Conference on Weather Modification, Fort Lauderdale, Florida, November 18-21, pp. 462-467.

Hill, G.E., 1977: Seedability of winter orographic storms in Utah. Utah Water Research Lab., College of Engineering, Utah State University, December, 67 pp.

Hobbs, P.V., 1969: Ice multiplication in clouds. J. Atmos. Sci., 26, 315-318.

Hobbs, P.V., J.D. Locatelli, and R.R. Weiss, 1976: Wave-like precipitation bands, precipitation cores, and generating cells associated with a warm front. 17th Weather Radar Conference, Seattle, Washington, October 26-29, pp. 249-256.

Houze, R.A., P.V. Hobbs, K.R. Biswas, W.M. Davis, 1976: Mesoscale rainbands in extratropical cyclones. Mon. Wea. Rev., 104, 868-878.

Kao, T.W., 1965: The phenomenon of blocking in stratified flows. J. Geophys. Res., 70, 4, 815-822.

Lindzen, R.S., and K.K. Tung, 1976: Banded convective activity and ducted gravity waves. Mon. Wea. Rev., 104, 1602-1617.

Mahrer, Y. and R.A. Pielke, 1975: A numerical study of the airflow over mountains using the two-dimensional version of the University of Virginia mesoscale model. J. Atmos. Sci., 32, 2144-2155.

Marwitz, J.D., 1974: An airflow case study over the San Juan Mountains of Colorado. J. Appl. Meteor., 13, 450-458.

Marwitz, J.D., 1975: The role of convection for seeding winter orographic storms. Abstracts of Special Regional Weather Modification Conference, San Francisco, California, pp. 21-26.

Marwitz, J.D., 1975: Dynamical processes in San Juan storms. Second WMO Conference on Weather Modification, Boulder, Colorado, August 2-6, pp. 85-92.

Marwitz, J.D., 1980: Winter storms over the San Juan Mountains. Part I: Dynamical processes. J. Appl. Meteor., 19, 913-926.

Marwitz, J.D., W.A. Cooper and C.P.R. Saunders, 1976: Structure and seedability of San Juan storms. Final Report to the Division of Atmospheric Water Resources Management, Bureau of Reclamation, July 1974 to August 1976, 329 pp.

Morris, R.K., 1979: Satellite studies of Sierra Nevada winter storms in support of weather modification. Masters Thesis, Department of Atmospheric Science, Colorado State University, Fort Collins, Colorado, 86 pp.

Mossop, S.C., 1976: Failure of cloud seeding projects caused by natural ice crystal multiplication. Second WMO Scientific Conference on Weather Modification, Boulder, Colorado, August 2-6, pp. 71-76.

Mossop, S.C., 1976: Production of secondary ice particles during the growth of graupel by riming. Quart. J. Roy. Met. Soc., 102, 45-57.

Mossop, S.C., and E.R. Wishart, 1976: Recent experiments on splinter production during riming. International Conference on Cloud Physics, AMS, Boulder, Colorado, July 26-30, pp. 148-151.

Myers, V.A., 1962: Airflow on the windward side of a large ridge. J. Geophys. Res., 67, 11, 4267-4291.

Nickerson, E.C., C.F. Chappell, and E.L. Magaziner, 1976: Effects of seeding on the dynamics of cold orographic clouds. Second WMO Scientific Conference on Weather Modification, Boulder, Colorado, August 2-6, pp. 123-130.

Orgill, M.M., 1971: Laboratory simulation and field estimates of atmospheric transport-dispersion over mountain terrain. Ph.D. Dissertation, Department of Civil Engineering, Colorado State University, Fort Collins, Colorado, 298 pp.

Orgill, M.M., J.E. Cermak and L.O. Grant, 1971: Laboratory simulation and field estimates of atmospheric transport dispersion over mountainous terrain. Fluid Mechanics Program, College of Engineering, Paper No. CER70-71MMO-JEC-LOGHO, Colorado State University, Fort Collins, Colorado, 301 pp.

Plooster, M.N., and L. Vardiman, 1976: Orographic snowfall prediction with a numerical model. Second WMO Scientific Conference on Weather Modification, Boulder, Colorado, August 2-6, pp. 131-134.

Polete, F.E., M.D. Hale, and D.A. Mathews, 1977: Bureau of Reclamation's environmental data network. 6th Conference on Planned and Inadvertent Weather Modification, Champaign-Urbana, Illinois, October 10-13, pp. 362-364.

Queney, P., 1947: The problem of airflow over mountains: a summary of theoretical studies. Bull. Amer. Met. Soc., 20, 16-26.

Queney, P., G.A. Corby, N. Gerbier, H. Koschmieder, J. Zierep, 1960: The airflow over mountains. Tech. Note No. 34, WMO, Geneva, 135 pp.

Reid, J., 1976: Dispersion in a mountain environment. Atmospheric Science Paper #253, Colorado State University, Fort Collins, Colorado, 150 pp.

Reid, J.D., L.O. Grant, R.A. Pielke, and Y. Mahrer, 1976: Observations and numerical modeling of seeding agent delivery from ground based generators to orographic cloud base. Second WMO Scientific Conference on Weather Modification, Boulder, Colorado, August 2-6, pp. 521-527.

Reynolds, D.W., and R.K. Morris, 1978: Satellite support to the Sierra Cooperative Pilot Project. Preprint Volume, Conference on Sierra Nevada Meteorology, AMS, San Francisco, California, June 19-21, pp. 141-148.

Reynolds, D.W., T.H. Vonder Haar and L.O. Grant, 1978: Meteorological satellites in support of weather modification. Bull. Amer. Met. Soc., 59, 3, 269-281.

Rhea, J.O., 1967: A weather typing scheme for the Park Range in northwestern Colorado. Presented at the AMS Conference on Weather Analysis and Forecasting, Fort Worth, Texas, November 6-8, 22 pp.

Rhea, J.O., 1972: Interpreting orographic snowfall patterns. Masters Thesis, Department of Atmospheric Science, Colorado State University, Fort Collins, Colorado, 123 pp.

Rhea, J.O., 1978: Orographic precipitation model for hydrometeorological use. Ph.D. Dissertation, Department of Atmospheric Science, Colorado State University, Fort Collins, Colorado, 198 pp.

Rhea, J.O., P. Willis and L.G. Davis, 1969: Park Range atmospheric water resources program. Final Report to Bureau of Reclamation, by EG&G, 385 pp.

Saucier, W.J., 1955: Principles of Meteorological Analysis. University of Chicago Press, Chicago, Illinois, 438 pp.

Sawyer, J.S., 1960: Numerical calculation of the displacement of a stratified airstream crossing a ridge of small height. Quart. J. Roy. Met. Soc., 86, 369, 326-345.

Schaffer, W., 1950: Pressure gradient associated with steeply inclined airflow. Bull. Amer. Met. Soc., 31, 8, 305-306.

Schuetz, J., 1957: The relationship between maximum echo top and stability. Proc. 6th Weather Radar Conference, March, Vol. 6, pp. 215-220.

Scorer, R.S., 1949: Theory of waves in the lee of mountains. Quart. J. Roy. Met. Soc., 74, 41.

Scorer, R.S., 1951: Forecasting the appearance of lee waves. Weather, 6, 99.

Scorer, R.S., 1953: A second kind of wave. Gliding, 4, 61.

Scorer, R.S., 1953: Theory of airflow over mountains: III-Airstream characteristics. Quart. J. Roy. Met. Soc., 80, 345, 417-428.

Seinfield, J.H., 1975: Air Pollution: Physical and Chemical Fundamentals. McGraw-Hill, Inc., New York, New York, 523 pp.

Smith, E.J., 1970: Effects of cloud-top temperatures on the results of cloud seeding with silver iodide in Australia. J. Appl. Meteor., 9, 800-804.

Stringer, E.T., 1972: Techniques of Climatology. W.H. Freeman and Company, San Francisco, California, 539 pp.

Vardiman, L., 1976: Ice multiplication by crystal fracture. International Conference on Cloud Physics, Boulder, Colorado, July 26-30, pp. 168-171.

Vardiman, L. and L.O. Grant, 1972: A study of ice crystal concentrations in convective elements of winter orographic clouds. Preprints: Third Conference on Weather Modification, AMS, Rapid City, South Dakota, June 26-29, pp. 113-118.

Vardiman, L., J.A. Moore and R.D. Elliott, 1976: Generalized seedability criteria for winter orographic clouds. Second WMO Scientific Conference on Weather Modification, Boulder, Colorado, August 2-6, pp. 41-48.

Wagner, N.K., 1960: An analysis of radiosonde effects on the measured frequency of occurrence of ducting layers. J. Geophys. Res., 65, 7, 2077-2085.

Wagner, N.K., 1960: The effects of the time constant of radiosonde sensors in the measurement of temperature and relative humidity discontinuities in the atmosphere. Bull. Amer. Met. Soc., 12, 5, 317-321.

Wallington, C.E., 1970: A computing aid to studies of airflow over
    mountains. The Meteorological Magazine, 99, 1175, 157-165.

Walsh, P.A., 1977: Cloud droplet measurements in wintertime clouds.
    Masters Thesis, University of Wyoming, Laramie, Wyoming, 170 pp.

Willis, P.T., 1970: A parameterized numerical model of orographic pre-
    cipitation. Prepared for the Bureau of REclamation (Contract No.
    14-06-D-5640), by EG&G, Inc., Boulder, Colorado, 67 pp.

Wong, K.K., and T.W. Kao, 1970: Stratified flow over extended obstacles
    and its application to topographical effects on vertical wind
    shear. J. Atmos. Sci., 27, 884-889.

APPENDIX A

In order to compare layer conditional instability and layer potential instability, the first stability analysis method must be defined in the normalized form called static stability.

$$E_{dry} = -g/\overline{T} \; (\Gamma_{environment} - \Gamma_{dry\;adiabatic})$$

$$E_{saturated} = -g/\overline{T} \; (\Gamma_{environment} - \Gamma_{saturated\;adiabatic})$$

<div align="right">(Saucier, 1955)</div>

The static stability normalizes the layer conditional instability by multiplying it by g, the acceleration of gravity, and dividing by the mean temperature in the layer. Other than these normalizing quantities, the static stability is nothing more than layer conditional instability.

$$\theta = T \; (P_o/P)^\kappa$$

$$d\theta/dZ = (P_o/P)^\kappa \; \frac{\partial T}{\partial Z} + T \; \frac{\partial (P_o/P)^\kappa}{\partial Z}$$

$$d\theta/dZ = (P_o/P)^\kappa + T \; [\; \frac{\frac{\partial (P_o)^\kappa}{\partial Z} \; P - (P_o)^\kappa \; \frac{\partial P^\kappa}{\partial Z}}{P^{2\kappa}} \;]$$

$$d\theta/dZ = (P_o/P)^\kappa \; \frac{\partial T}{\partial Z} + T \; [- \frac{\frac{\partial (P)^\kappa}{\partial Z}}{P^\kappa} \; (P_o/P)^\kappa \;]$$

$$d\theta/dZ = (P_o/P)^\kappa \; \frac{\partial T}{\partial Z} + T \; [- \frac{\kappa P^{\kappa-1} \; \partial P/\partial Z}{P^\kappa} \; (P_o/P)^\kappa]$$

$$d\theta/dZ = (P_o/P)^\kappa \; \frac{\partial T}{\partial Z} + T \; [- \frac{\kappa}{P} \; (P_o/P)^\kappa \; \frac{\partial P}{\partial Z} \;]$$

$$d\theta/dZ = T(P_o/P)^\kappa \; (1/T \; \frac{\partial T}{\partial Z} - \kappa/P \; \frac{\partial P}{\partial Z}) \qquad \theta = T(P_o/P)^\kappa \; \frac{\partial P}{\partial Z} = -\rho g$$

$$\kappa = R/c_p \qquad P = \rho RT$$

$$d\theta/dZ = \theta \; (1/T \; \frac{\partial T}{\partial Z} - 1/T \; g/c_p)$$

$$E_{dry} = g/\theta \, \frac{d\theta}{dZ} = -g/T \quad (\Gamma_{environment} - \Gamma_{dry\ adiabatic})$$

It is tempting to carry this analogy over to the saturated case by equating $1/\theta_e \, \partial\theta_e/\partial Z$, a normalized layer potential instability, to $E_{saturated}$ (similar to Fraser, et al., 1973).

$$\theta_e = \theta \exp \left(\frac{Lw}{c_p T}\right)$$

$$1/\theta_e \, \frac{d\theta_e}{dZ} = 1/\theta_e \left(\frac{d}{dZ} \, \theta \exp \frac{Lw}{c_p T}\right)$$

$$1/\theta_e \, \frac{d\theta_e}{dZ} = 1/\theta_e \left[\exp \left(\frac{Lw}{c_p T}\right) \frac{d\theta}{dZ} + \theta \, \frac{d}{dZ} \exp \left(\frac{Lw}{c_p T}\right)\right]$$

$$1/\theta_e \, \frac{d\theta_e}{dZ} = 1/\theta_e \left[\exp \left(\frac{Lw}{c_p T}\right) \frac{d\theta}{dZ} + \theta \exp \left(\frac{Lw}{c_p T}\right) \frac{d}{dZ} \frac{Lw}{c_p T}\right]$$

$$1/\theta_e \, \frac{d\theta_e}{dZ} = 1/\theta_e \left(\theta_e \, 1/\theta \, \frac{d\theta}{dZ} + \theta_e \, \frac{d}{dZ} \frac{Lw}{c_p T}\right)$$

$$g/\theta_e \, \frac{d\theta_e}{dZ} = E_{dry} + g \, \frac{d}{dZ} \frac{Lw}{c_p T}$$

$$E_{saturated} = -g/\overline{T} \quad (\Gamma_{environment} - \Gamma_{saturated\ adiabatic})$$

$g/\theta_e \, \frac{d\theta_e}{dZ}$ does not equal $E_{saturated}$.

The layer potential instability is composed of E_{dry} and the vertical gradient of latent heat. The first component is that part of the instability which is governed by the rules of layer conditional instability. The vertical gradient of latent heat, on the other hand, may also effect the sign of the layer potential instability. If this gradient happens to be more negative than E_{dry} is positive, the layer potential instability will be negative. This indicates that the layer will become convective if it becomes saturated. Clearly, $E_{saturated}$

or layer conditional instability alone cannot properly take the verti-
cal gradient of latent heat into account as the layer is in a state of
becoming saturated. Layer conditional instability, as well as layer
potential instability, is conditional upon moisture in the sense that
the layer must be cooled to saturation before the instability can be
realized. However, layer potential instability depends upon the
initial temperature and moisture gradients before and while the layer
is becoming saturated. Layer conditional instability is only dependent
upon the initial temperature gradient.

A potentially unstable layer will become convective, because, as
the layer is lifted dry adiabatically, the base of the layer will be-
come saturated first, due to the moisture gradient within the layer.
Then the layer base will cool moist adiabatically. As the layer is
lifted further, the top of the layer continues to be cooled dry
adiabatically until saturation, at which point it also cools moist
adiabatically. The initial moisture gradient can steepen the lapse
rate because of differential adiabatic cooling within the layer as it
becomes saturated. When the lapse rate is driven past the saturated
adiabatic value, the layer becomes conditionally unstable,
$\Gamma_{saturated} < \Gamma_{layer} < \Gamma_{dry\ adiabatic}$. Therefore, the lapse rate of the
layer has been altered by the original moisture gradient as lifting,
differential adiabatic cooling, and saturation has occurred. These
are the processes inferred by applying the layer potential instability
analysis method (Saucier, 1955; Hess, 1959).

As was stated before, airmass stretching may alter the lapse rate
within a layer, but now, layer potential instability describes how the
lapse rate can be changed by the initial temperature as well as

moisture gradients within the layer as it is lifted over the mountain barrier. In order to illustrate the effect of the temperature and moisture gradients in determining the differences between layer conditional instability and layer potential instability, an analysis was performed upon atmospheric layers of varying degrees of instability. An arbitrary layer base was chosen and various layer tops were chosen which represented the layer conditional instability classes of absolutely stable, and conditionally unstable. The change of equivalent potential temperature with height was calculated for each layer with varying moisture gradients so that the two stability analyses could be compared. The indicated stability represents the condition of the layer after being lifted to saturation.

From Tables V and VI, it can be seen that layer potential instability agrees with layer conditional instability in the most unstable classification. (Both methods will indicate instability under absolutely unstable conditions.) Layer potential instability, however, will attribute some instability to layers that would be classified as absolutely stable by layer conditional instability. This instability of apparently absolutely stable layers is brought about by the vertical gradient of latent heat which is present in the layer. Layer conditional instability is unable to identify this moisture effect.

TABLE V

CONDITIONALLY UNSTABLE LAYERS

	P(mb)	T(°C)	W_s(g/kg)	θ_{e_s}(°K)	W(g/kg)	θ_e(°K)	Layer Conditionally Instability	Layer Potential Instability
Layer Base	700	− 5	3.8	307.5				Unstable
Layer Top	600	−15.5	2.2	307.1			Unstable	Unstable
					2.0	306.6	Unstable	Unstable
					1.8	305.7	Unstable	Unstable
Layer Top	650	− 9.5	2.9	306.4			Unstable	Unstable
					2.7	305.9	Unstable	Unstable
					2.1	305.4	Unstable	Unstable
Layer Top	675	− 7.3	3.3	306.8			Unstable	Unstable
					3.0	305.7	Unstable	Unstable
					2.8	305.2	Unstable	Unstable

TABLE VI

ABSOLUTELY STABLE LAYERS

	P(mb)	T(°C)	W_s(g/kg)	θ_{e_s}(°K)	W(g/kg)	θ_e(°K)	Layer Conditional Instability	Layer Potential Instability
Layer Base	700	-5	3.8	307.5				
Layer Top	600	-11	2.8	311.4			Stable	Stable
					2.0	309.2	Stable	Stable
					1.5	307.8	Stable	Stable
					1.3	307.2	Stable	Unstable
Layer Top	650	-8	3.2	309.1			Stable	Stable
					3.0	308.5	Stable	Stable
					2.6	307.3	Stable	Unstable
					2.2	306.2	Stable	Unstable
Layer Top	675	-6.5	3.5	308.2			Stable	Stable
					3.3	307.7	Stable	Stable
					3.2	307.4	Stable	Unstable
					3.0	306.9	Stable	Unstable
					2.8	306.3	Stable	Unstable

APPENDIX B

This appendix contains the specific details of visual observations made within the Yampa Valley and vicinity from the ground as well as from the aircraft during the three case studies.

Case Study #1

The following is a description of the cloud system as it formed, precipitated, and dissipated. As can be seen, these observations agree well with the analyzed storm sequence in Figure 10a.

12-10-79 2130Z A thin layer of clouds are forming over the ridge.

12-10-79 2221Z A thin layer of clouds continue to form over the ridge.

12-10-79 2300Z Cirrus and stratus clouds move in from the west about Craig. Some small cumulus clouds form over the ridge along with the existing clouds.

12-11-79 0000Z Alto stratus is invading the valley. The orographic cloud which formed over the ridge has bases above ridge top.

12-11-79 0215Z The radar reports good cloud.

12-11-79 0421Z Precipitation is beginning at the radar.

12-11-79 0430Z Light precipitation is beginning at Craig and at the ridge top.

12-11-79 0445Z Snowing moderately on the ridge.

12-11-79 0545Z Snowing heavily on the ridge.

12-11-79 0800Z Snowing moderately on the ridge.

12-11-79 1310Z Snowing lightly on the ridge.

12-11-79 1400Z Snow has stopped on the ridge.

12-11-79 1430Z A thick orographic cloud still exists over the ridge while its base is well below crest.

12-11-79 1530Z Same as 1430Z.

12-11-79 2030Z The orographic cloud over the ridge is beginning to thin at its upwind edges.

12-11-79 2430Z The upwind edge is still dissipating. The cloud over the ridge is hugging the ridge, and bases are below the crest.

Case Study #2

The following observations made within the COSE study area (see Figure 2) helped to define the actual storm sequence with respect to the analysis time section of Figure 19a.

2-22-79 1600Z Skies are broken to clear to the west. Snow is falling on the Divide. Clouds are covering the ridge halfway up at Steamboat Springs.

2-22-79 2030Z The sky is overcast at Craig.

2-22-79 2255Z At Steamboat Springs, cloud bases are below 9000 feet, light snow is falling.

2-23-79 0000Z Snow is falling at Steamboat Springs.

2-23-79 0000Z It is overcast with snow at Craig, 50° winds at 4 knots.

2-23-79 0545Z Snow is falling at Steamboat Springs with the wind from the southeast.

2-23-79 0745Z Snow is falling at Steamboat Springs.

2-23-79 1115Z The sky is overcast at Craig.

2-23-79 1430Z Thin overcast lies to the north and west, thickening to the southeast with light flurries at Craig.

2-23-79 1841Z A few isolated scattered cumulus are forming over the mountaintops. As seen from the aircraft, it doesn't look ver continuous, they are all in nice puffy little cells.

2-23-79 1900Z Broken altostratus clouds reported over Craig.

2-23-79 2250Z From the aircraft, it can be seen that the ceiling is lowering over the ski area. The top of the area is obscured. The top of Storm Peak is not visible. To the west, the tops of the ridges east of Hayden are visible.

2-23-79 2300Z A brief snow shower was reported at Steamboat Springs.

2-23-79 2312Z From the aircraft it can be seen that just west of Craig, the cloud bases are about 10,000 feet and variable. The sun is dimly visible through the overcast. There is virga falling just west of Craig.

2-23-79 2333Z From the aircraft it can be seen that the top of the clouds look cumuliform. To the west stratiform decks are higher than the cumulus deck. Then they all interweave together. There is a cirrus deck quite a bit higher than the aircraft.

2-23-79 2354Z From the aircraft it can be seen that there is a lower ceiling over the Park Range now. The clouds look quite thick, at this point, towards the east. To the west, the deck is not solid. Blue sky is visible through it and the sun is visible, but the clouds seem to be getting thicker.

2-24-79 0400Z The sky is overcast and it is not snowing at Steamboat Springs.

2-24-79 0600Z Overcast skies are reported with snow falling at Craig.

2-24-79 0600Z Snow is falling at Steamboat Springs.

2-24-79 1345Z Overcast cirrostratus clouds are reported at Craig.

2-24-79 1500Z Light snow is falling at Steamboat Springs.

2-24-79 1630Z Clouds over the Park Range have cumuliform embedded with stratiform tops as observed from the aircraft.

2-24-79 1707Z There is a low cloud layer at about 9-10,000 feet, as observed from the aircraft. Clouds are very thin around Craig. Another thin cloud deck is at 12,000 feet.

Case Study #3

The following is an account of visual observations taken during

the storm period and should be compared to Figure 31a.

12-21-79 1400Z At Craig, the sky is broken to the north, east and west, while it is scattered towards the south.

12-21-79 1525Z At Craig, the east and west is all scattered with very few clouds on the southern horizon and heavier clouds to the north with mostly a stratiform structure.

12-21-79 1630Z Aircraft observations document a widespread orographic deck over the Park Range. No convection was observed, only smooth tops.

12-21-79 1649Z From the aircraft, it can be seen that broken clouds (a thin cloud deck) are drifting over the Park Range and the Yampa Valley.

12-21-79 2103Z At Craig, the sky is overcast. There is a snowshower at the airport.

12-22-79 0013Z Aircraft observations document some patchy scud clouds over the area and a higher cloud layer all the way up to 25,000 feet or so. There is just haze and scud clouds.

12-22-79 0215Z Clear skies are reported at Milner.

12-22-79 0545Z At Milner, the sky looks basically clear with stars missing to the southwest.

12-22-79 0850Z At Steamboat Springs, snow is reaching the ground.

12-22-79 0900Z At Hebron, no precipitation is falling, but the sky is overcast.

12-22-79 1036Z At Steamboat Springs moderate snowfall is reaching the ground, up to .5 cm agglomerates.

12-22-79 1227Z At Steamboat Springs, there is one inch of snowfall at the X band site, about .5 inch at the Ku site at Milner, and about 1 1/2 inches half way up the ridge. Snowfall is decreasing with time at the surface.

12-22-79 1430Z At Milner no snow is falling. There is 100% overcast present. Cloud bases are low in all quadrants.

12-22-79 1520Z At Craig snow is falling lightly from overcast skies.

12-22-79 1600Z Heavy snow is falling at Craig.

12-22-79 1600Z Snow has started falling at Milner.

12-22-79 1700Z Snow is lightly falling at Milner.

12-22-79 1820Z The snow has stopped falling at Craig.

12-22-79 2147Z There is light snow falling at Milner.

12-22-79 2340Z Overcast skies and light snow is reported at Craig.

12-23-79 0616Z Snow has been falling most of the evening at Craig.

12-23-79 1015Z Light snow is reaching the surface at Steamboat Springs.

12-23-79 1130Z Snow is still falling at Craig.

12-23-79 1400Z Snow is falling only lightly at Craig.

12-23-79 1400Z Overcast skies are reported at Milner. No snow is falling.